# THE EFFECTS OF ION BOMBARDMENT ON THE CHEMICAL REACTIVITY OF GaAs(100)

by

JUNE MIRIAM EPP

Dissertation submitted to the Faculty of the

Virginia Polytechnic Institute and State University

in partial fulfillment of the requirements for the degree of

**DOCTOR OF PHILOSOPHY**

in

CHEMISTRY

APPROVED:

John G. Dillard, Chairman

Larry C. Burton

John G. Mason

Larry T. Taylor

James P. Wightman

July, 1989

Blacksburg, Virginia

# THE EFFECTS OF ION BOMBARDMENT ON THE CHEMICAL REACTIVITY OF GaAs(100)

by

June Miriam Epp
John G. Dillard, Committee Chairman
Department of Chemistry

(ABSTRACT)

The effects of ion bombardment on the chemical reactivity of GaAs(100) were investigated by X-ray photoelectron spectroscopy. The enhancement in reactivity was shown to be related to the energy and mass of the bombarding ion. The oxidation results were compared to chemically cleaned (1:1 HCl(conc)/$H_2O$) and IHT (simultaneous ion/heat treatment) prepared GaAs(100).

Before ion bombardment, GaAs(100) was chemically cleaned with 1:1 HCl(conc)/$H_2O$ to remove surface oxides. Chemically cleaned GaAs was bombarded with 0.5-3 KeV $Ar^+$ ions (fluences = $10^{16}$-$10^{17}$ ions/cm$^2$) and with 3 KeV $Xe^+$, $Ar^+$, $^{20}Ne^+$, and $^{3}He^+$ ions (fluence = $10^{17}$ ions/cm$^2$) to investigate the effect of ion bombardment energy and mass on chemical reactivity. Ion bombardment results in the preferential sputtering of As and the amount of As depletion is dependent upon ion bombardment energy and mass. Following chemical cleaning and ion bombardment, GaAs was exposed to $10^7$-$10^{13}$ L $O_2$, $10^9$-$10^{13}$ L $H_2O$, $10^6$-$10^8$ L NO, and $10^7$-$10^{11}$ L $N_2O$ (1 Langmuir (L) = $1.3 \times 10^{-4}$ Pa•sec). Chemically cleaned GaAs produced equivalent amounts of $Ga_2O_3$ and $As_2O_3$ upon $O_2$ exposure. Oxygen exposure of ion bombarded GaAs resulted in the formation of $Ga_2O_3$, $As_2O_3$, and $As_2O_5$. Nitric oxide exposure produced $Ga_2O_3$ and $As_2O_3$, and $N_2O$ exposure produced only $Ga_2O_3$. Gallium oxide was preferentially formed for ion bombarded material and the relative amount of $Ga_2O_3$ increased with increasing ion energy. 3 KeV $Xe^+$ ion-bombarded GaAs exhibited

the greatest reactivity to $O_2$ and NO. Exposure of ion bombarded GaAs to NO produced the greatest amounts of $Ga_2O_3$. Ion bombarded GaAs was the least reactive to $N_2O$.

Exposure of ion bombarded GaAs to $H_2O$ resulted in the formation of GaOOH and $Ga(OH)_3$, with $Ga(OH)_3$ formation occurring only on 2 KeV $Ar^+$ and 3 KeV $Ar^+$ and $Xe^+$ ion-bombarded material at exposures above $10^{10}$ L.

It was shown that defects were responsible for the increased reactivity and that preferential formation of $Ga_2O_3$ on ion bombarded material was not determined by the Ga/As surface ratio. Exposing IHT prepared GaAs to $O_2$ produced equivalent amounts of $Ga_2O_3$ and $As_2O_3$ when the Ga/As ratio was $1.23 \pm 0.07$.

The damage caused by ion bombardment was investigated by optical reflectivity in the visible and near-ultraviolet region (1.6-5.6 eV), Raman spectroscopy, and capacitance-voltage measurements. Ion bombardment forms a damaged layer that is amorphous. The depth of damage is proportional to the energy of the bombarding ion and inversely proportional to the mass of the bombarding ion. The shallow damage depth for 3 KeV $Xe^+$ ion-bombarded GaAs offers some explanation for increased chemical reactivity.

The increased reactivity of ion bombarded GaAs with $O_2$ and NO is attributed to surface defects (broken surface bonds). It is suggested that these broken bonds are in the form of singly occupied dangling bonds. A model for the surface and possible reaction pathways for $O_2$ and NO reactions are discussed.

This Dissertation is dedicated to my family

# Acknowledgements

The author would like to thank her advisor, Dr. J. G. Dillard, for his encouragement, support and guidance during the pursuit of this degree.

Special thanks go to her committee members, Dr. J. P. Wightman, Dr. L. C. Burton, Dr. L. T. Taylor, and Dr. J. G. Mason for serving on her committee and for helpful suggestions.

Acknowledgement goes to Texas Instruments, the Virginia Center for Innovative Technology, and the National Science Foundation for supplying the funding to support this research project and to obtain the surface analysis equipment.

The author would like to extend thanks to for machining parts for the UHV reaction chamber and to for his work on the mass spectrometer.

The author would like to extend special thanks to for his help in keeping the surface analysis equipment in good working condition, for his generous help in training the author on that equipment, help in setting up and maintaining the UHV reaction chamber and helping her become familiar with the workings of UHV systems.

Recognition goes to Dr. Eric D. Cole and for performing the electrical measurements, as well as to Dr. Guofu Feng and for the optical measurements.

Finally, the author would like to thank her family, especially her Mother, for her long distance encouragement, and , not only for running various XRD samples, his mechanical assistance, and lessons on how to tighten nuts and bolts, but for all of his patience, encouragement, helpful advice, and support during the years at Virginia Tech.

# Table of Contents

**Chapter I: Introduction** . . . . . 1

**Chapter II: Literature Review** . . . . . 3

2.1 Gallium Arsenide . . . . . 3

2.1.1 Physical and Electrical Characteristics . . . . . 3

2.1.2 Growth of Bulk GaAs . . . . . 11

2.1.2.1 Horizontal Bridgman (HB) . . . . . 11

2.1.2.2 Liquid Encapsulated Czochralski (LEC) . . . . . 13

2.1.2.3 Epitaxial Growth Techniques . . . . . 14

2.2 Ion Bombardment . . . . . 14

2.3 Chemical Reactivity of GaAs . . . . . 23

2.3.1 Oxidation Studies of GaAs . . . . . 24

2.3.2 $O_2$ Adsorption Studies . . . . . 25

2.3.3 Chemical Composition of Oxides . . . . . 27

2.3.4 $H_2O$ Adsorption Studies . . . . . 28

2.3.5 Nitric Oxide Adsorption Studies . . . . . 30

2.3.6 Hydrogen Adsorption Studies . . . . . 31

2.3.7 Miscellaneous Gas Adsorptions . . . . . 32

2.4 Research Objectives . . . . . 34

**Chapter III: Experimental** . . . . . . 37

3.1 Materials . . . . . . 37

3.1.1 Wafers . . . . . . 37

3.1.2 XPS Standard Materials . . . . . . 37

3.1.3 Reactant Gases . . . . . . 38

3.2 Sample Preparations . . . . . . 38

3.2.1 GaAs Preparation . . . . . . 38

3.2.2 Simultaneous Ion/Heat Treatment (IHT) . . . . . . 40

3.2.3 Ion Bombardment . . . . . . 41

3.2.4 Reactant Gas Exposures . . . . . . 41

3.2.5 Standard Binding Energy Determinations . . . . . . 42

3.3 Reaction Chamber . . . . . . 43

3.4 Surface Analysis . . . . . . 46

3.4.1 Instrumentation . . . . . . 46

3.4.2 Sample Analysis . . . . . . 46

3.5 Electrical Studies . . . . . . 51

3.5.1 Sample Preparation . . . . . . 51

3.5.2 Electrical Measurements . . . . . . 54

3.6 Optical Studies . . . . . . 54

3.6.1 Raman Spectroscopy . . . . . . 54

3.6.2 Optical Reflectivity Measurements . . . . . . 56

**Chapter IV: Results and Discussion** . . . . . . 57

4.1 Effects of $Ar^+$ Ion Bombardment on the Chemical Reactivity of GaAs . . . . . . 57

4.1.1 Chemically Cleaned and $Ar^+$ Ion-Bombarded GaAs . . . . . . 57

4.1.2 $O_2$ Exposure . . . . . . 60

4.1.3 $O_2$ Reaction with IHT GaAs ..... 68
4.1.4 Chemical Forms of $O_2$ on GaAs Surface ..... 69
4.1.5 $H_2O$ Exposure ..... 70
4.2 Effect of Varying Bombarding Ion ..... 80
4.2.1 Ion Bombardment Effects on GaAs Surface Composition ..... 82
4.2.2 Depth and Composition of Damaged Layer ..... 90
4.2.3 The Chemical State of Ga and As in the Damaged Layer ..... 102
4.2.4 Ion Implantation ..... 104
4.3 Effect of Varying Bombarding Ion on Reactivity ..... 108
4.3.1 $O_2$ Exposure ..... 108
4.3.2 $H_2O$ Exposure ..... 115
4.3.3 NO Exposure ..... 118
4.3.4 $N_2O$ Exposure ..... 126
4.4 Possible Reaction Mechanisms with Ion Bombarded GaAs and a Model for the Ion Bombarded GaAs Surface ..... 130
4.4.1 GaAs(110) and Si(111) Surfaces ..... 136
4.4.2 Chemisorption of $O_2$ and O Atoms to GaAs(110) and Si(111) ..... 136
4.4.3 A Possible Surface Model for Ion Bombarded GaAs ..... 141
4.4.4 Possible Reaction Pathways for $O_2$ and NO ..... 143
4.5 Composition of Oxide Layers ..... 145

Chapter V: Summary ..... 150

Literature Cited ..... 154

Vita ..... 164

# List of Illustrations


Figure 2.1 The unit cube of the GaAs crystal lattice . . . . 4

Figure 2.2 Three basic crystal planes of the GaAs lattice . . . . 6

Figure 2.3 The partial energy band structures of GaAs and silicon . . . . 8

Figure 2.4 Drift velocity for GaAs and silicon . . . . 9

Figure 2.5 Energy states within the GaAs bandgap caused by impurity atoms or crystal defects . . . . 10

Figure 2.6 Schematic diagram of bulk growth of GaAs . . . . 12

Figure 2.7 Scheme of the main displacement processes that lead to surface damage . . . . 16

Figure 2.8 Mechanisms of energy dissipation for an incoming ion of mass $M_1$ and energy $E_0$ . . . . 17

Figure 2.9 Scheme of ion bombardment induced surface damage as a function of the total ion dose . . . . 22

Figure 3.1 Cutting and orientation of wafer for ion bombardment . . . . 39

Figure 3.2 Schematic of UHV reaction chamber . . . . 44

Figure 3.3 PHI model 10-360 hemispherical capacitor energy analyzer . . . . 47

Figure 3.4 Directional considerations in angular measurements . . . . 48

Figure 3.5 Substrate clamping arrangement during metal evaporation . . . . 53

Figure 3.6 Schematic diagram for a mounted diode . . . . 55

Figure 4.1 Representative spectra taken at 15° toa for chemically cleaned and $Ar^+$ ion-bombarded GaAs . . . . 59

Figure 4.2 XPS spectra for chemically cleaned and $Ar^+$ ion-bombarded GaAs exposed to $2x10^{11}$ L $O_2$ . . . . 61

Figure 4.3 XPS spectra for chemically cleaned and $Ar^+$ ion-bombarded GaAs exposed to $1x10^{13}$ L $O_2$ . . . . 62

Figure 4.4 Curve-resolved spectra for 3 KeV $Ar^+$ ion-bombarded GaAs exposed to $1x10^{13}$ L $O_2$ . . . . . . 64

Figure 4.5 Relative amounts of gallium and arsenic oxides for $O_2$ exposures at $2x10^{11}$ L and $1x10^{13}$ L . . . . . . 66

Figure 4.6 Curve-resolved spectra for 3 KeV $Ar^+$ ion-bombarded GaAs exposed to $2x10^{11}$, $1x10^{12}$, and $1x10^{13}$ L $O_2$ . . . . . . 71

Figure 4.7 XPS spectra for chemically cleaned and $Ar^+$ ion-bombarded GaAs exposed to $1x10^{10}$ L $H_2O$. . . . . . . 72

Figure 4.8 Curve-resolved spectra for 3 KeV $Ar^+$ ion-bombarded GaAs exposed to $10^{10}$, $10^{11}$, $10^{12}$, and $10^{13}$ L $H_2O$ . . . . . . 73

Figure 4.9 Relative amounts of GaO(OH) and $Ga(OH)_3$ for $H_2O$ exposure of $Ar^+$ ion-bombarded GaAs . . . . . . 76

Figure 4.10 Relative amounts of GaOOH and $Ga(OH)_3$ formed following $H_2O$ exposure for 3 KeV $Ar^+$ ion-bombarded GaAs . . . . . . 79

Figure 4.11 Ga/As atomic ratios as a function of take-off angle . . . . . . 84

Figure 4.12 Optical penetration depth for crystalline and amorphous GaAs . . . . . . 91

Figure 4.13 Reflectivity spectra obtained for crystalline, amorphous, and $Ar^+$ ion-bombarded GaAs . . . . . . 92

Figure 4.14 Reflectivity spectra obtained for crystalline, 3 KeV $Ne^+$, and $Xe^+$ ion-bombarded GaAs . . . . . . 95

Figure 4.15 Raman spectra obtained for crystalline, 3 KeV $^3He^+$, $Ne^+$, and $Xe^+$ ion-bombarded GaAs . . . . . . 96

Figure 4.16 Capacitance-Voltage characteristics for crystalline, 3 KeV $Ne^+$, $Ar^+$, and $Xe^+$ ion-bombarded GaAs . . . . . . 97

Figure 4.17 Schematic of a) depletion region under a metal contact on a semi-conductor and b) ion-bombarded . . . . . . 100

Figure 4.18 Atomic concentration of Xe and Ne found in GaAs following ion bombardment . . . . . . 106

Figure 4.19 XPS spectra for 3 KeV $^3He^+$ ion-bombarded GaAs exposed to $1x10^7$, $1x10^8$, and $2x10^{11}$ L $O_2$ . . . . . . 109

Figure 4.20 XPS spectra for 3 Kev $Ne^+$ ion-bombarded GaAs exposed to $1x10^7$, $1x10^8$, and $2x10^{11}$ L $O_2$ . . . . . . 110

Figure 4.21 XPS spectra for 3 KeV $Ar^+$ ion-bombarded GaAs exposed to $1x10^7$, $1x10^8$, and $2x10^{11}$ L $O_2$ . . . . . . 111

Figure 4.22 XPS spectra for 3 KeV $Xe^+$ ion-bombarded GaAs exposed to $1x10^7$, $1x10^8$, and $2x0^{11}$ L $O_2$ . . . 112

Figure 4.23 Relative amounts of gallium and arsenic oxides formed for 3 KeV $^3He^+$, $Ne^+$, $Ar^+$, and $Xe^+$ ion-bombarded GaAs after $O_2$ exposure . . . 113

Figure 4.24 GaAs(100) surface before and after ion bombardment. . . . 116

Figure 4.25 Relative amounts of gallium and arsenic oxides formed for 1 KeV $Ar^+$ and $Xe^+$ ion-bombarded GaAs exposed to $O_2$ . . . 117

Figure 4.26 Curve-resolved XPS spectra for 3 KeV $Xe^+$ and $Ar^+$ ion-bombarded GaAs exposed to $10^{13}$ L $H_2O$ . . . 119

Figure 4.27 XPS spectra for 3 KeV $Xe^+$ and $Ne^+$ exposed to NO $3x10^6$, $1x10^7$, and $1x10^8$ L NO . . . 122

Figure 4.28 Curve-resolved XPS spectra for 3 KeV $Xe^+$ and $Ne^+$ exposed to $10^8$ L NO . . . 123

Figure 4.29 Relative amounts of oxide produced for 3 KeV Xe+ and and $Ne^+$ as a function of NO exposure . . . 124

Figure 4.30 Spectra for 3 KeV $Xe^+$ ion-bombarded GaAs exposed to contaminated NO . . . 127

Figure 4.31 Curve-resolved O 1s spectra for contaminated NO exposure . . . 128

Figure 4.32 XPS spectra taken at 15° for 3 KeV $Xe^+$ and $Ne^+$ ion-bombarded GaAs following $1x10^7$, $1x10^8$, and $2x10^{11}$ L $N_2O$ exposures . . . 129

Figure 4.33 Relative amounts of oxide formed as a function fo $N_2O$ exposure for 3 KeV $Xe^+$ and $Ne^+$ ion-bombarded GaAs . . . 131

Figure 4.34 Bonding schemes for GaAs(110) and Si(111) . . . 137

Figure 4.35 Curve-resolved XPS spectra at various take-off angles for 3 KeV $Ar^+$ ion-bombarded GaAs exposed to $10^{13}$ L $O_2$ . . . 146

Figure 4.36 Curve-resolved XPS spectra at various take-off angles for 3 KeV $Xe^+$ ion-bombarded GaAs exposed to $10^{13}$ L $H_2O$ . . . 147

Figure 4.37 Relative amounts of oxide formed for (a) 3 KeV $Ar^+$ ion-bombarded GaAs exposed to $10^{13}$ L $O_2$ and (b) 3 KeV $Xe^+$ ion-bombarded GaAs exposed to $10^{13}$ L $H_2O$ as a function of take-off angle . . . 148

# List of Tables


Table 2.1 Room temperature (300 K) properties of GaAs . . . . . . . . . . . . . . . . . . . 5

Table 2.2a XPS shifts for oxides on GaAs relative to Ga and As of GaAs . . . . . . . 29

Table 2.2b Reference core shifts . . . . . . . . . . . . . . . . . . . . . . . . . . . . . . . . . . . . . . 29

Table 3.1 XPS sensitivity factors . . . . . . . . . . . . . . . . . . . . . . . . . . . . . . . . . . . . 50

Table 4.1 XPS results for chemically cleaned and $Ar^+$ ion-bombarded GaAs . . . . 58

Table 4.2 Binding energies for surface components . . . . . . . . . . . . . . . . . . . . . 65

Table 4.3 Atomic concentration of oxygen for 3 KeV $Ar^+$ ion-bombarded GaAs exposed to $H_2O$ . . . . . . . . . . . . . . . . . . . . . . . . . . . . . . . . . . . . 78

Table 4.4 Atomic radii and projected ranges for primary ions . . . . . . . . . . . . . . . 81

Table 4.5 Ga/As atomic ratios for GaAs bombarded with various ions . . . . . . . . . 83

Table 4.6 $T_{max}$ values . . . . . . . . . . . . . . . . . . . . . . . . . . . . . . . . . . . . . . . . . 85

Table 4.7 Heats of sublimation . . . . . . . . . . . . . . . . . . . . . . . . . . . . . . . . . . . . . 87

Table 4.8 Damage depths obtained from reflectivity and Raman measurements for $Ar^+$ ion-bombarded GaAs . . . . . . . . . . . . . . . . . . . . . . . . . . . . . . . 94

Table 4.9 Energy differences $\Delta E$ between Ga 3d and As 3d photopeaks for various bonding states . . . . . . . . . . . . . . . . . . . . . . . . . . . . . . . . . . 103

Table 4.10 3 KeV $Xe^+$ and $Ar^+$ ion-bombarded GaAs exposed to $10^{13}$ L $H_2O$ . . . 120

# Chapter I: Introduction

It was once said within the semiconductor community that "gallium arsenide is the material of the future, and it always will be [1]." Since its creation by Goldschmidt [2] in the 1920s and the first publication on the electronic properties of III-V compounds in 1952 [3], scientists in universities and industries have struggled for more than thirty years to understand gallium arsenide (GaAs) and to produce practical processes and devices that offer high performance and reliability [1]. Now, the above statement is no longer true. GaAs is currently the leading member of the III-V compound family from a commercial standpoint [4] as is evidenced by the large number of semiconductor companies that are now establishing prototype or full-scale GaAs production facilities, such as the newly established facility to produce MMIC (microwave monolithic integrated circuits) devices by ITT in Roanoke, Virginia.

The interest in GaAs is driven by several factors. One such factor is in the problems that have been introduced for silicon based technology by the need to reduce the size of devices required for both large scale integration and high speed, low power devices. Silicon based devices have encountered atomic limitations. As a semiconductor, GaAs has two basic advantages over silicon. It has a direct band gap which allows opto-electronic devices such as junction lasers and LEDs to be fabricated on the same substrate as other electronic circuitry. It also has a higher carrier mobility than silicon both at low and high field conditions. This characteristic allows higher frequency or faster operation of semiconductor devices that is not possible with silicon; GaAs can operate at microwave frequencies where silicon devices are unable to function [5]. The ability to operate at microwave frequencies has made its development of great interest to the military.

GaAs will not replace silicon, but serves to fill in the gaps in the industry that silicon based technology is not able to handle. One reason GaAs cannot replace silicon is that

there is no stable native oxide that can "passivate" the surface in the manner that $SiO_2$ does for silicon. This means that there are no GaAs analogs to the metal-oxide semiconductor (MOS) devices that are a foundation of silicon device technology [6].

There are many aspects involved in device fabrication from the cleaning and preparation of materials to the making of the actual devices. Among the many methods are wet chemical etching; photolithography; electron beam, ion beam, and x-ray lithography; plasma enhanced deposition; and dry etching techniques (plasma assisted etching, reactive ion etching, reactive ion beam etching, and ion milling). All of these techniques involve a great deal of chemistry and altering of materials' surfaces. With the size of devices becoming increasingly smaller, one must be concerned with the chemical nature of the surface and the interface with the materials used for making devices during and after processing by any of the above techniques. The surface chemistry resulting from these treatment steps has a strong influence on subsequent device performance.

One example is the use of ion bombardment to produce clean surfaces for device manufacturing [7] and to etch submicrometer structures in GaAs. Since this process involves bombardment of the substrate with energetic particles, devices can suffer radiation damage. Ion bombardment produces an amorphous layer at the surface containing defects and implanted ions all of which cause degradation of devices [7-10] and chemical changes in the surface structure [11-13] which affect the surface reactivity [14].

The purpose of this research is to investigate the effects of ion bombardment on the chemical reactivity of GaAs and to determine how these changes may affect device performance. It is therefore of interest to investigate how the changes in the chemical reactivity of GaAs induced by ion bombardment could be used for the selective control of chemical reactions at the surface perhaps to control the properties of GaAs devices [15].

# Chapter II: Literature Review

## 2.1 Gallium Arsenide

### *2.1.1 Physical and Electrical Characteristics*

GaAs is a III-V compound semiconductor having the zinc blende crystal structure which consists of two interpenetrating face-centered cubic lattices that are offset with respect to each other by half the diagonal of the fcc cube. The distance between the nearest neighbors is 2.44Å - equal to the sum of the atomic radii of As(1.18Å) and Ga(1.26Å). The unit cube of the GaAs crystal lattice is shown in Figure 2.1 and a number of the room temperature (300 K) GaAs properties are listed in Table 2.1. The bonding in GaAs is a mixed ionic/covalent type due to the shift of valence charge from gallium to arsenic atoms increasing the bond strength compared to the covalent bond in germanium and silicon. The valence electron configurations of the atoms Ga and As are $4s^2 4p^1$ and $4s^2 4p^3$, respectively. The structure of GaAs utilizes $sp^3$ covalent bonding where each atom of one kind is surrounded tetrahedrally by the atoms of the other kind. There is an admixture of ionic and covalent bonding with the covalency being 0.63 [18,19].

Three basic crystal planes of the GaAs lattices are shown in Figure 2.2. Each As atom on the (100) surface has two bonds with Ga atoms from the layer below and two other bonds are free. The (110) plane has the same number of Ga and As atoms. Each atom has one bond with the layer below. GaAs crystals are easily cleaved along the (110) planes. Atoms on the (111) surface have three bonds with the Ga atoms from the layer below and the fourth bond is free [20].

There are two main advantages for GaAs over silicon. One is its ability to operate at higher frequencies and the other is its direct band gap. The partial band structures

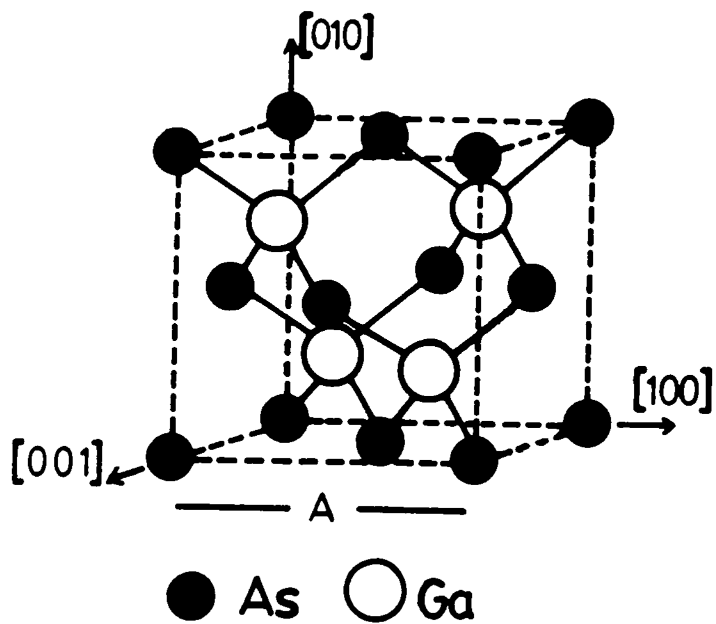


**Figure 2.1** The unit cube of the GaAs crystal lattice [16].

**Table 2.1** Room temperature (300 K) properties of GaAs [17].

| Property | Value |
|---|---|
| Lattice constant | 5.65 Å |
| Density | 5.317 $g/cm^3$ |
| Atomic density | $4.4279 \times 10^{22}$ $atoms/cm^3$ |
| Molecular weight | 144.642 |
| Bulk modulus | $7.55 \times 10^{11}$ $dyn/cm^2$ |
| Sheer modulus | $3.26 \times 10^{11}$ $dyn/cm^2$ |
| Linear expansion coefficient | $5.73 \times 10^{-6}$ $K^{-1}$ |
| Specific heat | 0.327 J/g-K |
| Lattice thermal conductivity | 0.55 W/cm-K |
| Dielectric constant | 12.85 |
| Bandgap | 1.423 eV |
| Threshold field | 3.3 KV/cm |
| Peak drift velocity | $2.1 \times 10^7$ cm/s |
| Electron mobility (undoped) | 8500 $cm^2/V$-s |
| Hole mobility (undoped) | 400 $cm^2/V$-s |
| Melting point | 1238 °C |

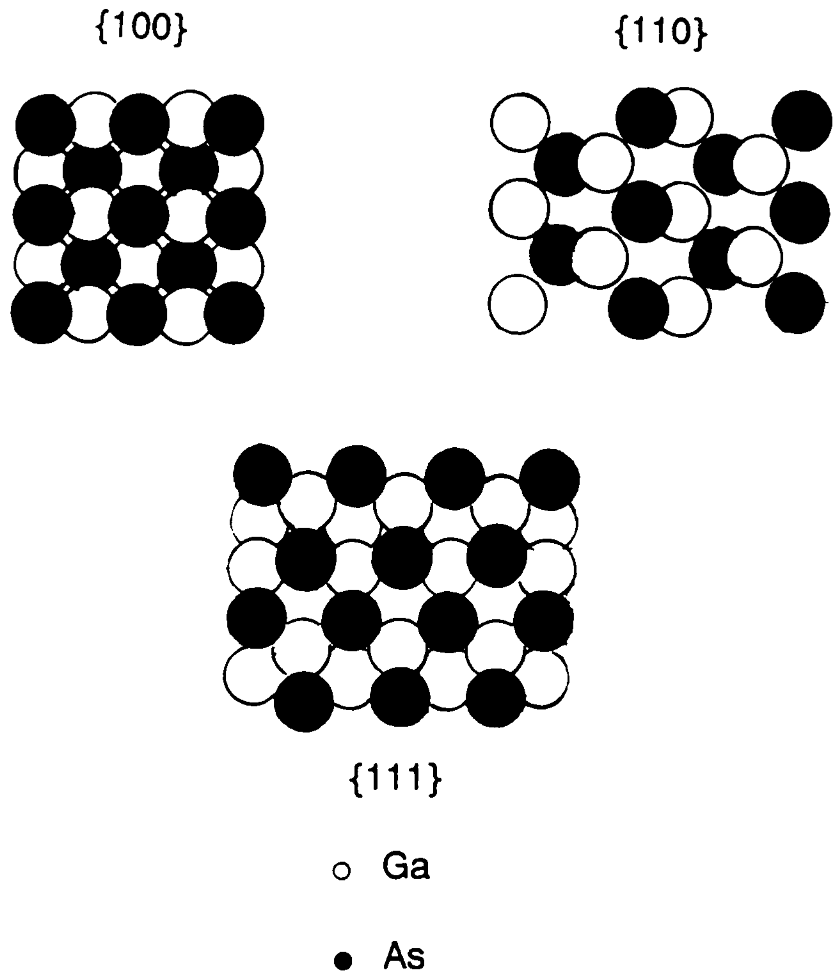


**Figure 2.2** Three basic crystal planes of the GaAs lattice [20].

showing the uppermost valence band and lower conduction band along two principal directions in the crystals are shown in Figure 2.3. GaAs is a direct band gap semiconductor because the minimum of the conduction band is directly over the maximum of the valence band. Therefore, electrons can make the transition between bands simply by emitting or absorbing a photon without a change in momentum. This makes GaAs ideal for making optical devices such as lasers and LEDs.

The drift velocity of electrons in GaAs and silicon is shown in Figure 2.4, which illustrates the speed advantage of GaAs over silicon. Subjecting a carrier (electrons or holes) to an electric field causes the carrier to achieve a velocity that is a function of the electric field. The increase in speed is a function of many factors including temperature and impurity concentrations, but from Figure 2.4 it can be seen that the drift velocity for GaAs is greater than that for silicon. This means that electrons can travel faster in GaAs than in silicon and devices can operate at higher frequencies [21].

The energy band diagram of GaAs shown in Figure 2.3 was for a pure semiconductor. No semiconductor is without crystal or surface defects, or dopant atoms, whose presence changes the energy band structure causing other energy levels to appear within the bandgap (Figure 2.5). Most doping is done intentionally and in controlled amounts for the purpose of increasing either the electron or hole concentration. Impurity atoms that increase the electron concentration are donors or n-type dopants. Si is a typical n-type dopant for GaAs with Si occupying a Ga site in the lattice. Introducing extra electrons creates extra energy levels that are near the conduction band. The electrons have enough thermal energy to jump into the conduction band thus increasing the conductivity of the semi-conductor.

The principal deep electron trap (EL2) in GaAs is located 0.76 eV below the conduction band. It is said to be related to the presence of an As atom on a Ga lattice site (the antisite defect $As_{Ga}$) and is called a deep electron trap because it can trap electrons far

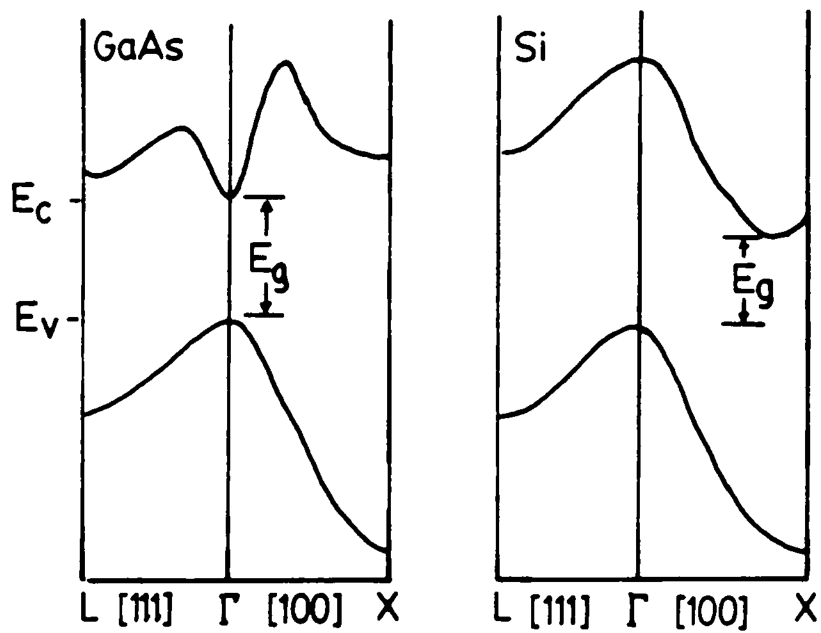


**Figure 2.3** The partial energy band structures of GaAs and silicon [22,23].

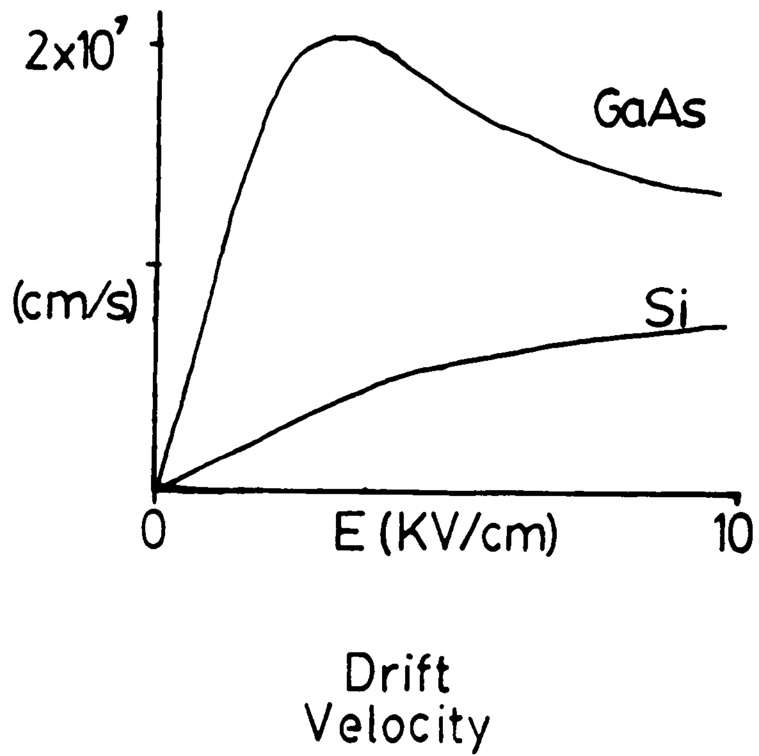


**Figure 2.4** Drift velocity for GaAs and silicon [21,49].

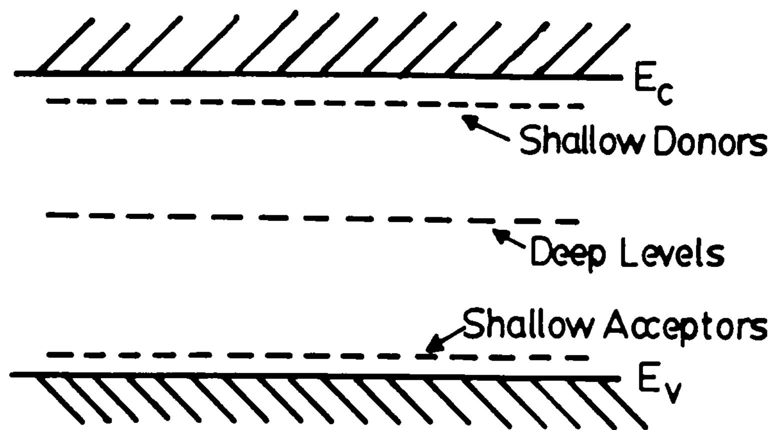


**Figure 2.5** Energy states within the GaAs bandgap caused by impurity atoms or crystal defects [24].

from the conduction band edge.

### *2.1.2 Growth of Bulk GaAs*

Bulk GaAs is grown in crystal ingots, called boules, and oriented single-crystal wafers are cut and polished from the ingot. The two principal methods for growing GaAs single crystal material are the horizontal Bridgman (HB) and liquid encapsulated Czochralski (LEC) techniques [25]. Other technologies have been developed for the formation of active device layers on single crystal substrates. These techniques utilize molecular beam epitaxy(MBE) and metal-organic chemical vapor deposition(MOCVD) in which the substrate, usually LEC grown material, is used to minimize the possibility of impurity outdiffusion into epitaxial regions [20]. Because of its use as a substrate material for epitaxial processing and its successful use in ion implantation device fabrication, LEC grown GaAs has gained in popularity. The HB technique is used when highly conducting n-type material is needed [27]. This section will discuss the two methods of bulk GaAs growth and briefly discuss MBE and MOCVD techniques.

#### 2.1.2.1 Horizontal Bridgman (HB)

In the horizontal Bridgman growth technique, either gallium or polycrystalline GaAs are placed in a boat, a GaAs seed crystal is placed at one end and elemental arsenic is placed at the other end of a sealed quartz ampoule backfilled with an inert gas (Figure 2.6a). The tube is placed in a resistance-heated multizone furnace where a temperature profile is generated so that arsenic is evaporated (600-625 °C), the seed crystal temperature is just below the melting point of GaAs and the melt material is at or above the melting point of GaAs (>1240 °C). The As reacts with Ga to produce GaAs and the temperature front is moved along the length of the boat with crystal growth following the temperature front. Since this method involves growth in a quartz boat, chemical contamination from the boat

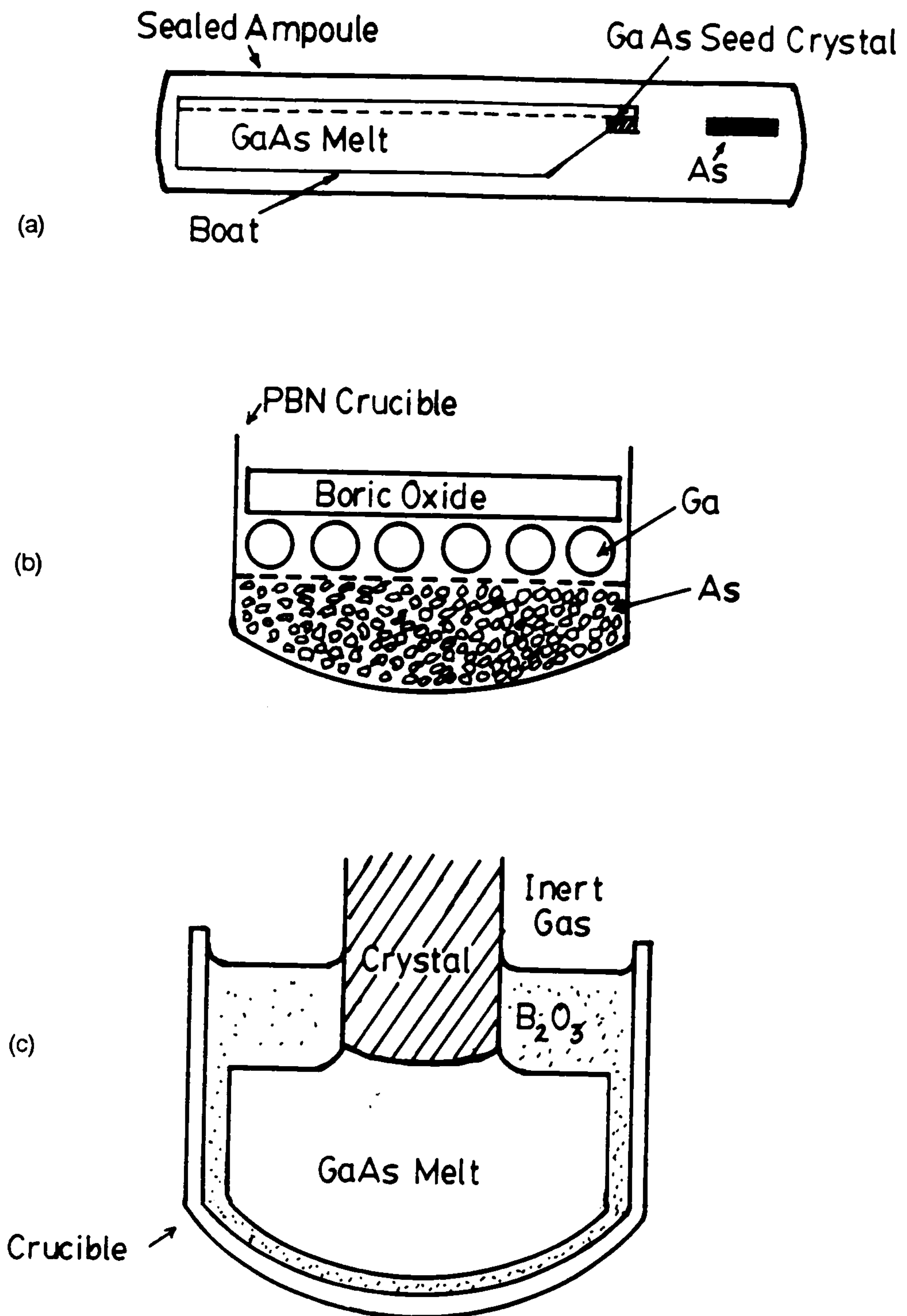


**Figure 2.6** Schematic diagram of bulk growth of GaAs.
(a). Horizontal Bridgman (HB) growth system [25].
(b). Liquid encapsulated Czochralski (LEC) growth before heating [26].
(c). LEC growth system during GaAs crystal growth [26].

can cause problems [4]. Crystal growth is usually in the <111> direction and resulting slices sawed perpendicular to its axis are (111) material and usually are D-shaped due to the configuration of the boat. Round boules can be obtained by growth in a verticle crucible. However, GaAs(100) material is usually desired for epitaxial growth and is obtained by sawing at an angle of 54.7° with respect to the axis of the ingot.

#### 2.1.2.2 Liquid Encapsulated Czochralski (LEC)

The LEC method was first applied to III-V materials by Mullin *et al.* [28,29]. Crystals of GaAs are grown by vertically pulling an ingot from a melt. This technique utilizes crystal growth machines called pullers. Two types of pullers and processes are used for LEC growth: low pressure, operated at about 1 atmosphere and high pressure, operated at up to 50 atmospheres.

The process begins by combining elemental Ga (top layer) and As in a high-purity pyrolytic boron nitride crucible (PBN) and topping with a layer of boric oxide ($B_2O_3$) (Figure 2.6b). The crucible is heated under an initial argon chamber pressure of 600 psi. The Ga melts first (mp≈30 °C) and covers the As, then the $B_2O_3$ melts (450-500 °C) and flows around the Ga and As melt, shielding the melt from crucible contamination. The melt temperature is maintained at about 800 °C where the formation of GaAs occurs rapidly. High argon overpressures are used, which combined with the presence of $B_2O_3$, prevent any significant loss of As via evaporation.

Crystal growth is initiated by the contact of a seed crystal with the melt through the boric oxide layer. The crystal is slowly pulled from the melt (Figure 2.6c) forming a neck with a diameter smaller than the seed crystal. The crystal diameter is then allowed to increase to the desired diameter and this dimension is maintained throughout the pulling process. LEC crystal growth is generally in the <100> direction so that GaAs(100) material is obtained when the ingot is sliced [26].

#### 2.1.2.3 Epitaxial Growth Techniques

Epitaxial growth techniques allow the production of material of the highest purity. These techniques allow defects and impurity concentrations to be controlled below $10^{15}$ $cm^{-3}$, which cannot be achieved by ingot growth [27]. Liquid phase epitaxy (LPE) was the first of these techniques used to grow epitaxial layers on GaAs crystals, but MBE and MOCVD processes are becoming the attractive techniques for producing very thin layers (<100 Å by MOCVD) and superior control of doping levels (control of monolayers by MBE).

MOCVD involves the pyrolysis of a vapor phase mixture of arsine and trimethyl- or triethyl gallium; whereby free Ga and $As_4$ molecules are formed and recombine on a hot substrate surface to form GaAs. MBE involves the growth of elemental, compound, and alloy semiconductor films from the impingement of molecular beams onto a heated crystalline substrate under UHV conditions [25,30]. In both techniques the concentrations of gallium and arsenic vapor species are the parameters which control the growth rate, stoichiometry, and impurity concentrations. Another advantage of these techniques is that electronic materials can be produced at relatively low temperatures (900 - 1000 K). Their major advantage is in the control of material production and potential for variety that can be introduced at the atomic level, especially for MBE grown material.

## 2.2 Ion Bombardment

Ion bombardment induced surface damage was first linked to changes in chemical reactivity by Sherburne and Farnsworth [31]. They reported that the catalytic yield of some reactions increased with ion bombardment of the substrate. Since then, increased surface reactivity following ion bombardment has been reported in the literature [14,32,33]. Farnsworth and Woodcock [34] reported almost a ten-fold increase in the catalytic activity of

Ni after argon ion bombardment. The effects have been explained by the removal of surface impurities, such as oxides, and the creation of new adsorption sites.

Defects on the surface, whether induced by ion bombardment or by other means (cleavage steps, etc.), play an important role in the oxidation process of GaAs by providing initial adsorption sites and assisting in the dissociation of $O_2$ molecules [14,35-41]. Surfaces with high defect densities adsorb oxygen faster than ones with a low density [36,40,42,43]. GaAs surfaces containing defects specifically caused by ion bombardment exhibit a different reactivity towards oxygen than cleaved GaAs [14,40,43]. Ion bombardment used for surface cleaning [7], or in the reactive ion process, induces changes in break down voltages, barrier heights, trapping levels and the optical properties of GaAs [8,44-48]. Ion bombardment also produces changes in the surface structure so that the chemical surface reactivity is altered [14]; preferential sputtering of As leads to changes in the chemical composition of the surface; and the extent of change is related to ion energy [11-13,50,51].

Modification of surfaces by ion bombardment can produce many different results from the microscopic to the macroscopic (results visible to the naked eye). The results depend upon the substrate that is bombarded, the identity of the bombarding ion, ion energy, and bombardment time period.

Energetic ions that impinge upon a surface can set many different processes into motion. Figures 2.7 and 2.8 illustrate some of the processes that can occur when a particle of energy $E_o$ strikes a surface. The mechanism for these processes is considered to be a hard-sphere mechanism as described by Carter and Colligon [52]. An initial amount of energy $E_\epsilon$ is lost by the primary ion through electronic excitations when it first collides with the surface. The other energy losses are due to collisions with the atoms in the matrix. These collisions continue through a cascade process, whereby all of the collisions are considered to be isolated two body collisions (elastic collisions [54]), in which, after displacement, each of the displaced atoms is available to make further collisions in a

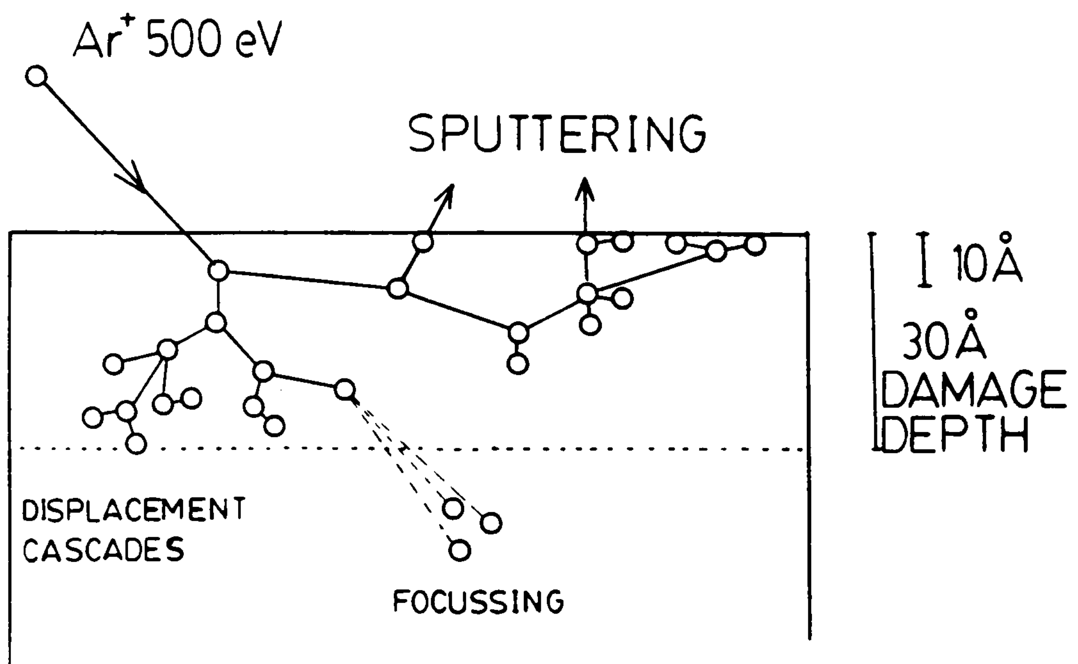


**Figure 2.7** Scheme of the main displacement processes that lead to surface damage [59].

## COLLISION CASCADE

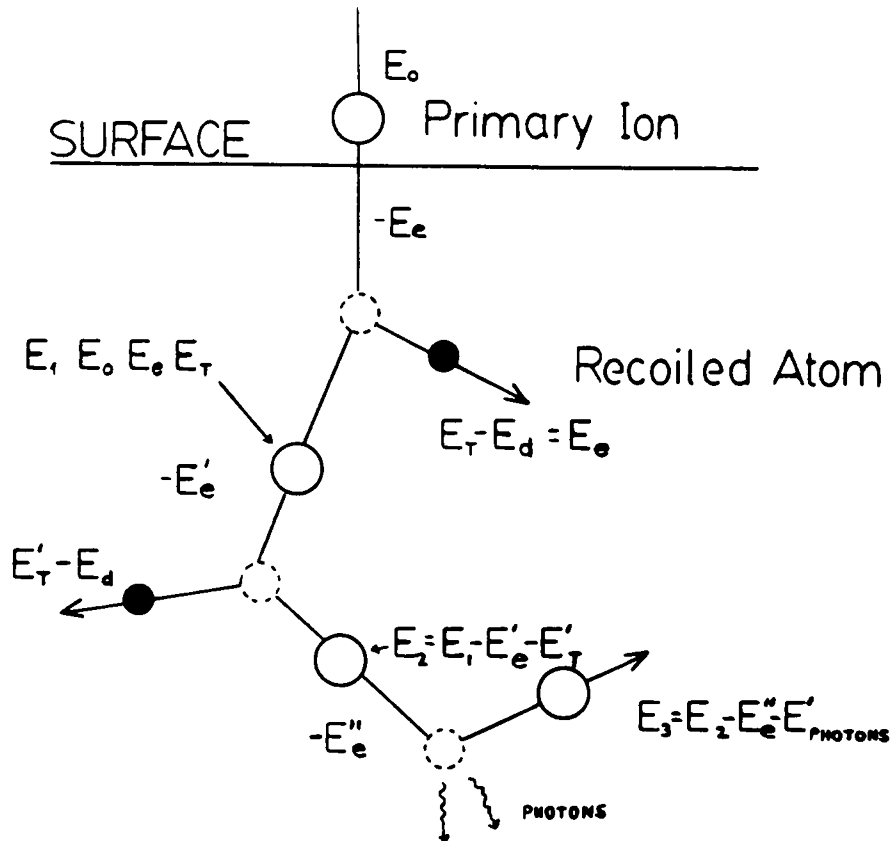


$E_o$ = Kinetic energy of incoming ion (1 KeV)

$E_e$ = Energy dissipated through electron excitation

$E_T$ = Transferred energy (nuclear stopping)

$E_d$ = Displacement energy (25 eV)

$$E_T = \frac{4\,M_1 M_2}{(M_1 + M_2)^2} \quad E_o \sin^2 \theta/2$$

**Figure 2.8** Mechanisms of energy dissipation for an incoming ion of mass $M_1$ and energy $E_o$ [59].

cascade-like process [52].

Since the conservation laws of energy and momentum limit the energy transfer between two atoms in an elastic collision, the maximum amount of energy, $T_{max}$, that can be transferred from the primary ion to another atom at rest in the target is [55]

$$T_{max} = \gamma E_o = \frac{4 M_1 M_2}{(M_1 + M_2)^2} E_o \tag{2.1}$$

where $\gamma$ is the maximum energy transfer factor, $M_1$ and $M_2$ are the respective atomic masses, and $E_o$ is the energy of the primary ion.

If the primary ion has an energy less than 1 KeV, the penetration depth is relatively small, ranging from 10 to 20 Å. However, because of the cascade process, the displaced atoms cause damage much deeper into the surface, ranging from 30 to 100 Å. Other processes such as focussing or channeling can also cause damage deeper into the surface. When the energy of the original ion is dissipated throughout the lattice of the material, the collision cascade comes to an end.

During ion bombardment, processes occur that induce surface and lattice changes in the material. The amount of damage induced depends upon the total ion dose (ions/cm$^2$). One of these processes, known as sputtering, is the ejection of surface ions and neutrals into the surrounding vacuum and is caused by sufficient energy being transferred to a surface atom to overcome its binding energy [53,54]. There are two types of sputtering that can occur: physical and chemical sputtering [55]. Physical sputtering involves the transfer of kinetic energy from the incident ion to the target atoms and subsequent ejection through the target surface of those atoms which have acquired enough kinetic energy to overcome the binding forces exerted by the target. Chemical sputtering involves a chemical reaction induced by the primary particle which produces an unstable compound at the surface.

Physical sputtering effects occur at incident-particle energies ranging from the medium to upper eV region into the MeV region, but tend to be weaker in the lower eV region compared to chemical sputtering effects which may persist down to much smaller energies. Chemical sputtering usually occurs by bombardment of targets with reactive-gas ions such as hydrogen, oxygen, or nitrogen. Bombardment with these ions can lead to the formation of volatile chemical compounds which may be released from the surface and contribute to surface erosion [54]. The main concern in this thesis is with physical sputtering.

Sputtering yields are affected by the masses of the primary ion and the target, the angle of incidence, and the efficiency of momentum transfer. Sigmund [56] derived the following equation expressing the sputtering yield as a function of ion energy for orthogonal incidence:

$$S(E_i) = \frac{0.42}{U} \alpha(M_t/M_i)\, \sigma_n(E_i,Z_i,Z_t) \tag{2.2}$$

where $E_i$, $M_i$ and $Z_i$ are the energy, mass, and charge of the primary ion, respectively, and $M_t$ and $Z_t$ are the mass and charge of the target, respectively. The factor $\alpha(M_t/M_i)$ describes the efficiency of the momentum transfer upon elastic collisions, $\sigma_n$ is the nuclear stopping cross section for atom-atom collisions and is evaluated assuming Thomas-Fermi interactions. For elemental targets, the heat of sublimation is used for the binding energy, U.

Surface orientation and the angle of ion incidence also play a role in determining the sputter yield, with the sputtering yield increasing for greater angles of incidence (with respect to the surface normal). The maximum in the sputtering yield typically occurs at an angle $\delta$ of 50 to 80° [53], where $\delta$ is the angle of incidence with respect to the surface normal. The angular dependence of the sputtering yield can be approximated from

Sigmund's theory as

$$\frac{S(E_i,\delta)}{S(E_i,0)} = (\cos\delta)^{-f} \quad (2.3)$$

where f depends on the ratio of $M_t/M_i$ and varies from $\approx$5/3 for $M_t/M_i<3$ to 1 for $M_t/M_i \geq 7$ [54,56].

The displacement of atoms from their original positions in the lattice which causes lattice defects is another process resulting from ion bombardment. The average number of displaced atoms, $n_d$, is given by the equation

$$n_d = E_i/2E_d \quad (2.4)$$

where $E_i$ is the energy of the incident ion and $E_d$ is the displacement energy [52].

Most of what has been discussed up to now involves ion bombardment of an elemental target. A phenomenon that occurs when sputtering multicomponent systems is that of preferential sputtering where the sputtering of one component is more rapid than that of the other component and the surface layer develops a composition that is different from the bulk. Kelly [57] has summarized the understanding of the sputtering of multicomponent systems. In general, the most common result is that the target usually develops a layer that is rich in the heavier component, because the lighter component is sputtered away. By examining the maximum energy transfer factor, $\gamma$, in equation 2.1, it can be predicted that the lighter atom in the target acquires a larger portion of the energy dissipated by the primary ion [58] and will therefore be preferentially sputtered. This is a very important fact that must be observed in the area of surface analysis since preferential sputtering can cause problems in depth profiling and quantitative analysis.

Another phenomenon known as a thermal spike occurs in the bulk [54]. It is caused by a recoiled atom that does not have enough energy to cause any more displacements.

However, it may carry enough energy to raise the temperature of the surrounding atoms above the melting point of the solid as it transfers the remaining energy to the lattice. This increase in temperature of such a small volume can greatly accelerate defect production such as defect migration, amorphization, or disordering.

A process that occurs during bombardment that does not induce surface damage is photon production. A photon is produced when a particle does not contain enough energy to cause a displacement. The energy is transferred to the target atom and is dissipated as a photon.

The processes described above can cause many types of surface changes ranging from those on the atomic scale to those on a macroscopic scale. These changes depend on the total ion dose received by the material. Figure 2.9 lists most of the surface changes induced by ion bombardment as a function of total ion dose. Some of these defects will be discussed in more detail in the following paragraphs.

Low ion doses ($10^{11}$-$10^{15}$ ion/cm$^2$) produce indirectly detectable surface damage as illustrated in Figure 2.9(a-d). As atoms are ejected from their normal lattice positions, the surface changes result in point defects and small clusters of point defects. These defects sometimes appear as amorphization of the surface [60]. As the ion dose is increased in this range, random steps may form and even some facetting may occur. Heavier doses produce dislocation half-loops that are caused by the collapse of discs of vacancies.

In the dose range of $10^{15}$-$10^{17}$ ions/cm$^2$, surface damage becomes visible. Large clusters of defects form, dislocation loops become aligned and grow and microfacetting becomes visible by microscopic techniques such as SEM. Ion bombardment can cause the crystalline state to become amorphous and the surface can develop a bumpy appearance. However, in the case of argon ion bombarded GaAs, no topography develops even with doses $>10^{17}$ ions/cm$^2$, in contrast to similar sputtering of metal targets where conical protrusion always occurs [61].

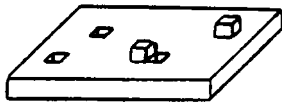

(A) Point defects (vacancies, adatoms)

$n_d = 10^{13}$-$10^{14}$ cm$^{-2}$

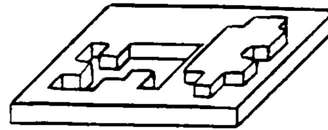

(B) Clusters of point defects

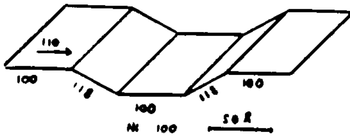

(C) Random steps → Facetting

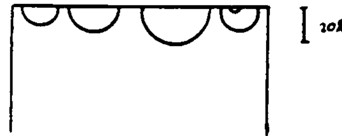

(D) Dislocation half loops

$n_d = 10^{8}$-$10^{12}$ cm$^{-2}$

ION BOMBARDMENT INDUCED SURFACE DAMAGE

| | ON ATOMIC SCALE | ON MICROSCOPIC SCALE | ON MACROCOPIC SCALE |
|---|---|---|---|
| TOTAL ION DOSE | $10^{11}$ .................. $10^{15}$ | ..................... $10^{17}$ | ............... $10^{19}$ ions/cm$^2$ |
| | INDIRECT DETECTABLE DAMAGE | VISIBLE DAMAGE | DEVELOPED SURFACE STRUCTURE |
| | Individual defects, cluster, planer faults, amorphization | Large clusters, tangling of dislocations, dislocation loops alignment, micro-facetting, crystallization, and amorphization | Ion etching, facets, terraces, steps, grooves, furrows, selective sputtering, equilibrium state, and blistering |

**Figure 2.9** Scheme of ion bombardment induced surface damage as a function of the total ion dose (A to D increasing ion doses) [59,60].

At higher doses ($>10^{17}$ ions/cm$^2$), ion erosion becomes so effective that topographical features begin to develop and can be visible even to the naked eye. Such features include facets, terraces, blisters from release of trapped gases, cones and pyramids. The type of topography that develops depends on the condition of the starting material. Material purity and surface structure can dictate the topography that develops. Cones and pyramids usually develop on surfaces from preferential sputtering. If the surface contains impurities or oxides, then certain areas will erode more easily than others thus developing cone-like structures on the surface; the cones being the material more resistant towards sputtering.

The bombarding ions can also become trapped or incorporated into the surface layer as has been reported by many investigators [53,62-64]. The probability is dependent upon temperature and angle of incidence and on the energy of the primary ion. The probability of an incident ion becoming trapped in the target lattice increases with increasing impingement energy and decreasing ion mass. The maximum concentration of trapped ions is inversely proportional to the target sputtering yield and at high doses $\sim 10^{14}$ to $10^{15}$ ions/cm$^2$ the available traps are saturated and a steady state is reached between trapping and reemission processes [53,62].

## 2.3 Chemical Reactivity of GaAs

The purpose of this research is to examine the effects of ion bombardment on the chemical reactivity of GaAs. Therefore, it would be important first to understand and to examine what chemical studies have been completed on clean, cleaved GaAs surfaces and on GaAs containing defects. This section will be divided into a discussion of the oxidation of GaAs and the reactivity with other species such as $H_2$ and fluorocarbons.

### *2.3.1 Oxidation Studies of GaAs*

The construction of metal-oxide semiconductor (MOS) devices requires the growth of a suitable dielectric material on the semiconductor substrate. For this purpose, the oxide layer must be isolating, chemically stable, and the interface between the oxide and the semiconductor bulk should contain a small number of interface states [5,65]. The growth of native oxides on silicon has been very successful, but it is more difficult for GaAs. The compound nature of GaAs gives rise to a different surface chemistry for each constituent and the oxides have low decomposition temperatures (600-800 °C). It is for these reasons that the oxidation of GaAs has been the focus of considerable effort over the years. The oxidation of GaAs has included reactions with $O_2$ [14,35-39,41,65-105], excited $O_2$ [77,101,106], air [101,107,108], $H_2O$ [79,80,101,109-113], $N_2O$ [114,115], and NO [116-119]. Most of these studies have dealt with the oxidation of the GaAs(110) surface. The oxidation has been studied by many methods including, Auger electron spectroscopy (AES), X-ray photoelectron spectroscopy (XPS), ultraviolet photoelectron spectroscopy (UPS), low energy electron diffraction (LEED), electron energy loss spectroscopy (ELS), reflection high energy electron diffraction (RHEED), high resolution electron energy loss spectroscopy (HREELS), extended x-ray absorption fine structure (EXAFS), thermal desorption spectroscopy (TDS), ion scattering spectroscopy (ISS), and secondary ion mass spectroscopy (SIMS), all in an effort to determine the actual mechanism of adsorption, the chemical composition of the oxides formed, the local atomic structure of the oxides, and the relationship between the chemical composition and local atomic structure of the oxides. Despite the numerous studies, there has not been any direct and conclusive evidence in support of a particular oxidation mechanism [97]. Explanations of the data advanced by the numerous investigators will be considered in chronological order to examine how the understanding of surface oxidation has progressed.

### *2.3.2 $O_2$ Adsorption Studies*

Some of the earliest investigations of the adsorption of oxygen on GaAs were completed by Rosenberg and co-workers [120,121] for vacuum-crushed samples. They found that two adsorption processes occurred: a fast chemisorption and a reversible physical adsorption. Oxygen adsorption on argon bombarded and annealed polar surfaces of GaAs was studied by Arthur [122]. Differences in the reactivity were noted for the two surfaces and the adsorption was shown to have a very small activation energy. The chemisorption process was studied volumetrically and by ellipsometry [123,124]. It was determined that the absolute saturation coverage was about 60% of an oxygen monolayer (a monolayer is two oxygen atoms for every surface molecule of GaAs). This was in close agreement with the results obtained by Dorn *et al.* [88], which led to the development of two bonding models that were consistent with their data. One model involves an $H_2O$-like bond of one oxygen atom, bonding to two nearest neighbors of different atoms. The other model involves a peroxide bridge configuration in which an $O_2$ molecule is bonded with two next nearest atoms of the same kind.

It was clear from these early studies that information was needed on the binding site of oxygen on GaAs to help clarify some aspects of the various GaAs surface-state models. Froitzheim and Ibach [125], Gregory *et al.* [126], and Dorn *et al.* [88] suggested that oxygen preferentially binds to surface arsenic atoms. However, Ludeke and Koma [100] and Arthur [122] implied that oxygen bonds to surface gallium atoms. Pianetta *et al.* [92] attempted to clarify these disagreements by studying the oxidation of GaAs(110) using x-ray photoemission spectroscopy and examining the shifts in the As and Ga 3d core levels as a function of oxygen exposure in the range $10^4$ to $10^{13}$ L ($1L=1.3x10^{-4}$ Pa•sec). They observed large chemical shifts in the As 3d levels while the Ga 3d levels were shifted by less than 1 eV. They concluded that oxygen bonded directly to As at the surface, supporting the results of Dorn *et al.*, Froitzheim and Ibach, and Gregory *et al.*

However, Ludeke [86,90] disagreed with the results of Pianetta *et al.* [92] and argued that Ga surface atoms were involved in the oxidation process. This sparked a disagreement between the two groups, with each one qualifying their conclusions based on their own data [83]. Since then, theories and conclusions based on experimental results have not totally agreed on a specific bonding site for oxygen in the initial steps of the oxidation process. Theoretical calculations of Barton *et al.* [41] suggest that an oxygen atom initially chemisorbs to an As surface atom, which is in agreement with the results presented above and other studies [72,79,91,97]. However, Chye *et al.* [14] and Brundle and Seybold [36] conclude that oxygen bonds to both surface As and Ga atoms, because of chemical shifts in both the As and Ga 3d photopeaks. Su *et al.* [66] have proposed an adsorption model that involves both nonbridging oxygen (As=O) and bridging oxygen (Ga-O-As and Ga-O-Ga).

One conclusion that most agree upon is the fact that "disordered" surfaces adsorb oxygen more readily than ordered surfaces. For the chemisorption of oxygen to occur on any of these surfaces a defect site is required [14,35,36,41,43,127,128] which may then catalyze the decomposition of $O_2$ [41,83]. Clearly, there is no agreement on whether oxygen chemisorbs only to As atoms or if it initially bonds to Ga atoms or to both As and Ga atoms.

Theoretical studies favor bonding to As sites but disagree on whether oxygen bonds in molecular or atomic form. The theoretical predictions of Goddard *et al.* [83] indicate that molecularly adsorbed $O_2$ should not be expected on GaAs. From studies of the O 1s photopeak, Brundle and Seybold [36] (XPS and UPS measurements) came to the conclusion that $O_2$ dissociates into chemisorbed atomic oxygen. The O 1s photopeak binding energy (BE) occurs at 531 eV which is in the range where adsorbed dissociated oxygen and bulk oxide oxygen values occur. A chemisorbed molecular oxygen species would be expected to have an O 1s BE several eV higher than that for the oxide [36]. These results are sup-

ported by the work of Stöhr *et al.* [38] using surface EXAFS in which they find oxygen chemisorbed in atomic form. Thus the consensus is that the adsorption of oxygen occurs in a two-step process [14,38,43,77,104]. On an initially ordered surface, oxygen is first adsorbed at residual native defect sites and produces additional disorder by the release of exothermic adsorption energy. Second, oxygen accumulates towards a monolayer in a chemisorbed atomic oxygen form and, above a monolayer, begins to form a complex oxide.

In recent experiments Frankel *et al.* [103,105] studied the adsorption of $O_2$ on cleaved GaAs(110) at low temperatures with UV photoemission. At 50 K, they observed physisorbed molecular $O_2$, which upon warming to 300 K was transformed to chemisorbed atomic oxygen - the state normally observed at room temperature. Their results do not contradict the belief that oxygen is chemisorbed in an atomic form, but imply that a transition from a physisorbed molecule to the chemisorbed atom occurs as a function of temperature.

### *2.3.3 Chemical Composition of Oxides*

GaAs oxidation and the Ga-As-O equilibrium phase diagram were the subject of an investigation by Schwartz *et al.* [129,130] in an attempt to predict the phases and their composition which result from the oxidation of GaAs. Bulk layers of oxide with varying thicknesses have been formed in many ways by long term exposure to $O_2$ or air [101,104, 118,131,133], thermal oxidation in air [130], anodization [76,130], and plasma oxidation [134]. XPS has probably been one of the best and most used techniques for examining the chemical composition of surface oxide layers. XPS yields information on the valence state of the surface atoms in the first 60 Å for GaAs. The type of oxidation and extent of oxidation have been determined by observing changes in the photopeaks of the Ga 3d, As 3d, and O 1s levels. The As and Ga 3d photopeaks in the oxides exhibit shifts to higher binding energies compared to the observed binding energies for Ga and As in GaAs. The Ga 3d photopeak due to oxide exhibits a smaller shift (<2 eV) from the Ga(GaAs) photopeak than

does the As 3d photopeak due to oxide (>3 eV). This makes it possible to identify the amount and type of species on oxidized GaAs. Table 2.2 summarizes the chemical shifts observed for bulk and surface oxides formed on GaAs reported in the literature (Table 2.2a) and reference chemical shifts for oxides of known composition (Table 2.2b) [130].

Generally, most studies on the oxidation of GaAs report the valence state of Ga atoms to be $Ga^{3+}$ and the valence state of the As to be $As^{3+}$ or $As^{5+}$ (depending on oxidation conditions), suggesting Ga in the form of $Ga_2O_3$, and As in the form of $As_2O_3$ and $As_2O_5$ or $GaAsO_4$. The ratios of Ga : As : O in these studies yield information on the stoichiometry with respect to the particular oxide phases.

### 2.3.4 *$H_2O$ Adsorption Studies*

Water adsorption has been studied to a lesser extent than oxygen, but is nevertheless important because of its presence during cleaning processes. Water in small amounts in oxygen has been shown to enhance the oxidation process [101].

Very little controversy exists regarding the mechanism for $H_2O$ adsorption on GaAs. The data support a model for a two step process [79,111]. For exposures below $10^6$ L, UPS data indicate an initial step of molecular adsorption via the oxygen lone pair orbital [79,105]. Webb and Lichtensteiger [79] and Childs *et al.* [109] have shown that $H_2O$ adsorbs predominantly to Ga atoms associated mostly with defect sites. However, the adsorption does not appear to be defect controlled over the range of 5 to $10^6$ L as much as oxygen adsorption depends upon defects. Childs *et al.* [109] have also shown that $H_2O$ adsorbs two to three orders of magnitude faster than $O_2$. The adsorption of $H_2O$ could occur faster because it does not go through a dissociation step like $O_2$ to chemisorb on the surface [104,105].

For exposures above $10^6$ L, a physisorbed or condensed $H_2O$ layer is found [70,112]. For doses above $10^9$ L dissociative adsorption becomes apparent in the formation of Ga-OH

**Table 2.2a** XPS shifts for oxides on GaAs relative to Ga and As of GaAs [137].

| Bulk Oxides | Atomic State | Chemical Shift(eV) | Reference |
|---|---|---|---|
| Molecular $O_2$, RT<br>30Å | As 3d<br>Ga 3d | 3.3-3.4<br>1.1 | 131,133 |
| Thermal oxide, air 500 °C<br>200Å | As 3d<br>Ga 3d | 3.4<br>1.4 | 130 |
| Thermal oxide, $O_2$ 500 °C<br>200Å | As 3d<br>Ga 3d | 4.7<br>1.4 | 130 |
| Anodic oxide<br>300Å | As 3d<br>Ga 3d | 3.4<br>1.4 | 130 |
| **Surface Oxides** | | | |
| Molecular $O_2$<br>$10^7$-$10^{13}$ L | As 3d<br>Ga 3d | 3.0<br>1.0 | 14 |
| Molecular $O_2$<br>$1.2x10^8$-$10^{14}$ L | As 3d<br>Ga 3d | 3.1<br>1.0 | 36 |
| Molecular $O_2$<br>$10^7$-$5x10^7$ L | As 3d<br>Ga 3d | 2.9<br>not reported | 132 |
| "Excited" $O_2$*<br>$10^5$ L | As 3d<br>Ga 3d | 2.9<br>1.0 | 132 |
| "Excited" $O_2$*<br>$10^6$-$10^7$ L | As 3d<br>Ga 3d | 4.6<br>1.1 | 134 |

**Table 2.2b** Reference Core Shifts [135,130].

| Material | Core Shift (eV) |
|---|---|
| As 3d: Relative to As in GaAs | |
| $As_2O_3$ | 3.4±0.4 |
| $As_2O_5$ | 4.7±0.5 |
| $GaAsO_4$ | 4.7±0.5 |
| Ga 3d: Relative to Ga in GaAs | |
| $Ga_2O_3$ | 1.4±0.2 |
| $GaAsO_4$ | 1.4±0.3 |

bonds as found in the UPS and XPS results of Webb and Lichtensteiger. The only question is in determining the identity of the surface species formed, such as $Ga(OH)_3$ and $GaO(OH)$.

### *2.3.5 Nitric Oxide Adsorption Studies*

The adsorption of NO on transition metals, including Pd, Ru, Ni, Pt, Ir, and Rh has been studied. These studies have been reviewed [136,137]. The adsorption behavior at room temperature ranges from complete dissociation on Ru, Rh, and Ni, to partial dissociation on Ir, to molecular adsorption on Pd and Pt [137]. The interaction of NO with GaAs has been reported less frequently in the literature [116-119], although there is extensive literature on the adsorption of NO on Si [118].

One of the earliest investigations of NO adsorption on GaAs(100) [116] considered the effect of NO on the surface photovoltage spectrum of sputter-disordered GaAs(100). Bermudez [117] reported the use of AES to investigate the influence of low-intensity visible/near-ultraviolet radiation on the oxidation of n- and p-type GaAs(110) in which he compares $O_2$ and NO adsorption. The results showed that NO exhibited a smaller sticking coefficient and a much smaller photoeffect than $O_2$.

Recently, detailed studies of NO interaction with GaAs were reported [118,119]. A principal thrust of these studies was to clear up the controversy regarding GaAs oxidation. It was thought that results for a similar reactive, but heteronuclear, diatomic molecule could be compared with the large amount of data on the $O_2$ reaction and could possibly provide new insight into the oxidation mechanism [118]. It has also been suggested that adsorption of $N_2O$ on GaAs might also be a useful means of providing atomic O without the need for dissociating the $O_2$ molecule [41,115,118]. $N_2O$ requires only 1.7 eV to dissociate compared to 5.1 eV for $O_2$ [115] and 6.5 eV for NO [118].

It has been suggested by almost all investigators that a rate-limiting step in $O_2$ chemisorption is the dissociation of the oxygen molecule itself and that this dissociation step

is also controlled by the presence of defect sites. In the photoemission study of NO on GaAs(110), Bermudez *et al.* [117] report that defect sites might also be important in the NO reaction. NO reacts slower than $O_2$ at lower exposures (<$10^7$ L) for which defects are thought to be important. They also report the dissociative adsorption of NO on GaAs at room temperature, which is similar to that reported for $O_2$. If the step controlling the reaction is the dissociation of the molecule, then comparing two diatomic molecules with different dissociation energies could help to elucidate the oxidation mechanism on cleaved as well as sputtered GaAs, especially if defects play an important role in the dissociation of the molecule.

So and Ho [119] reported on the interaction of laser radiation with NO adsorbed on GaAs(110) at 90K. They observed molecular adsorption with a partial reaction to form a small amount of $N_2O$. The results are similar to those reported by Frankel *et al.* [103,105] for $O_2$ adsorption at 90 K.

### 2.3.6 Hydrogen Adsorption Studies

Hydrogen interacts very strongly with semiconductor surfaces, saturating dangling bonds, and altering the surface reconstruction [138]. Hydrogen is usually present as a carrier gas in chemical vapor deposition processes, and is also present in the compounds used to form GaAs. Improvements in the electrical and optical properties of GaAs grown in the presence of hydrogen were reported [82,139,140]. Hydrogen plasmas are used to clean GaAs surfaces and atomic hydrogen introduced by the plasma passivates certain electrically active deep-level defect sites [139,141,142].

Pretzer and Hagstrum [143] used ion neutralization spectroscopy to study the effects of various gases, including $H_2$, on the surfaces of clean GaAs. An exposure of $10^5$ L $H_2$ at room temperature caused no changes in the ion neutralization spectrum. It was concluded by Pretzer and Hagstrum and other investigators [94,144] that $H_2$ does not adsorb at

significant rates at room temperature on GaAs. However, atomic hydrogen, usually formed from molecular $H_2$ by exposure of the gas to a hot tungsten filament, does react readily with GaAs surfaces [94,102,138,140,144-148].

EELS studies by Bartels *et al.* [102] found that the work function decreased for p-type and increased for n-type materials with hydrogen exposures up to 5 L. This effect was associated with the formation of depletion layers from the chemisorptive loss of As atoms in the topmost layers due to hydrogen adsorption. From these results, they concluded that hydrogen initially bonds to arsenic atoms. Astaldi *et al.* [145] also confirm the loss of As atoms upon hydrogen exposure. From core level XPS and LEED studies, Bringans and Bachrach [138,147] concluded that atomic hydrogen bonds to As atoms; however, the hydrogen saturated surface is always As-rich and the properties of the saturated surface are independent of the composition of the original surface. They found that the surface becomes As-rich even if the initial surface is Ga-rich.

Through the use of HREELS and other techniques such as RHEED, other investigators were able to identify hydrogen atoms bonded to gallium and arsenic atoms on the GaAs surface from the observation of stretching vibrations of both As-H and Ga-H [140,145,146, 148]. Hou *et al.* [148] observed the participation of both As and Ga atoms in the adsorption process, but only at high exposures (1000 L). They reported that the initial hydrogen interaction occurs only with Ga atoms.

### *2.3.7 Miscellaneous Gas Adsorptions*

The adsorption of other gases, such as CO [149], $H_2S$ [80], $CH_3OH$ [112], HCOOH [150,151], $CH_3COOH$, and $CF_3COOH$ [149], on GaAs have been studied by HREELS, ELS, and LEED. Studies of other gases are important to understand molecular adsorption and decomposition reactions on solid surfaces that could play roles in epitaxial growth and for doping of semiconductors from the gas phase [151]. Formic acid was studied by Mattern-

Klosson *et al.* [150] because of its simple structure, thus serving as a model for molecules with more complex structures. Acetic acid and trifluoroacetic acid were chosen for their importance in helping to understand the details in the complex reaction mechanisms that take place during reactive ion etching (RIE) where gases such as $CCl_4$ and $CF_4$ are involved. $CF_3COOH$ was chosen to produce reactive $CF_3$ groups on the surface without involving electron or ion beams. In the reactive ion etching process, interaction of the material to be etched with the gas phase species follows a sequence of steps [152,153], the first being the nondissociative adsorption of the gas phase species at the surface. Winters [152] showed that this step cannot be ignored when attempts are made to understand the complex mechanism involved in the etching process.

The results of the reaction of formic acid with GaAs give insight into the changes of the electronic structure of cleaved GaAs surfaces [150,151]. During adsorption, formic acid decomposes to form an adsorbed formate species($HCOO^-$) and adsorbed hydrogen (H). $HCOO^-$ is bound to the surface in a bidentate configuration with two Ga-O bonds and H is adsorbed on As sites. Different changes in the work function observed for n- and p-type materials as a result of the adsorption give information about intrinsic and extrinsic surface states. On p-type GaAs, depletion layers disappear upon exposure to HCOOH. This implies that for p-type materials, intrinsic donor-like surface states have to be assumed which are responsible for an initial depletion layer. From the work function changes found on n-type materials, an adsorbate induced depletion layer is assumed.

The adsorption results of $CF_3COOH$ are of importance in determining some of the initial reactions that occur during the RIE process. The adsorption process of $CF_3COOH$ involves first the adsorption of the hydrophilic end to Ga surface atoms. The H atom is split off and is bonded to a neighboring As surface atom. The "intermediate" $CF_3COO$ breaks apart between the two C atoms, evolving $CO_2$ which desorbs leaving the $CF_3$ group on the surface [149]. The results indicate that $CF_3$ groups are bonded to Ga surface atoms. The

purpose of the work completed by Förster *et al.* [149] was to demonstrate the possibility for studying the adsorption of charged reactive complexes in order to understand the chemical surface reactions underlying the reactive ion etching process. Instead of generating reactive complexes by electron or ion bombardment, decomposition reactions of suitable larger molecules might yield the same complexes that are already bonded to adsorption sites during reactive ion etching [149].

## 2.4 Research Objectives

Goddard and Barton *et al.* [41,83] concluded from theoretical calculations that the chemisorption of $O_2$ should not readily occur on cleaved GaAs surfaces. It is generally agreed that for chemisorption of $O_2$ to occur, defect sites are required to catalyze the dissociation of $O_2$ [14,35,36,41,43,83,127,128]. It was shown by Su *et al.* [14] that a surface disordered by ion bombardment adsorbs more oxygen than a clean, cleaved surface. The disordered surface should have an increased number of defect sites compared to that of cleaved GaAs and will therefore provide the necessary conditions for the chemisorption of $O_2$. It is the purpose of this research to investigate in more detail the effects of ion bombardment on the chemical reactivity of GaAs by examining the effects of ion bombardment energy and ion bombardment mass on the reaction chemistry by exposing the ion bombarded surfaces to several different reactant gases.

It is known that ion bombardment causes damage to a surface and the amount of damage is dependent upon the energy and mass of the bombarding ion. If defects are required in order for chemisorption of oxygen to occur, then ion bombardment could be used to impart different amounts of damage to the GaAs crystal by changing the mass and energy of the bombarding ions. Consequently, an effect should be observed in the reactivity of the ion bombarded surface that is different from a non-ion bombarded surface. If defects are caused by ion bombardment and if they are required for dissociation of the

reactant molecule, then the effect observed should be an enhanced reactivity compared to non-ion bombarded material (at least for $O_2$). In this study, the mass and energy of the bombarding ion were varied ($Ar^+$ at 0.5-3 KeV and $^3He^+$, $^{20}Ne^+$, $Ar^+$, and $Xe^+$ at 3 KeV) to investigate the effect of these parameters on the crystal surface stoichiometry and reactivity.

It has been suggested that the initial chemisorption of $O_2$ at defect sites on GaAs involves the formation of a negative complex [66,118,195] and that the dissociation of molecules on GaAs is related to the bond dissociation energy of the reactant molecule [115]. These two possibilities could be investigated by exposing ion bombarded GaAs to different reactant gases. Defects, which are produced by ion bombardment by the breaking of surface bonds, could be in the form of dangling bonds. If defects are playing a role in the dissociation and the formation of a negative complex is the desired reaction pathway, then an enhanced reactivity will be observed for GaAs exposed to reactant molecules that will easily form a negative complex. If the reactivity is not related to defects but to the dissociation energy of the molecule, then enhancement of the reactivity should not be observed by inducing different amounts of damage by changing the ion bombardment conditions. Then the reactivity observed for a series of gases should be related to the bond dissociation of the reactant molecule. $O_2$, NO, and $N_2O$ were chosen for this study for several reasons. $O_2$ was chosen because there is a great deal of data in the literature to compare with the results observed for ion bombarded GaAs to determine if there is actually an enhanced reactivity as a result of ion bombardment. NO and $N_2O$ were chosen to investigate the possibility that the bond dissociation energy of the molecule could control the reactivity. $N_2O$ was shown to oxidize GaAs more readily than $O_2$ [115] because the bond dissociation energy for $N_2O$ is much less than $O_2$ (D($N_2$-O) 1.5 eV and D(O-O) 5.6 eV, respectively). If defects have no effect on the reactivity, then $N_2O$ should oxidize ion bombarded GaAs more readily than $O_2$ or NO.

The presence of $H_2O$ in $O_2$ has been shown to enhance the oxidation of GaAs,

therefore it was of interest to investigate the effect of $H_2O$ itself on the oxidation of ion bombarded GaAs. Based on the results observed for the different ion bombardment conditions and the various reactions it should be possible to suggest a model for an ion bombarded GaAs surface and to determine if defects are important to the chemical reactions on GaAs.

# Chapter III: Experimental

## 3.1 Materials

### *3.1.1 Wafers*

GaAs wafers were obtained from the Morgan Semiconductor Division of Ethyl Corporation. All wafers were either LEC or HB grown with a crystal orientation of (100) ± 0.5° or (100) 2.0° off toward (110). The wafers were Si doped (n-type) in the melt and had a doping density in the range $2.3 \times 10^{16}$ - $5.3 \times 10^{17}$ $cm^{-3}$.

### *3.1.2 XPS Standard Materials*

The following materials were used as model compounds for the determination of XPS binding energies (BE), full-width-at-half-maxima (FWHM), and atomic ratios: $Ga_2O_3$ (Alfa, 99.99%), $As_2O_3$ (Aldrich, 99.999%), $As_2O_5$ (Fisher, 99.2%), and GaO(OH) (synthesized) [158,159].

GaO(OH) was prepared by dissolving Ga metal (Alfa, 99.99999%) in concentrated HCl. The hydroxide was precipitated by the addition of $NH_4OH$ to attain pH 8. The precipitate was digested at 75 °C for one hour, washed with deionized $H_2O$, and left to age overnight in deionized $H_2O$. The precipitate was then centrifuged, rinsed until the wash water measured pH 7 and there were no detectable traces of $Cl^-$, washed with acetone, and dried under vacuum. X-ray diffraction measurements confirmed the preparation of crystalline GaO(OH) (JCPDS 6-0180). The X-ray diffraction instrument consisted of a Picker Nuclear Goniometer (Model 3668A) on a Picker Nuclear Generator (Model 42215A), and a Cu x-ray tube with curved graphite monochromator. Generator settings were 30 KV and 15 mA.

### *3.1.3 Reactant Gases*

The reactant gases used in this study were $O_2$, $H_2O$, NO, and $N_2O$. Ion bombarding gases were $^3$He, $^{20}$Ne, Ar, and Xe. The source, purity, and any further purification of each gas are listed below.

$O_2$: Airco, Grade 4.3, 99.993%, Alltech gas purifier with indicating drierite and 5 Å molecular sieve was added in line.

NO: Matheson, C.P. 99.0%, purified by passing through a stainless steel 1/4" tubing loop containing 60-200 mesh silica gel (previously baked under vacuum) at dry-ice/acetone bath temperature [154]. A 7 micron, stainless steel, in-line filter was installed after the silica gel loop to protect the UHV system from particle contamination.

$N_2O$: Scott Gases, SFC grade

$H_2O$: boiled, cooled by bubbling $N_2$ through the liquid, placed in a stainless steel Nupro sample cylinder and connected to the reaction chamber. Further purification was by a freeze/thaw cycle under vacuum.

$^3$He: Isotec Inc., Standard Grade, 99.9%

$^{20}$Ne: Isotec Inc., 99.95%

Ar: Union Carbide, Research Grade(XPS) /Air Products, Research Grade, 99.9995% (reaction chamber)

Xe: Airco, Research Grade, 99.995% (natural isotopic abundance)

## 3.2 Sample Preparations

### *3.2.1 GaAs Preparation*

Samples were cut from the GaAs wafers using a diamond scribe and oriented for ion bombardment as indicated in Figure 3.1. All specimens were cleaned in 1:1 (by vol.)

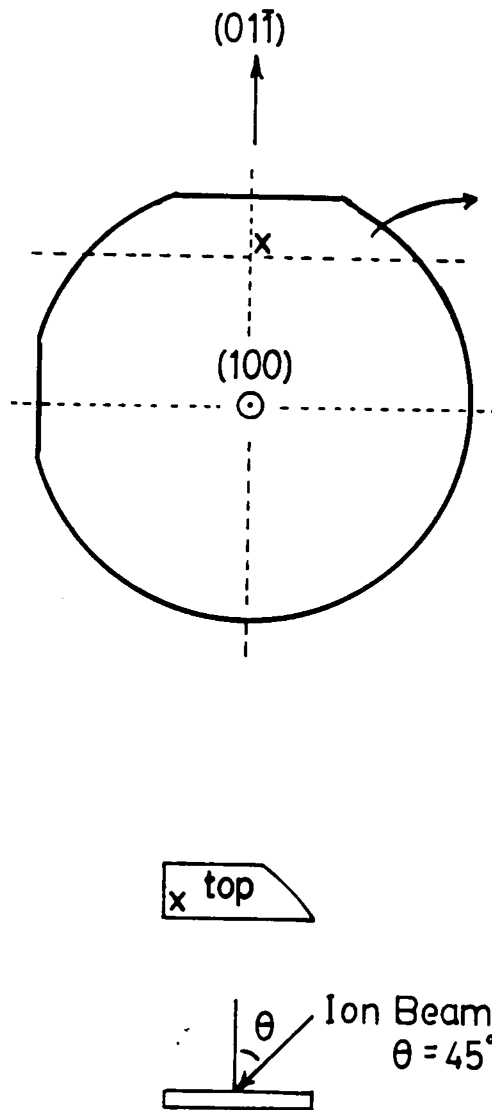


**Figure 3.1** Cutting and orientation of wafer for ion bombardment.

$HCl(conc)/H_2O$ at room temperature for 10 minutes to remove surface oxides. The samples were rinsed in deionized water and transferred in air to the XPS chamber. These samples are referred to as ***chemically cleaned*** GaAs.

An alternative method used for cleaning involved etching the GaAs samples. The etching solution consisted of 8:1:1 (by vol.) $H_2SO_4$(conc): $H_2O_2$(30%) : $H_2O$. The samples were etched in the solution with constant stirring for 8 minutes. The etch rate for a GaAs(100) surface in this solution is 1.2 $\mu m{\cdot}min^{-1}$ [155]. The etched samples were rinsed in deionized water and immediately treated by the standard 1:1 $HCl(conc)/H_2O$ cleaning described above. These samples are referred to as ***chemically etched*** GaAs.

### *3.2.2 Simultaneous Ion/Heat Treatment (IHT)*

A cleaning procedure developed by Oelhafen *et al.* [156] to obtain clean, well-ordered surfaces of GaAs(100) was followed to aid in the effort to compare the properties of chemically cleaned and ion-bombarded GaAs. The procedure consisted of bombarding GaAs with low energy $Ar^+$ ions (<400 eV) while simultaneously heating the GaAs substrate. These samples will be referred to as ***IHT*** GaAs.

This procedure was carried out in the UHV reaction chamber using a PHI Model 04-161 ion gun, mounted perpendicular to the sample surface. The samples were chemically cleaned and pre-heated (outgassed) for at least 2 hours at 400 °C before IHT to insure a beginning base pressure of $<7x10^{-6}$ Pa in the reaction chamber. The ion bombardment energy was 200 eV and ion currents in range of 1-2 $\mu amps{\cdot}cm^{-2}$ were used. The temperature of the GaAs was maintained at 400 °C. The IHT treatment time was typically 1-2 hours. This time was fixed by measuring the XPS spectra for O 1s, As 3d, and Ga 3d regions. When the O content was <10 atomic percent (at.%) and only species due to GaAs were present, the IHT treatment was stopped. These samples were allowed to cool for

approximately 45 minutes before any reactions were carried out. During cooling, the sample was analyzed by XPS.

### *3.2.3 Ion Bombardment*

Ion bombardment was carried out in a Perkin-Elmer PHI Model 5300 XPS system equipped with a 04-300 differentially pumped ion gun, mounted at 45° with respect to a line perpendicular to the specimen surface. $Ar^+$ ion bombardment was carried out at energies of 500, 1000, 2000, and 3000 eV using a 1 $cm^2$ rastered beam with ion currents in the range of 0.2 - 40 $\mu$amps (measured with a Keithley 610A Electrometer). The time of bombardment was adjusted to give fluences in the range of $2x10^{16}$ - $9x10^{17}$ ions·$cm^{-2}$. $^3He^+$, $^{20}Ne^+$, and $Xe^+$ ion bombardments were carried out at 3000 eV with ion currents in the range 20-30 $\mu$amps. The time of bombardment was adjusted to give fluences in the range 6-$9x10^{17}$ ions·$cm^{-2}$. The samples were oriented such that ion bombardment was in the (111) direction (see Figure 3.1). The base pressure before ion bombardment was $3x10^{-6}$ Pa or less. Chamber pressures during ion bombardment were generally about $1x10^{-5}$ Pa.

### *3.2.4 Reactant Gas Exposures*

Following ion bombardment, the sample was transferred under vacuum into the UHV reaction chamber attached to the XPS system, where exposure at room temperature to the reactant gases, $O_2$, $H_2O$ vapor, NO, or $N_2O$ was carried out. $O_2$ exposures ranged from $10^7$-$10^{13}$ L, $H_2O$ exposures were in the range $10^9$-$10^{12}$ L, NO exposures were $10^6$-$10^8$ L, and $N_2O$ exposures were $10^7$-$10^{11}$ L. Since NO is known to interact strongly with stainless steel [118,137], the chamber was passivated following bake-out and before any exposures were performed by exposing the chamber to 13 Pa (continuous flow) for at least 45 min (>$1x10^8$ L). The NO gas flow was monitored by the mass spectrometer before and after the passivation for the presence of contamination in the gas, particularly $NO_2$. For the NO

results reported in this thesis, no $NO_2$ was detected before or after NO exposure. After these experiments, a new NO tank and a new silica gel coil were introduced to the system. Due to an in-line leak or improper bake-out of the silica gel, the NO was contaminated with $NO_2$, even with the dry-ice/acetone bath in place. Any NO exposures performed with contaminated NO were found to differ from that of the previous NO exposures. The results with contaminated NO are discussed in the section on NO exposures, but are not included in any of the NO results reported.

All filaments were turned off before and during gas exposure to avoid exposure of the sample to excited oxygen (or other excited gases) [70] and the filaments were left off during evacuation of the chamber until the sample was transferred back into the XPS chamber. Time for transfer was generally <2 minutes following the end of a gas exposure, except in the case of $H_2O$ which took a longer time to evacuate. Exposures of $10^8$ L and less were carried out with continuous gas flows and the pressure was measured by a Hastings thermocouple gauge. Above $10^8$ L, the reaction chamber was back-filled with the reactant gas to atmospheric pressure (measured by an Omega general service gauge) or to $3.2 \times 10^3$ Pa for $H_2O$. The exposure time was 5 min or longer depending on the exposure level needed.

### *3.2.5 Standard Binding Energy Determinations*

The oxides (except GaO(OH)) were dried at 110 °C prior to XPS analysis and the powders were mounted using double-stick tape on a stainless steel probe. The binding energies were determined by sputtering a thin layer of gold onto the sample (Edwards Sputter Coater; Model S150B) and referencing the binding energies to the Au $4f_{7/2}$ level at 83.8 eV [157,193]. The FWHMs and atomic concentrations were determined from spectra obtained before the deposition of Au onto the sample. The average measured binding energies, FWHMs, and atomic concentrations were determined from at least three separately

prepared samples for each of the oxides. The measured binding energies agreed with the literature values [135,157].

The binding energy of ion-bombarded GaAs was determined by sputtering a layer of Au that was thick enough to obscure the Ga 3d and As 3d photopeaks before ion bombardment onto a chemically cleaned (1:1 HCl(conc)/$H_2O$) sample. The sample was then ion bombarded with 3 KeV $Ar^+$ ions to remove the Au. The area of bombardment was adjusted so that the analysis area would still contain non-bombarded material. The single photopeaks in each of the Ga 3d and As 3d regions were then referenced against the Au $4f_{7/2}$ peak at 83.8 eV [157,193].

## 3.3 Reaction Chamber

A stainless steel, ultra-high vacuum (UHV) reaction chamber was constructed and attached to the XPS chamber to facilitate carrying out in situ reactions. A schematic of the chamber is illustrated in Figure 3.2.

The XPS chamber and reaction chamber were isolated by a high vacuum stainless steel gate valve (MDC Model GV-1500M, 1.5 in I.D.). The chamber was pumped by a water cooled turbomolecular pump (Balzers Model TPU 050) and a two-stage rotary vane vacuum pump (forepump) (Balzers Model DUO 016B). The pumps were isolated from the reaction chamber during atmospheric gas exposures by a high vacuum stainless steel gate valve (MDC Model GV-2500M, 2.5 in I.D.) The chamber pressure was monitored by a Bayard-Alpert ionization gauge with dual tungsten filaments. During reactant gas exposures, the chamber pressure was monitored by a thermocouple gauge (Hastings vacuum gauge) for pressures in the range 3-13 Pa and by an Omega general service gauge that measures pressures in the range $133\text{-}2\times10^5$ Pa.

Samples were transferred into the reaction chamber from the XPS chamber using a PHI

a)

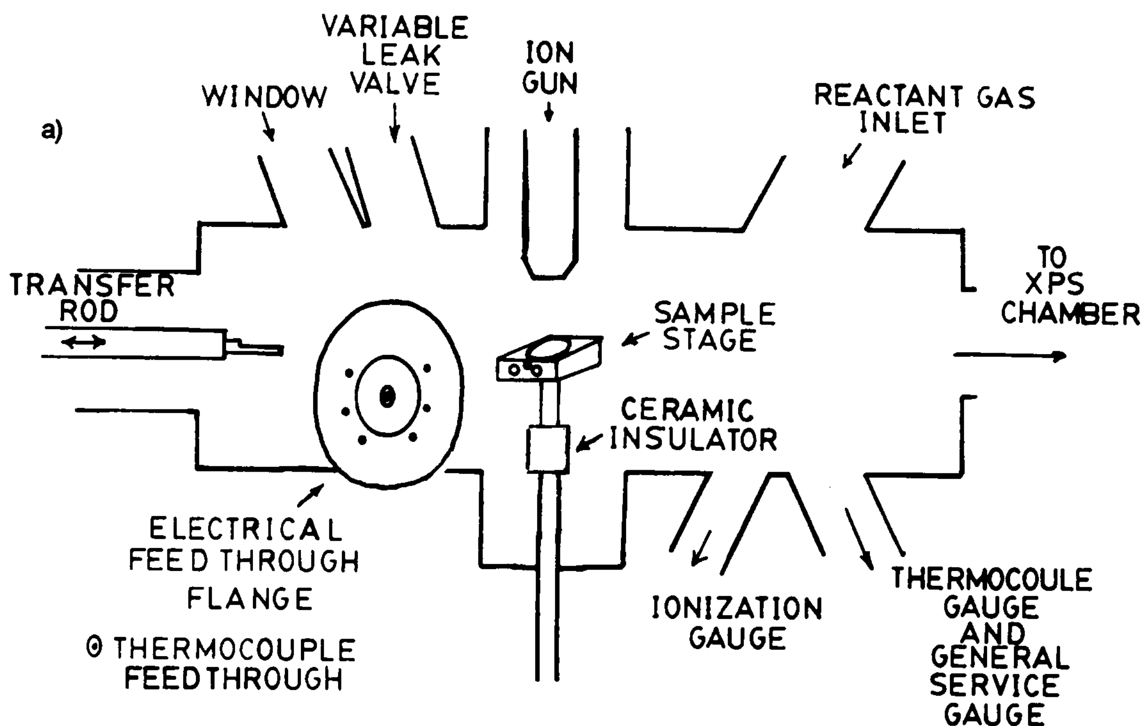


b)

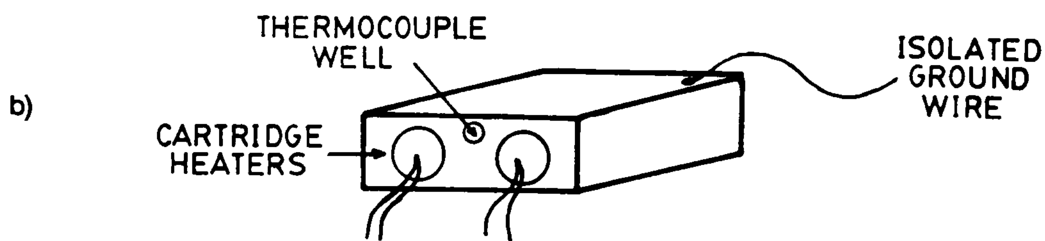


c)

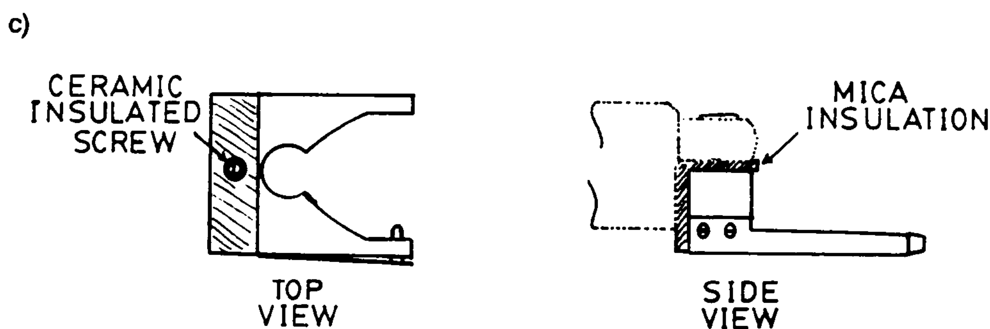


**Figure 3.2** Schematic of UHV reaction chamber. (a) chamber, (b) sample stage, and (c) transfer fork.

Model 04-745 linear transport attachment. Ion bombardment in the reaction chamber was carried out using a PHI Model 04-161 ion gun that was mounted perpendicular to the sample surface. Ion currents (measured with a Keithley 610A Electrometer) were detected by touching the heater stage to the sample probe that contained an isolated ground (Pt wire) that was connected to an electrical feedthrough flange (see figure 3.2b). The sample probe was also electrically isolated from the transfer device by placing a ceramic tube through the screw holding the fork and a sheet of mica across the part of the fork that would come into contact with the transfer rod (see figure 3.2c). The heater stage consisted of a block of stainless steel (1.5 x 1.5 x 0.5 in), with holes for cartridge heater elements and a thermocouple. It was held in place by a wobble stick device (Hastings Vacuum Generators) and electrically isolated from the wobble stick by ceramic. The cartridge heater power was supplied by a variac and temperature was monitored by a type K thermocouple whose output was monitored by an Omega programmable temperature controller. The thermocouple was also electrically isolated from the stage by a ceramic tube inserted into the thermocouple well. The thermocouple was inserted into the vacuum chamber and sealed by a 1/16 in. swagelok.

Reactant gases were admitted by two means. One was through a stainless steel variable leak valve, for small controlled doses, and the other was through a Nupro stainless steel bellows valve (series SS-4H), for atmospheric doses. The gases in the chamber were monitored by a mass spectrometer (UTI 100C Precision Mass Analyzer). The quadrupole was mounted between the reaction chamber and the turbomolecular pump. Mass spectra were acquired on an IBM PC-AT computer utilizing the Teknivent Vector/One PCSPEC acquisition and processing control program.

The chamber was wrapped with silicone-coated heating tape and baked-out for at least 8 hours before and in between reactions.

## 3.4 Surface Analysis

### 3.4.1 *Instrumentation*

The surface analyses were carried out using a Perkin-Elmer PHI Model 5300 XPS system. X-ray generation occurs in the PHI Model 04-500 X-ray source equipped with both Mg and Al anodes. Mg $K_\alpha$ radiation was utilized in these studies with the anode power set at 250 watts. Photoelectrons emitted from samples are focussed into the spectrometer input slit at the appropriate kinetic energy by the PHI Model 10-360 Precision Energy Analyzer (Figure 3.3), a concentric hemispherical analyzer. The electron signals are detected by a position sensitive detector that consists of two 2.5 cm diameter channel electron multiplier arrays [160].

Auger analysis was carried out on a Perkin-Elmer Model 610 Scanning Auger Microprobe using a 3 or 5 KeV primary electron beam and was used strictly for qualitative analysis.

### 3.4.2 *Sample Analysis*

Photoelectrons were produced using Mg $K_\alpha$ radiation ($h\nu$=1253.6 eV) as the excitation source. The analysis chamber pressure was less than $3 \times 10^{-6}$ Pa. Spectra were obtained immediately following chemical cleaning, ion bombardment, IHT, and also following reactant gas exposures. Spectra were acquired at 90° and 15° take-off angles (toa) measured as the angle between the sample surface and the photoelectron analyzer (Figure 3.4). Compositional analysis as a function of depth was carried out for some samples in which case the toa was varied between 90° and 15°. Ninety-five percent of the observed photoelectron signal comes from a layer $3\lambda\sin\theta$ thick where $\lambda$ is the mean free path of the photoelectron and $\theta$ is the take-off angle [162]. For the Ga 3d and As 3d core levels $\lambda$ is approximately 22 Å, therefore the analysis depths are approximately 66Å and 17Å for 90° and 15° toas,

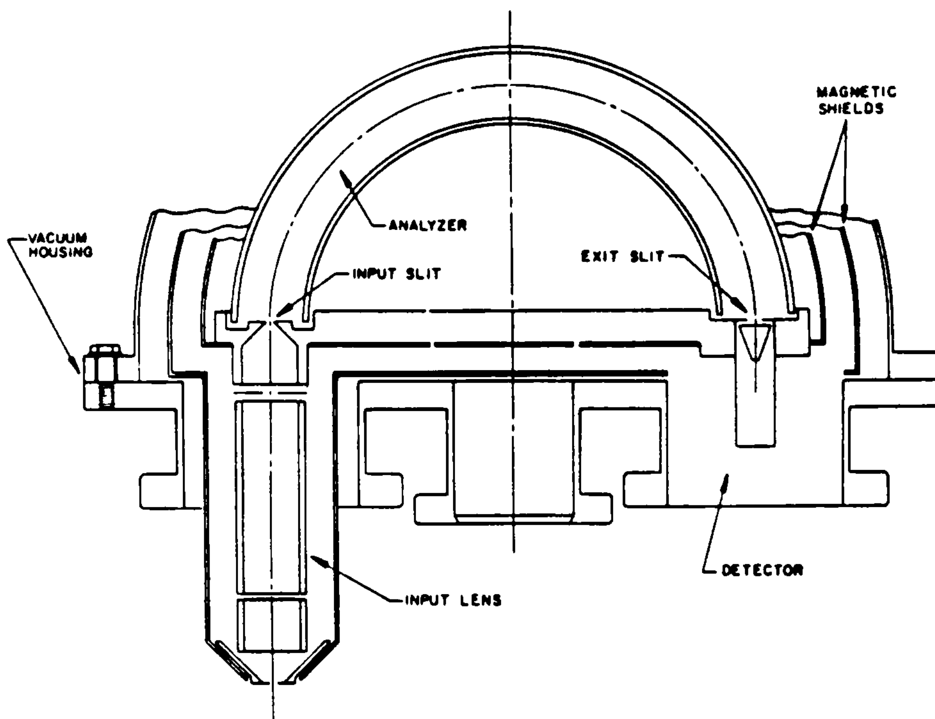


**Figure 3.3** PHI model 10-360 hemispherical capacitor energy analyzer [160].

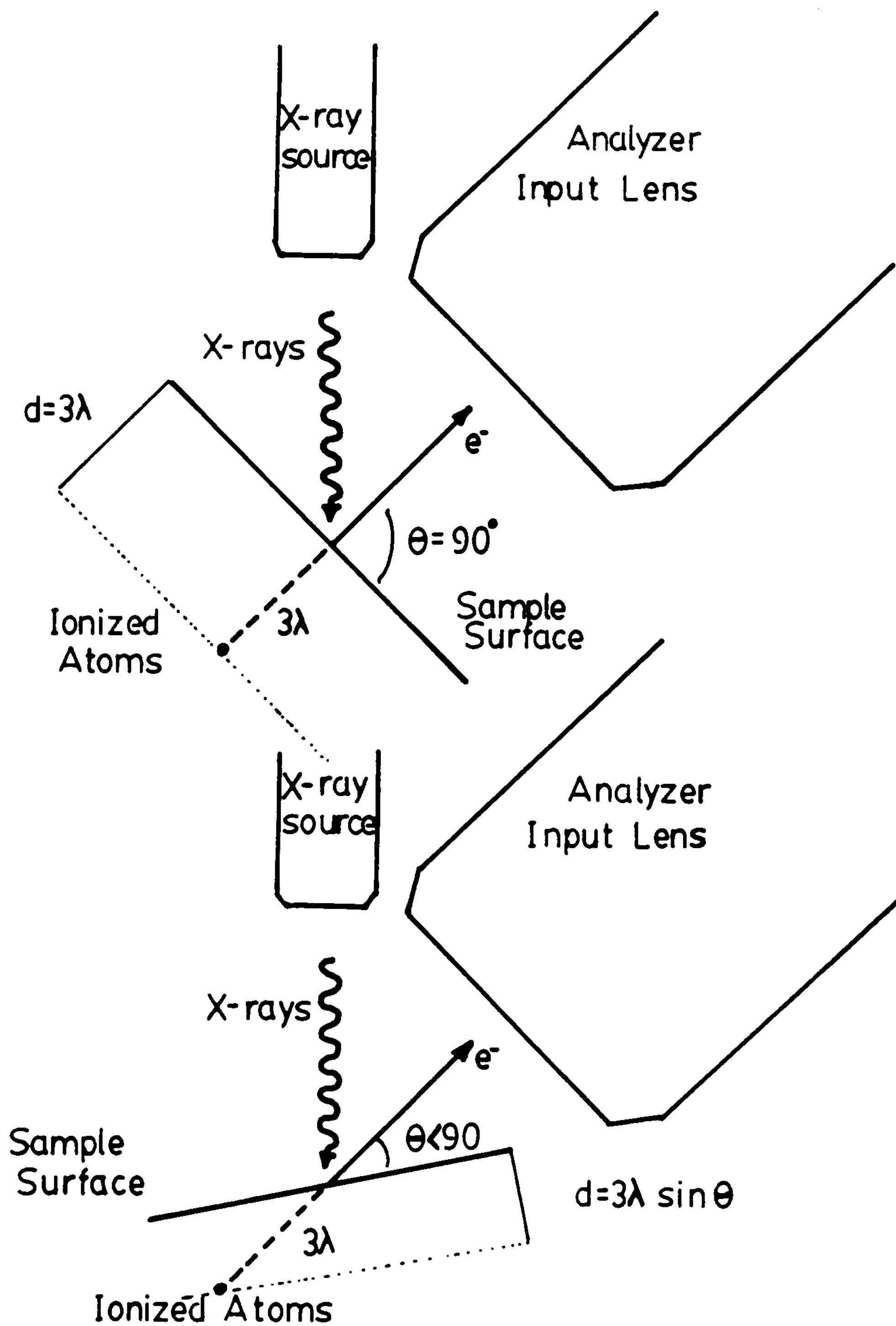


**Figure 3.4** Directional considerations in angular measurements [160].

respectively.

The photopeaks were analyzed by subtracting the X-ray source line width (deconvolution), smoothing, and curve-resolving the data using the software routines available with the PHI 5300 system. The atomic concentrations were evaluated from the photopeak areas (determined by curve-resolution) using the sensitivity factors listed in Table 3.1.

The PHI X-ray line deconvolution routine is based on a deconvolution technique known as Van Cittert's method [160]. It functions to reduce the line width by reducing or removing the contribution of the x-ray source line width when exciting the specimen. Deconvolution (2 iterations) was performed on the raw XPS data before smoothing.

Smoothing was utilized to reduce noise in the spectra. The smoothing routine in the PHI 5000 series software is accomplished using the Savitzky-Golay convolution algorithm [160], which is an expanded calculation of a moving average. A 15-point smooth was used in this study.

The peak positions, FWHMs, and areas were determined using the curve-fitting routine. Standard Gaussian peaks were superimposed on the deconvoluted and smoothed data after a background subtraction in the integrated mode was performed. Peak heights, widths, and positions were adjusted to simulate the peak structure of the experimentally obtained peaks. Peak widths and positions were obtained from the standard oxide measurements and were used to assist in curve-fitting. Curve-fits were obtained by manual manipulation of the photopeaks so as to keep reasonable widths and positions for peaks.

Atomic concentrations were determined using the following expression:

$$\%\ \text{AC for species X} = \frac{\text{Area(X)}/\sigma(\text{X})}{\sum_{i=1}^{n} \text{Area(i)}/\sigma(\text{i})} \times 100 \tag{3.1}$$

where n is the number of chemical species (i.e. Ga(GaAs), As(GaAs), Ga($Ga_2O_3$) As($As_2O_3$), etc.), I is the peak area determined from the curve-fit routine, and $\sigma$ is the sensitivity factor (Table 3.1).

**Table 3.1** XPS sensitivity factors [161].

| Level | Sensitivity Factor ($\sigma$) |
|---|---|
| Ga 3d | 0.31 |
| As 3d | 0.53 |
| O 1s | 0.66 |
| N 1s | 0.42 |
| Xe $3d_{5/2}$ | 6.6 |
| Ne 1s | 1.5 |
| Ar 2p | 0.96 |

## 3.5 Electrical Studies

Ion-bombardment causes damage to a surface [8,11-13,44]. XPS is only able to probe ~60Å into the surface and the only evidence for ion bombardment damage is the change in the Ga/As ratio and the presence of implanted ions. To probe the damage effects and perhaps obtain some correlation between ion bombardment and reactivity, electrical studies of GaAs were conducted. The electrical measurements included:

- Current-Voltage (I-V) characteristics (290 K)
- Capacitance-Voltage (C-V) characteristics (290 K)

of Schottky diodes on ion bombarded and non-bombarded GaAs.

### *3.5.1 Sample Preparation*

The GaAs samples used in these studies were the same as described in section 3.1.1 (only LEC grown material was used) and the following procedures (except ion bombardment) were performed by and are taken from the Master's thesis of S. Sen [163] in the VPI & SU Electrical Engineering Department. A set of samples, all prepared at the same time from the same wafer, consisted of four 0.5 $in^2$ pieces, where three pieces were subjected to ion bombardment and the fourth was kept as a control sample. Before ohmic contact formation, the samples were cleaned by boiling in tetrachloroethylene (10 min), followed by a soak in warm methanol (10 min), rinsed in deionized water, treated to a 10 min cleaning in 1:1 (by vol.) HCl(conc)/$H_2O$, rinsed in deionized water, treated for 4 minutes in 8:1:1 (by vol.) $H_2SO_4$(conc): $H_2O_2$(30%) : $H_2O$ in a rotating beaker (rotation speed ~22 rpm), followed by a final rinse in deionized $H_2O$ and kim-wipe dried.

Following the above cleaning procedure, ohmic metal was deposited. Au-Ge (88%-12%) alloy was used as an ohmic material. The thermal evaporation was carried out in a Denton-503 high vacuum evaporating unit. The alloy was evaporated upwards from a resistance heated tungsten boat. Chamber pressure was ~$5x10^{-4}$ Pa during evaporation and the rate

of deposition was ~400Å/min. A quartz crystal thickness monitor (Kronos model-311) and a rotating shutter were used in conjunction to control the thickness of the deposited film. The Au-Ge contacts had a circular geometry of 1/32 in. diameter and a film thickness of ~2000Å. The placement of the contacts was controlled by the use of a stainless steel shadow mask illustrated in Figure 3.5. Following Au-Ge evaporation, Ni was deposited over the Au-Ge layer with a thickness of ~600Å to prevent "beading up" of the Au-Ge layer during the ohmic annealing step.

Following Au-Ge/Ni deposition, the samples were annealed in a Thermolyne (Type 21100) tube furnace at 440 °C for 2 minutes under forming gas (90% $N_2$ / 10% $H_2$). Temperature was controlled by an Omega temperature controller and gas flow was controlled by a Matheson flowmeter.

After the ohmic anneal, the samples were again etched in 8:1:1 (by vol.) $H_2SO_4$(conc): $H_2O_2$(30%) : $H_2O$ solution for 4 minutes, rinsed in deionized $H_2O$, and stored in a glass desiccator until the time of ion bombardment. Prior to ion bombardment, the samples were again cleaned in 1:1 (by vol) HCl(conc)/$H_2O$ for 10 minutes, rinsed with deionized $H_2O$, mounted on a stainless steel probe and immediately transferred to the XPS chamber for ion bombardment. The ion bombardment conditions were identical to those described in section 3.2.3. The control sample was treated to the same chemical cleaning step (1:1 HCl(conc)/$H_2O$) as the ion-bombarded samples. After ion-bombardment the samples were stored in a glass desiccator and backfilled with an inert gas (He or Ar) until the Schottky metal could be deposited (on the same day).

Schottky metal (aluminum) was deposited using the same evaporator as for the ohmic metal deposition. A separate stainless mask was used to form 1/32 in. diameter Schottky contacts, with a thickness of ~2000Å. The metal deposition rate was ~60-100Å/min and increased to ~400Å/min when a layer of about 500Å had been deposited.

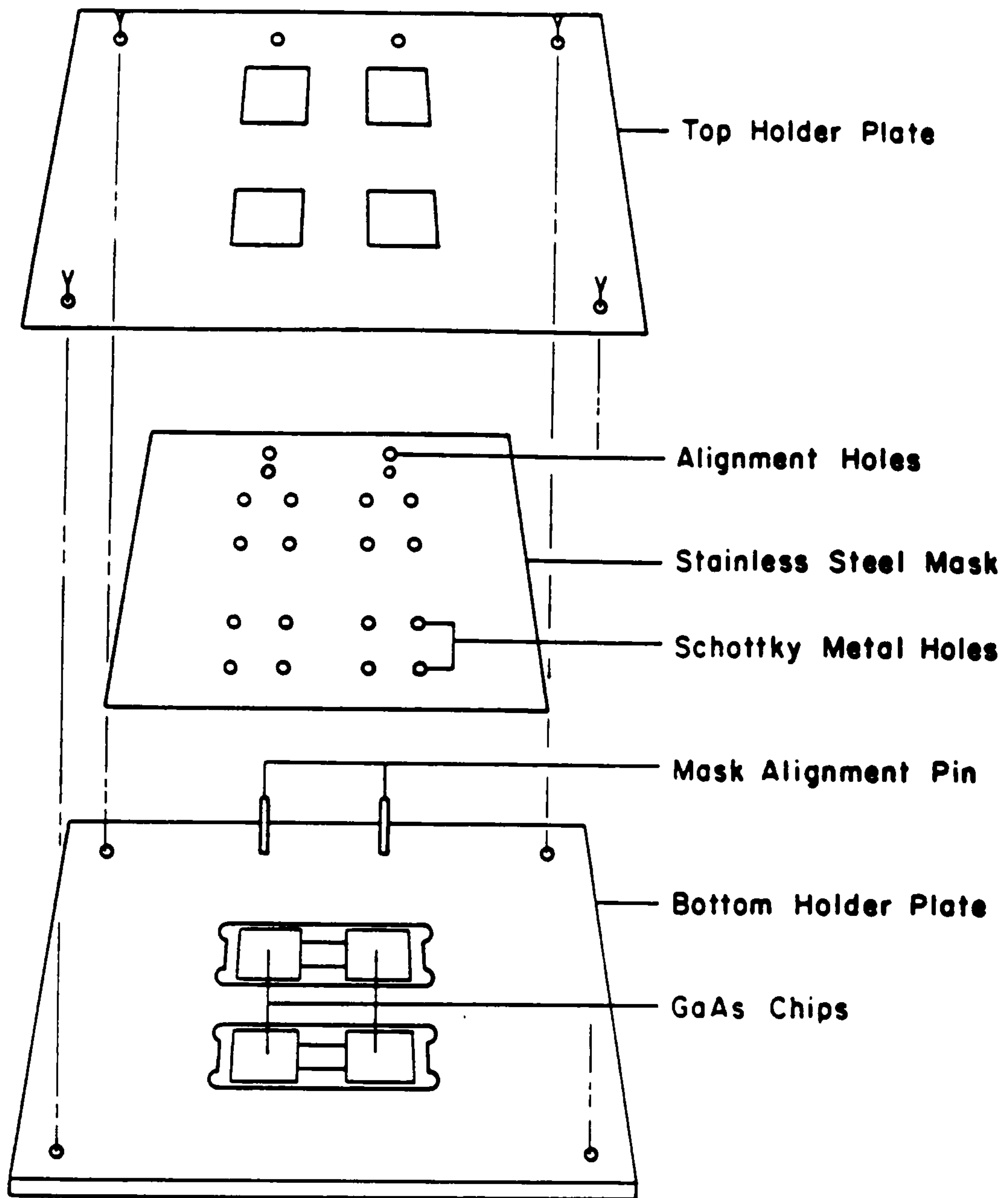


**Figure 3.5** Substrate clamping arrangement during metal evaporation [163].

### *3.5.2 Electrical Measurements*

All electrical measurements were made at room temperature (290 K). Individual diodes were scribed and cut from the larger chips and mounted into a TO-8 package by means of a thermally conductive grease. The mounted diode was electrically connected to the TO-8 header by 1 mil thick gold wires bonded by EPO-TEK H20E conductive epoxy cured at 150 °C for 5 min. Figure 3.6 shows the schematic of a mounted diode.

Current-voltage and capacitance-voltage measurements were done using a Hewlett-Packard 4140B pA/voltage source meter and 4280A 1MHz C meter, respectively. The data collection was performed through an IBM PC-AT by the means of Medusa [164,165], an automated electrical analysis system for device characterization.

## 3.6 Optical Studies

Optical studies were conducted as another means of investigating ion bombardment damage deeper into the GaAs samples than is allowed by XPS measurements. $Ar^+$ ion bombardment damage as a function of ion energy, as well as damage at 3 KeV for $^{3}He^+$, $^{20}Ne^+$, $Ar^+$, and $Xe^+$ ion bombarded samples was studied optically. For both the Raman and UV-Vis studies, measurements were taken for ion-bombarded samples and control samples from the same GaAs wafer.

### *3.6.1 Raman Spectroscopy*

The apparatus and conditions used to acquire the Raman spectra are described in the theses of M. Holtz [166] and G. Feng [167]. Raman spectra were acquired for 3 KeV $^{3}He^+$, $^{20}Ne^+$, $Ar^+$, and $Xe^+$ ion-bombarded GaAs samples. Prior to ion bombardment, the samples were treated to the chemical cleaning step (1:1 HCl(conc)/$H_2O$). The relative Raman intensity measurements were made using crystalline GaAs as a reference that was also treated with the chemical cleaning step (1:1 HCl(conc)/$H_2O$). The Raman spectra were

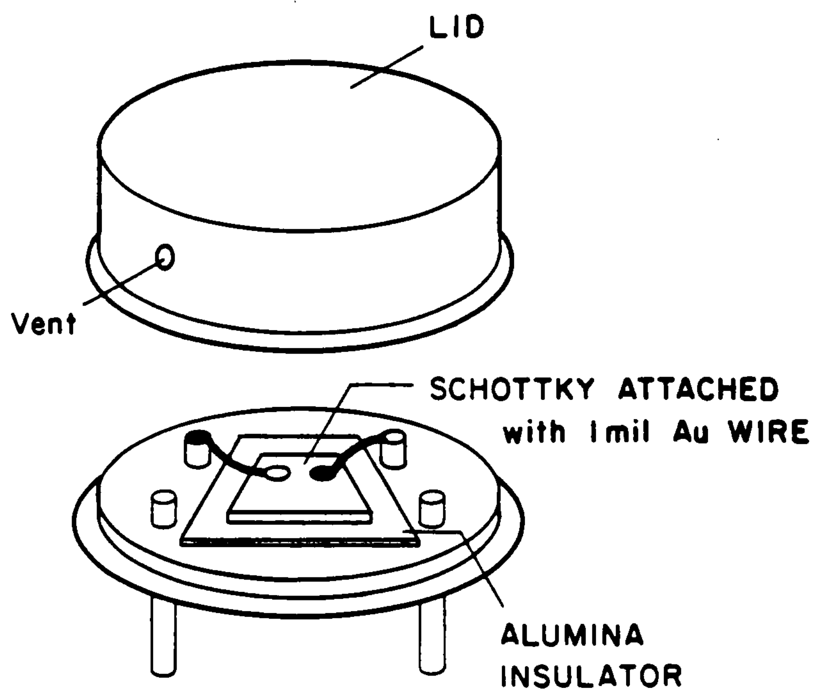


**Figure 3.6** Schematic diagram for a mounted diode [165].

acquired by A. Siochi in the VPI & SU Physics Department.

### *3.6.2 Optical Reflectivity Measurements*

Optical reflectivity spectra in the visible and near-ultraviolet region (vis-near-uv, photon energy E ranging form 1.6 to 5.6 eV) were taken at room temperature for samples ion bombarded with 0.5-4 KeV $Ar^{+}$ ions and 3 KeV $^{20}Ne^{+}$ and 3 KeV $Xe^{+}$ ions. The instrumentation for the optical reflectivity measurements is described in the thesis of G. Feng [167]. The measurements were taken in the VPI & SU Physics Department by G. Feng ($Ar^{+}$ ion-bombarded samples) and A. Siochi (3 KeV $^{20}Ne^{+}$ and $Xe^{+}$ ion-bombarded samples). The control sample and the ion-bombarded samples (prior to ion bombardment) were treated to the chemical cleaning step (1:1 HCl(conc)/$H_2O$).

# Chapter IV: Results and Discussion

## 4.1 Effects of $Ar^+$ Ion Bombardment on the Chemical Reactivity of GaAs

Since changes in the chemical reactivity of GaAs have been linked to defects caused by ion bombardment [14,40,43], it is the purpose of this section to fully examine the interaction of $O_2$ and $H_2O$, over the exposure range $10^7$ to $10^{13}$ L, with chemically cleaned and $Ar^+$ ion-bombarded (0.5-3 KeV) GaAs surfaces.

### *4.1.1 Chemically Cleaned and $Ar^+$ Ion-Bombarded GaAs*

The surface atomic composition and the relative amounts of Ga(GaAs) and As(GaAs) on the surface of GaAs following chemical cleaning and $Ar^+$ ion-bombardment determined from XPS measurements taken both at 15° and 90° toas are summarized in Table 4.1. Representative spectra for chemically cleaned and ion bombarded GaAs are shown in Figure 4.1.

Following chemical cleaning, the surface is arsenic-rich (Table 4.1). Single photopeaks are observed in the Ga 3d and As 3d regions that indicate only Ga and As of GaAs are present on the surface and no oxide species are present. However, oxygen is detected on the surface (BE 532.0 eV) that is most likely due to adsorbed oxygen [36,168,169]. No evidence for contamination from the HCl solution was detected. These observations are similar to those obtained by Bertrand [168] for HCl treated GaAs(100).

Ion bombardment of GaAs removes residual oxygen from the chemically cleaned surface; more oxygen being removed with increasing ion bombardment energy. Ion bombardment also results in the preferential sputtering of arsenic, as indicated by the increasing Ga/As atomic ratio. This finding is consistent with the results obtained by others for ion bombarded GaAs [11,13,48]. It should be noted that the oxygen content also decreases with increasing ion bombardment time up to a point where a steady-

**Table 4.1** XPS Results for Chemically Cleaned and $Ar^+$ Ion-Bombarded GaAs.

| Treatment | | ATOMIC PERCENT, toa 15°: Ga | As | O | ATOMIC PERCENT, toa 90°: Ga | As | O | Ga/As (±0.05): 15° | 90° |
|---|---|---|---|---|---|---|---|---|---|
| Chemically Cleaned | | 28.0 | 35.9 | 36.1 | 39.5 | 44.4 | 16.1 | 0.78 | 0.89 |
| **Ion Energy** | **Fluence** | | | | | | | | |
| 500 | $2\pm1\times10^{16}$ | 36.8 | 49.5 | 13.7 | 48.2 | 47.9 | 3.9 | 0.74 | 1.01 |
| 1000 | $2\pm3\times10^{16}$ | 53.2 | 42.1 | 4.7 | 54.7 | 42.8 | 2.5 | 1.26 | 1.28 |
| 2000 | $9\pm3\times10^{17}$ | 59.8 | 40.2 | $<2.0$ | 58.8 | 41.2 | $<2.0$ | 1.49 | 1.43 |
| 3000 | $9\pm4\times10^{17}$ | 60.4 | 39.6 | $<2.0$ | 60.8 | 39.2 | $<2.0$ | 1.52 | 1.55 |

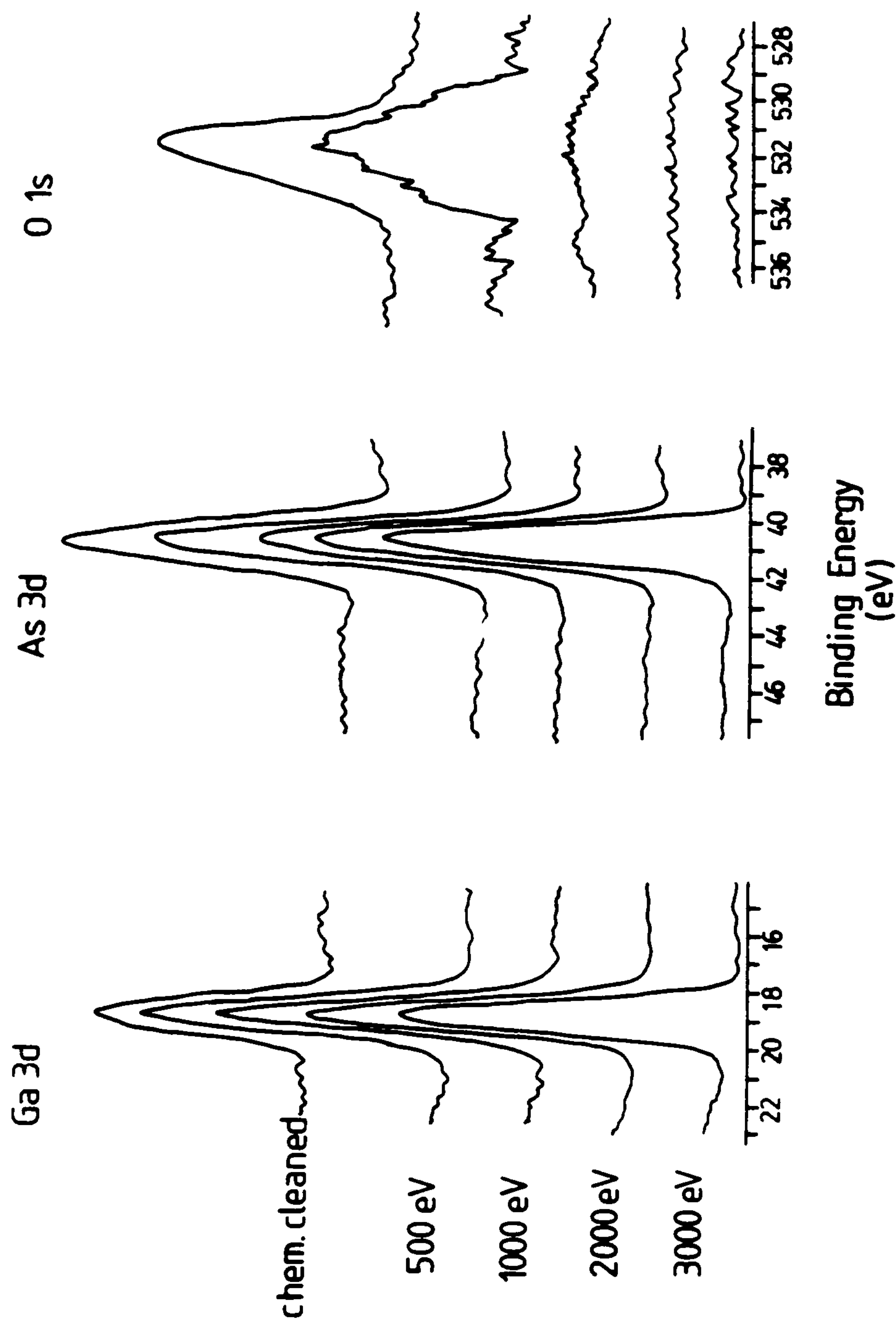


**Figure 4.1** Representative spectra taken at 15° toa for chemically cleaned and $Ar^+$ ion-bombarded GaAs.

state is reached (for the fluences used in this study) such that no change in either residual oxygen content (for 0.5 and 1 KeV) or the Ga/As atomic ratio was found. No signal is detected in the O 1s region for 2 and 3 KeV $Ar^+$ ion-bombarded GaAs samples at the fluences indicated. The <2 at.% detection limit is based on the following data. After ion bombardment at 2 and 3 KeV, the O 1s peak area was less than 400 counts-ev/sec. Corresponding Ga 3d and As 3d areas were ≈8000-9000 counts-eV/sec. From the Ga 3d, As 3d, and O 1s peak areas, the atomic concentrations were calculated according to equation 3.1, using the appropriate sensitivity factors (Table 3.1). From this calculation, a value of <2 at.% was obtained for the O 1s detection limit.

The Ga/As atomic ratios for the samples at different toas can be used qualitatively to evaluate the depth of damage caused by ion bombardment within the XPS depth sensitivity limit. The Ga/As atomic ratio for chemically cleaned GaAs is less than 1.0 at both toas indicating that an As-rich surface extends at least to 60Å into the surface. For the lowest ion bombardment energy, 500 eV, the As-rich layer is being sputtered away by ion bombardment. This is noted by the 15° Ga/As atomic ratio that is As-rich (<1.0) and the 90° Ga/As atomic ratio that is near unity (1.0). For 3, 2, and 1 KeV $Ar^+$ ion-bombarded samples, the Ga/As values at both 15° and 90° toas for the respective ion energies are equivalent within the experimental error, indicating that an As-depleted layer extends to a depth of at least 60Å. The results of McGuire [13] and Holloway *et al.* [170] state that the surface composition is dependent on both the energy and mass of the incident bombarding ion. Results presented later in this thesis for GaAs bombarded with $^3He^+$, $Ne^+$, and $Xe^+$ at the same energy support some of these results.

#### *4.1.2 $O_2$ Exposure*

The XPS spectra obtained at a 15° toa are presented for the Ga 3d, As 3d, and O 1s levels for chemically cleaned and $Ar^+$ ion-bombarded GaAs following $2x10^{11}$ L (Figure 4.2) and $10^{13}$ L (Figure 4.3) $O_2$ exposure, respectively. The Ga 3d and As 3d photopeaks both

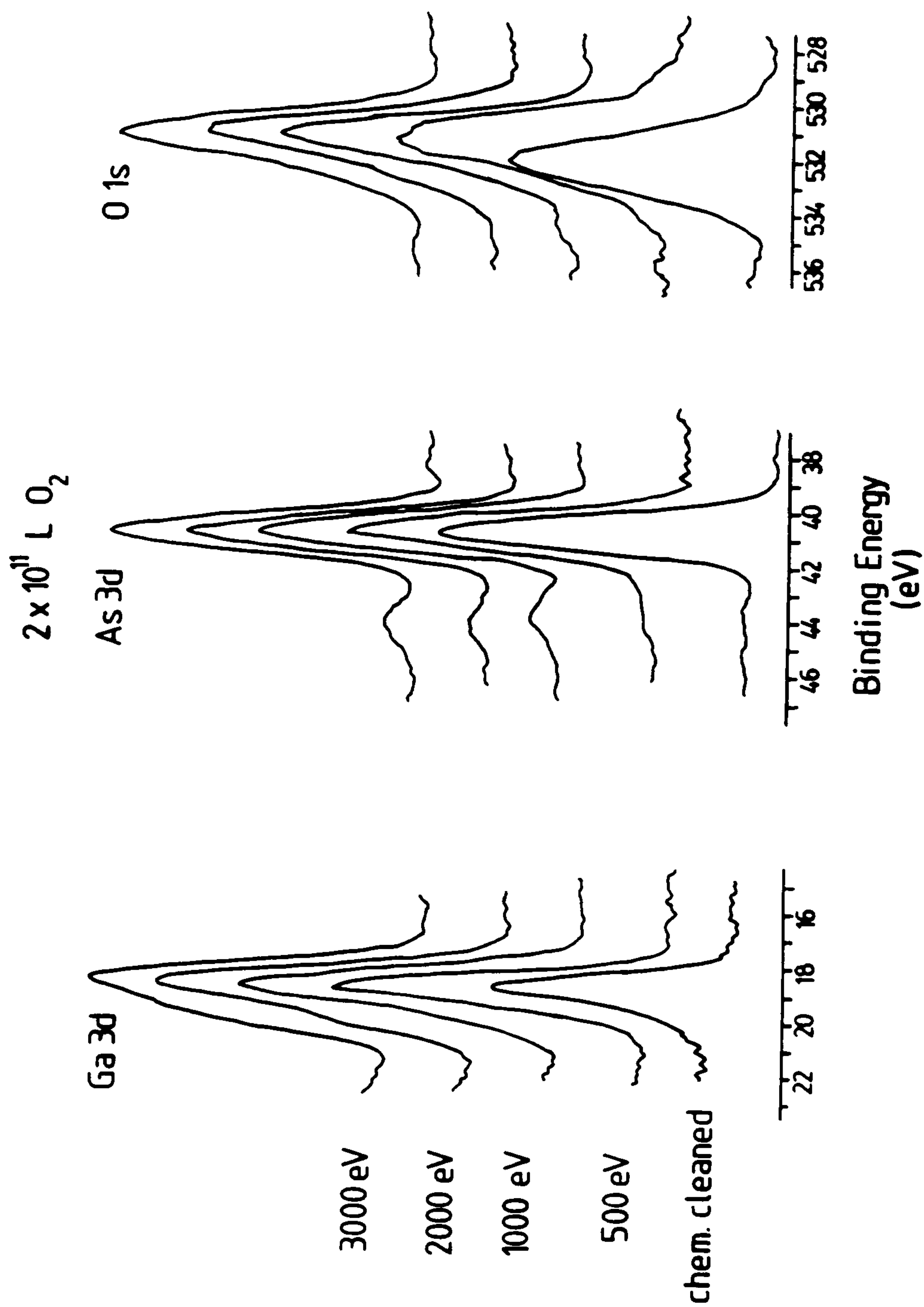


**Figure 4.2** XPS spectra for chemically cleaned and $Ar^+$ ion-bombarded GaAs exposed to $2x10^{11}$ L $O_2$.

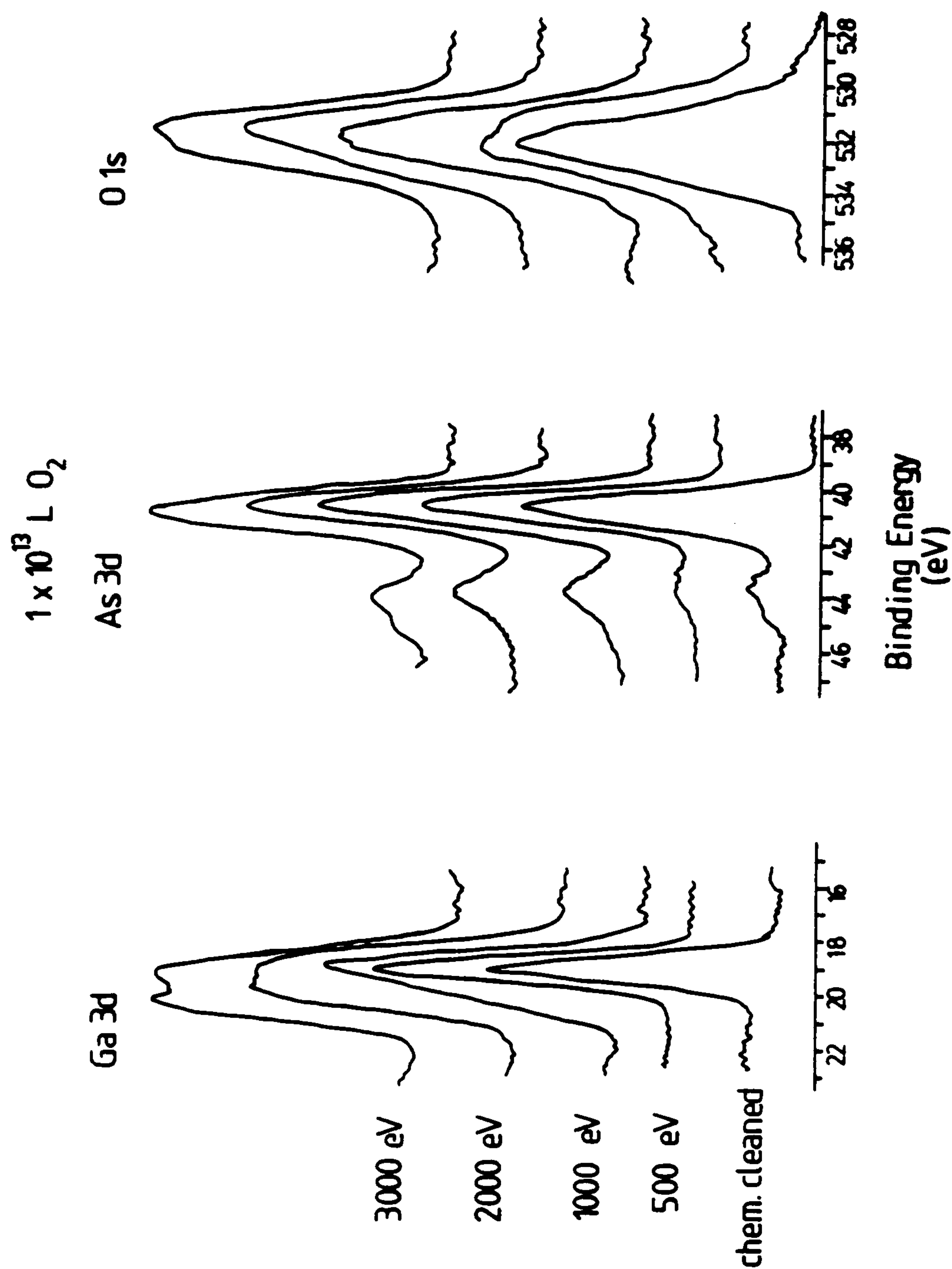


**Figure 4.3** XPS spectra for chemically cleaned and $Ar^+$ ion-bombarded GaAs exposed to $1x10^{13}$ L $O_2$.

exhibit evidence for the formation of oxides by the appearance of photopeaks on the high binding energy side of the respective substrate photopeaks. Evaluation of the percent oxide(s) in the photopeaks was accomplished by curve-resolution. The peak positions and the FWHMs used in the curve-resolution were determined by measuring XPS spectra for standard oxide compounds. The FWHM and peak positions for the Ga 3d and As 3d due to GaAs were determined from the spectra for ion bombarded GaAs. Oxygen peak intensities were selected based on knowledge of the oxygen/gallium or oxygen/arsenic ratios for the respective gallium($Ga_2O_3$) and arsenic($As_2O_3$, $As_2O_5$) oxides.

Typical curve-resolved spectra are shown in Figure 4.4 for 3 KeV $Ar^+$ ion-bombarded GaAs exposed to $10^{13}$ L $O_2$. These spectra are characterized by the photopeaks due to Ga(GaAs), As(GaAs), Ga($Ga_2O_3$), As($As_2O_3$, $As_2O_5$), O($Ga_2O_3$, $As_2O_3$, $As_2O_5$), and O(ad). Table 4.2 summarizes the binding energies obtained for the surface oxides on GaAs following $O_2$ exposure.

The relative amounts of gallium and arsenic oxides produced as a result of $O_2$ exposure are shown in Figure 4.5 following $2\times10^{11}$ L and $1\times10^{13}$ L $O_2$ exposure. The relative quantities of gallium or arsenic oxide produced are represented as:

$$\mathrm{Ga(Ga_2O_3)\ or\ [As(As_2O_3 + As_2O_5)]\ /\ [Ga(total) + As(total)]} \qquad (4.1)$$

The zero point corresponds to the results obtained for chemically cleaned GaAs. It can be seen from the relative amounts of oxides (Figure 4.5) and the changes in the XPS spectra (Figures 4.2 and 4.3) that the reactivity of ion bombarded GaAs is quite different from that of chemically cleaned GaAs.

Exposure of chemically cleaned GaAs to $O_2$ produces only $Ga_2O_3$ and $As_2O_3$. On the chemically cleaned surface the relative amounts of arsenic and gallium oxide are nearly equivalent. This is consistent with the results obtained by others for reaction on cleaved

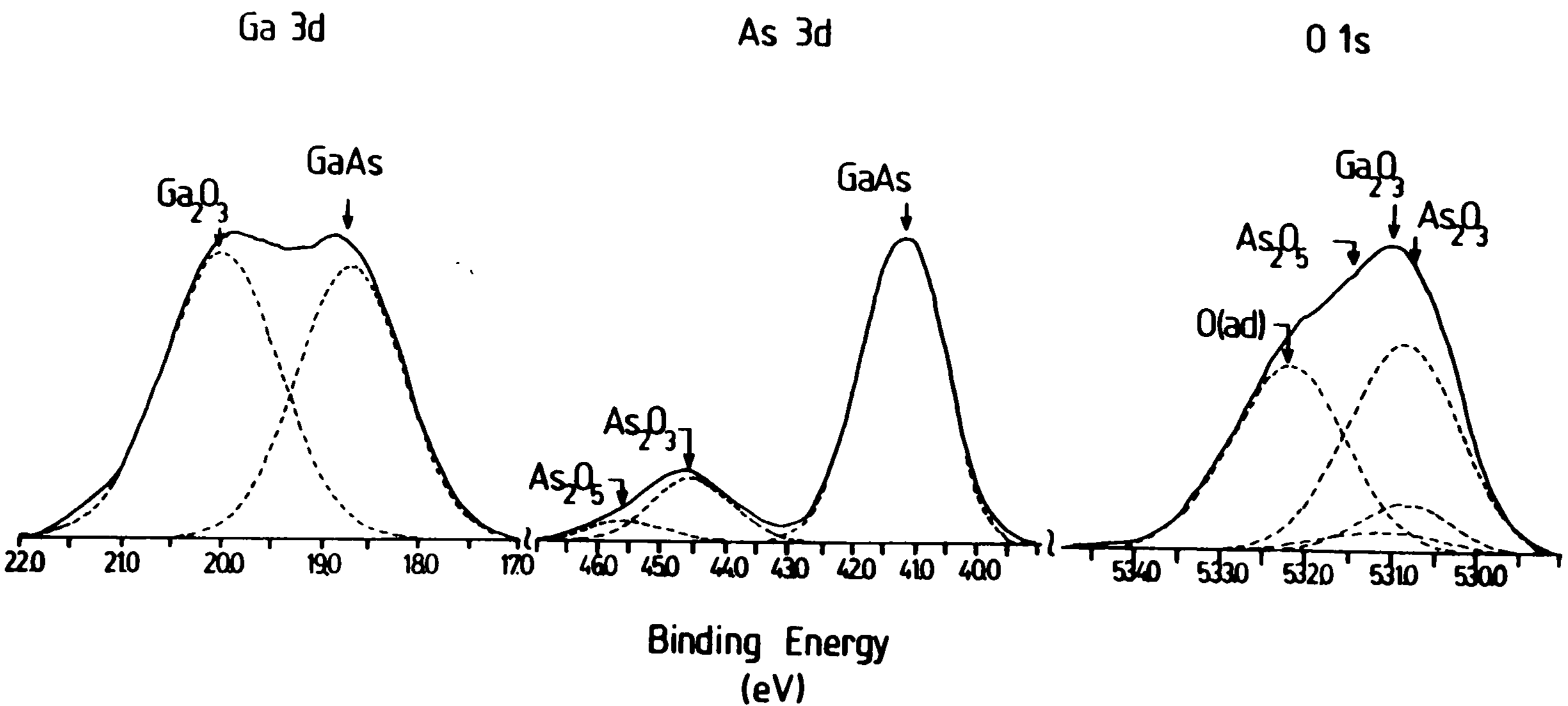


**Figure 4.4** Curve-resolved spectra for 3 KeV $Ar^+$ ion-bombarded GaAs exposed to $1x10^{13}$ L $O_2$.

**Table 4.2** Binding energies for surface components.

| Component | BE (eV) | FWHM (eV) | STANDARDS[a] (eV) | LITERATURE[b] (eV) |
|---|---|---|---|---|
| Ga(GaAs) | 18.8±0.2 | 1.2±0.2 | -------- | 19.0±0.4 |
| As(GaAs) | 40.8±0.2 | 1.5±0.2 | -------- | 41.0±0.4 |
| Ga($Ga_2O_3$) | 20.0±0.2 | 1.4±0.2 | 20.0±0.2 | 20.4±0.2 |
| Ga(GaO(OH)) | 19.9±0.2 | 1.7±0.2 | 19.8±0.4 | -------- |
| Ga($Ga(OH)_3$) | 20.9±0.2 | 1.6±0.2 | -------- | -------- |
| As($As_2O_3$) | 44.2±0.3 | 1.5±0.2 | 43.9±0.2 | 44.6±0.3 |
| As($As_2O_5$) | 45.5±0.3 | 1.6±0.2 | 45.5±0.2 | 45.7±0.1 |
| O($Ga_2O_3$) | 531.3±0.4 | 1.5±0.2 | 530.6±0.2 | 531.4±0.2 |
| O($As_2O_3$) | 530.3±0.4 | 1.3±0.2 | 530.6±0.2 | 531.6±0.2 |
| O($As_2O_5$) | 530.8±0.4 | 1.6±0.2 | 531.1±0.2 | 531.6±0.1 |
| O(ad) | 532.6±0.4 | 1.6±0.2 | -------- | 532.8[c] |
| O(Ga**O***(OH)) | 530.8±0.5 | 1.7±0.2 | 530.3±0.3 | ~530.3[c] |
| O(GaO(**O***H)) | 531.8±0.5 | 1.7±0.2 | 531.6±0.3 | ~531.5[c] |
| O($Ga(OH)_3$) | 531.8±0.5[e] | 1.7±0.2 | -------- | ~531.5[c] |
| O($H_2O$ ad) | 532.6±0.5 | 2.0±0.3 | -------- | ~533[d] |

a) This study.
b) From Reference 157.
c) From Reference 174.
d) From Reference 175.
e) No standard compound was measured for this. The binding energy is assumed to be nearly equivalent to that for -OH in GaO(OH) as explained in the text.

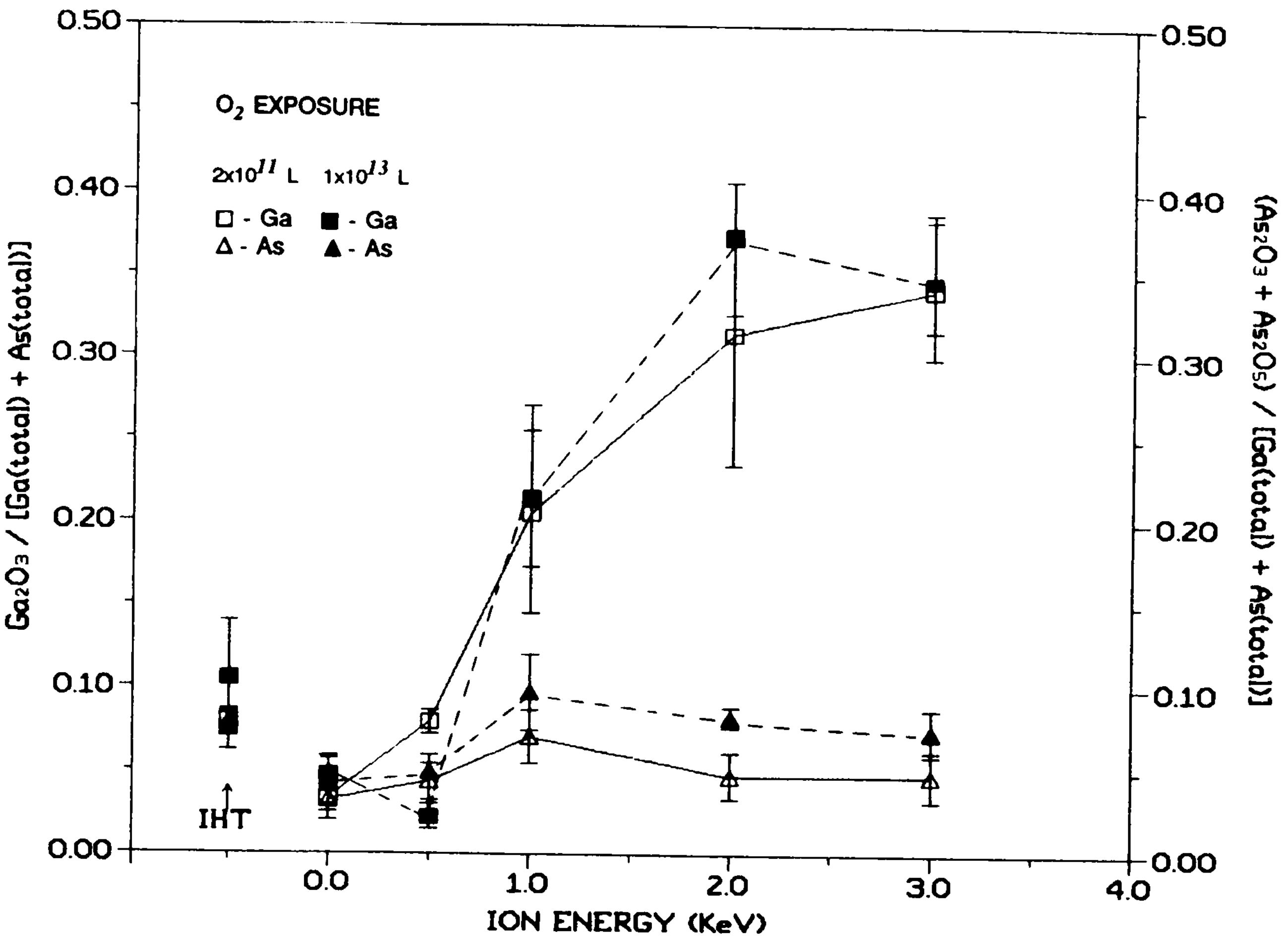


**Figure 4.5** Relative amounts of gallium and arsenic oxides for $O_2$ exposures at $2x10^{11}$ L and $1x10^{13}$ L.

and atomically clean GaAs [14,135]. Exposure of $Ar^+$ ion-bombarded GaAs to $O_2$ produces $Ga_2O_3$, $As_2O_3$, and $As_2O_5$ with preferential formation of $Ga_2O_3$. The relative amount of $Ga_2O_3$ on the surface increases with increasing $Ar^+$ ion-bombardment energy up to 2 KeV. On the other hand, the reaction of $O_2$ with ion bombarded surfaces produces approximately the same quantity of arsenic oxides as found for chemically cleaned GaAs.

The preferential formation of $Ga_2O_3$ on the ion bombarded material could be due to the larger amount of Ga(GaAs) at higher ion bombardment energies. More $Ga_2O_3$ forms because more gallium is present on the surface. It has been suggested by Chye *et al.* [14] that once the surface becomes disordered by ion bombardment, bulk thermodynamics take precedence forming gallium oxides more readily than arsenic oxides; the free energy of formation of $Ga_2O_3$ is -1004 kJ/mol and of $As_2O_3$ is -661 kJ/mol [101]. Chye *et al.* [14] note that Mark *et al.* [43] suggested that oxidation takes place first on residual defect sites and that additional disorder occurs by the exothermic release of adsorption energy. Chye *et al.* [14] argue that if $O_2$ adsorbs on native defect sites and subsequently generated defect sites, one would expect to observe roughly equal amounts of arsenic and gallium oxides on both ordered and disordered surfaces. They did not take into account the fact that the disordered surface produced by ion bombardment has a different surface Ga/As ratio than an ordered(cleaved) surface; a result of preferential sputtering of arsenic. Therefore, Chye *et al.* [14] should observe more $Ga_2O_3$ than $As_2O_3$ formation due to the presence of more gallium on the surface. Mark *et al.'s* [43] proposal of increased disorder to produce more defect sites would still influence the reactivity, but the ratio of Ga/As would also be expected to play a role in the final amount of gallium and arsenic oxides produced. However, taking into account the increasing Ga/As ratio and bulk thermodynamics or the ideas of Mark *et al.* [43] to explain the increased amount of $Ga_2O_3$ formed on ion bombarded material does not entirely account for all of the results obtained in this study.

### 4.1.3 $O_2$ Reaction with IHT GaAs

To determine what role the Ga/As ratio plays in the formation of oxides, a GaAs surface was prepared by a method other than chemical cleaning or ion bombardment, using the procedure outlined by Oelhafen *et al.* [156]; subsequently referred to as IHT treated GaAs. An IHT treated GaAs surface was obtained containing only Ga(GaAs) and As(GaAs) with a Ga/As atomic ratio of 1.23 ± 0.07 (at 15° toa) and with ≈10 at.% adsorbed oxygen on the surface. The IHT treated GaAs was exposed to $2x10^{11}$ and $1x10^{13}$ L $O_2$ and the relative amounts of gallium and arsenic oxides were approximately equal (see Figure 4.5). If the Ga/As ratio were to determine solely the amount of gallium and arsenic oxides formed following $O_2$ exposure, one would expect results similar to that for 1 KeV $Ar^+$ ion-bombarded GaAs exposed to $O_2$, where the Ga/As ratio before exposure was 1.26 (15° toa). However, the results for IHT treated GaAs are similar to those for chemically cleaned GaAs (Ga/As = 0.6). The amount of oxide formed following $O_2$ exposure of IHT treated GaAs is also similar to the amount of oxide formed for a cleaved GaAs(110) surface exposed to $O_2$. Approximately equal amounts of gallium and arsenic oxides are formed on a cleaved GaAs(110) surface exposed to $O_2$ ($10^7$-$10^{13}$ L) [66]. The result that less gallium oxide forms on a surface rich in Ga but which was not ion bombarded demonstrates that ion bombardment influences the reaction chemistry of GaAs. It is reasonable that ion bombardment produces defects and/or disordered GaAs as the ion bombardment energy increases and that reaction takes place at defect sites [14,35,36,40,41,43,70,72,77,83,102,127,171]. Goddard *et al.* [83] suggest that defect sites with broken Ga-As bonds are needed to form a strong bond to molecular $O_2$ and that the defect sites catalyze the dissociation of $O_2$ into chemisorbed O atoms which can then attack nearby Ga or As atoms to form oxides. For ion bombarded GaAs, greater production of $Ga_2O_3$ would occur with increasing ion bombardment energy; a result of the generation of disordered sites around Ga atoms since As is preferentially removed by sputtering.

There is a small amount of oxygen detected (<5 at.%) on 0.5 and 1 KeV $Ar^+$ ion-bombarded material as well as IHT material (<10 at.%). The presence of this small amount of oxygen would appear to be affecting the adsorption of oxygen (less being adsorbed by 0.5, 1 KeV, and IHT material) and the overall results would be less oxide formation due to the presence of an initial amount of adsorbed oxygen which would block further oxygen adsorption. However, there is experimental evidence that the presence of <10 at.% oxygen will not affect the adsorption and oxide formation. Three samples, 3 KeV $Ar^+$ ion-bombarded, contained an average of 8 at.% oxygen before $O_2$ exposure. Following $O_2$ ($10^{11}$-$10^{13}$ L) exposure, they produced the same relative amounts of oxide (within experimental error) as those samples that contained no detectable oxygen before exposure. Therefore, it would appear that the presence of a small amount of oxygen (<10 at.%) before $O_2$ exposure does not affect the final adsorption results and the presence of defects are controlling the reaction.

### *4.1.4 Chemical Forms of $O_2$ on GaAs Surface*

The adsorption of $O_2$ on chemically cleaned and ion bombarded materials at room temperature yields chemisorbed molecular oxygen and atomic oxygen by dissociative adsorption. Brundle and Seybold [36] discussed the reaction of $O_2$ with cleaved GaAs(110) over the exposure range $10^5$ to $10^{14}$ L and noted that only dissociatively adsorbed oxygen forms gallium and arsenic oxides directly. In the XPS study of O 1s photopeaks, Brundle and Seybold [36] observed oxygen only with a binding energy near that for $Ga_2O_3$ and $As_2O_3$ (~531 eV). However, in this study (see curve fits in Figure 4.4) the oxygen photopeak is composed of species due to oxides and an additional photopeak at higher binding energy, 532.6 eV, which is attributed to chemisorbed molecular oxygen [36,171,174]. The amount of chemisorbed molecular oxygen increases with increasing $O_2$ exposure. A likely process is that dissociative adsorption takes place first to form the oxides and then

molecular oxygen is adsorbed onto the oxide layer. That this process occurs is more apparent for 3 KeV ion-bombarded GaAs exposed to $O_2$ (see Figure 4.6). An increase in the amount of oxides (both Ga and As) is evident by the increased intensity of higher binding energy Ga and As photopeaks relative to Ga(GaAs) and As(GaAs) peaks. At the same time the O 1s peak intensity at higher binding energy increases more significantly with increasing exposure. This indicates that the majority of oxide formation takes place up to $10^{11}$ L and increased exposure does not significantly increase the amount formed. The initial exposure to oxygen probably forms a protective layer of $Ga_2O_3$ (the major component), $As_2O_3$, and $As_2O_5$. Any further oxide formation would either depend upon the inward diffusion of oxygen through the oxide layer to oxidize underlying GaAs or by the outward diffusion of either As or Ga where the breaking of crystal bonds would be the limiting step in the oxidation process [172]. Thus, only an increase in molecularly adsorbed $O_2$ relative to chemisorbed oxygen is noted in the O 1s photopeak for $O_2$ exposures above $10^{11}$ L.

### *4.1.5 $H_2O$ Exposure*

The XPS spectra are presented in Figure 4.7 for the Ga 3d, As 3d, and O 1s levels for chemically cleaned and $Ar^+$ ion-bombarded GaAs following $H_2O$ exposure at $10^{10}$ L. After $H_2O$ exposure, a broadening occurs on the higher binding energy side of the Ga 3d photopeak while no change is observed for the As 3d photopeak. Broadening of the Ga 3d photopeak was also observed by Webb and Lichtensteiger [79] for GaAs exposed to $H_2O$.

Curve-resolved XPS spectra for the Ga 3d and O 1s photopeaks for the 3 KeV $Ar^+$ ion-bombarded GaAs as a function of $H_2O$ exposure are shown in Figure 4.8. For $H_2O$ exposures of $10^{10}$ L, the FWHM of the higher binding energy photopeak in the Ga 3d region was slightly broader than what had been previously observed for the same peak following $O_2$ exposures (the photopeak due to $Ga_2O_3$). The FWHM of the Ga 3d photopeak for GaO(OH) is generally broader than that for $Ga_2O_3$; 1.7±0.2 and 1.4±0.2, respectively. For

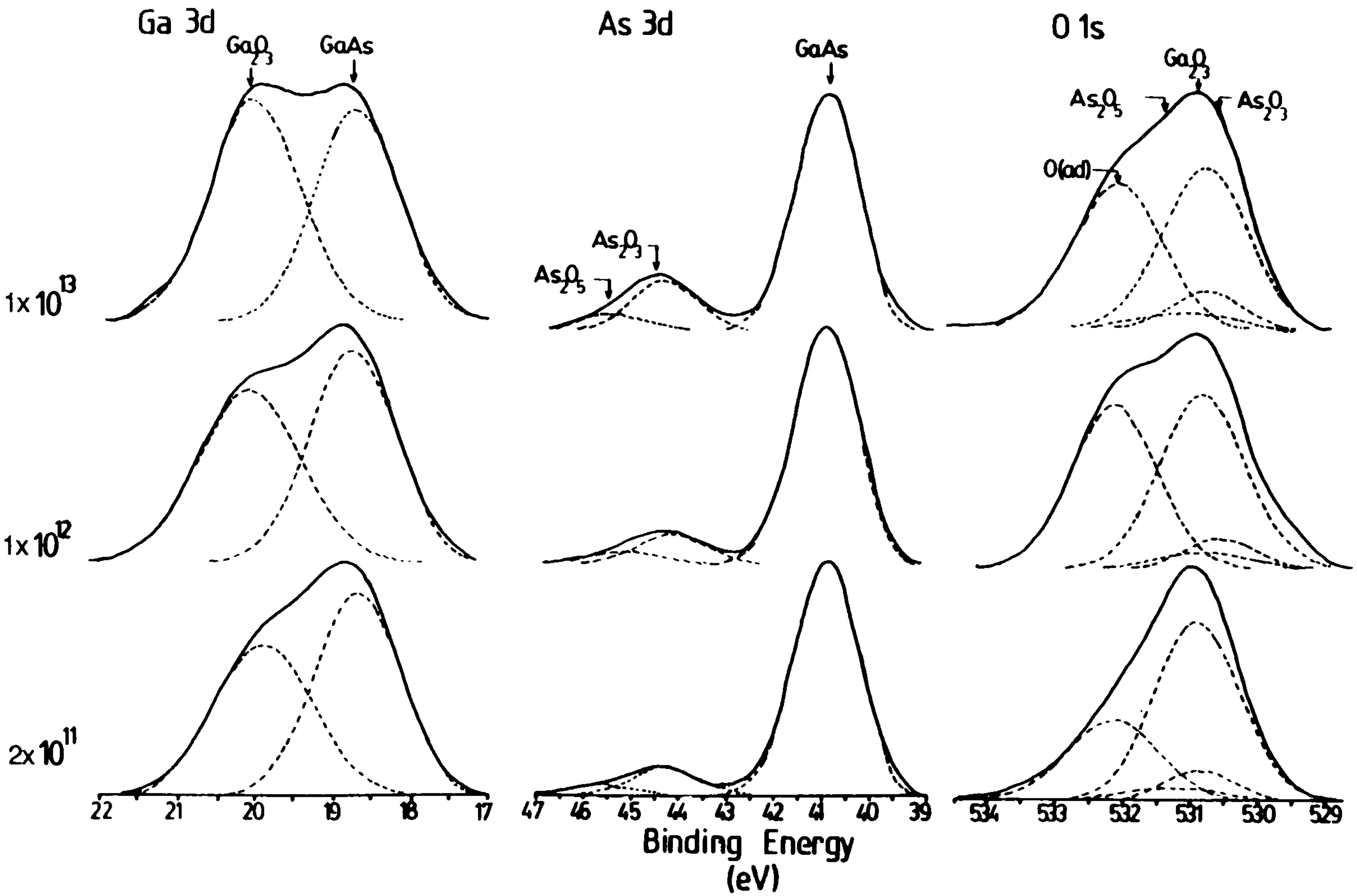


**Figure 4.6** Curve-resolved spectra for 3 KeV $Ar^+$ ion-bombarded GaAs exposed to $2x10^{11}$, $1x10^{12}$, and $1x10^{13}$ L $O_2$.

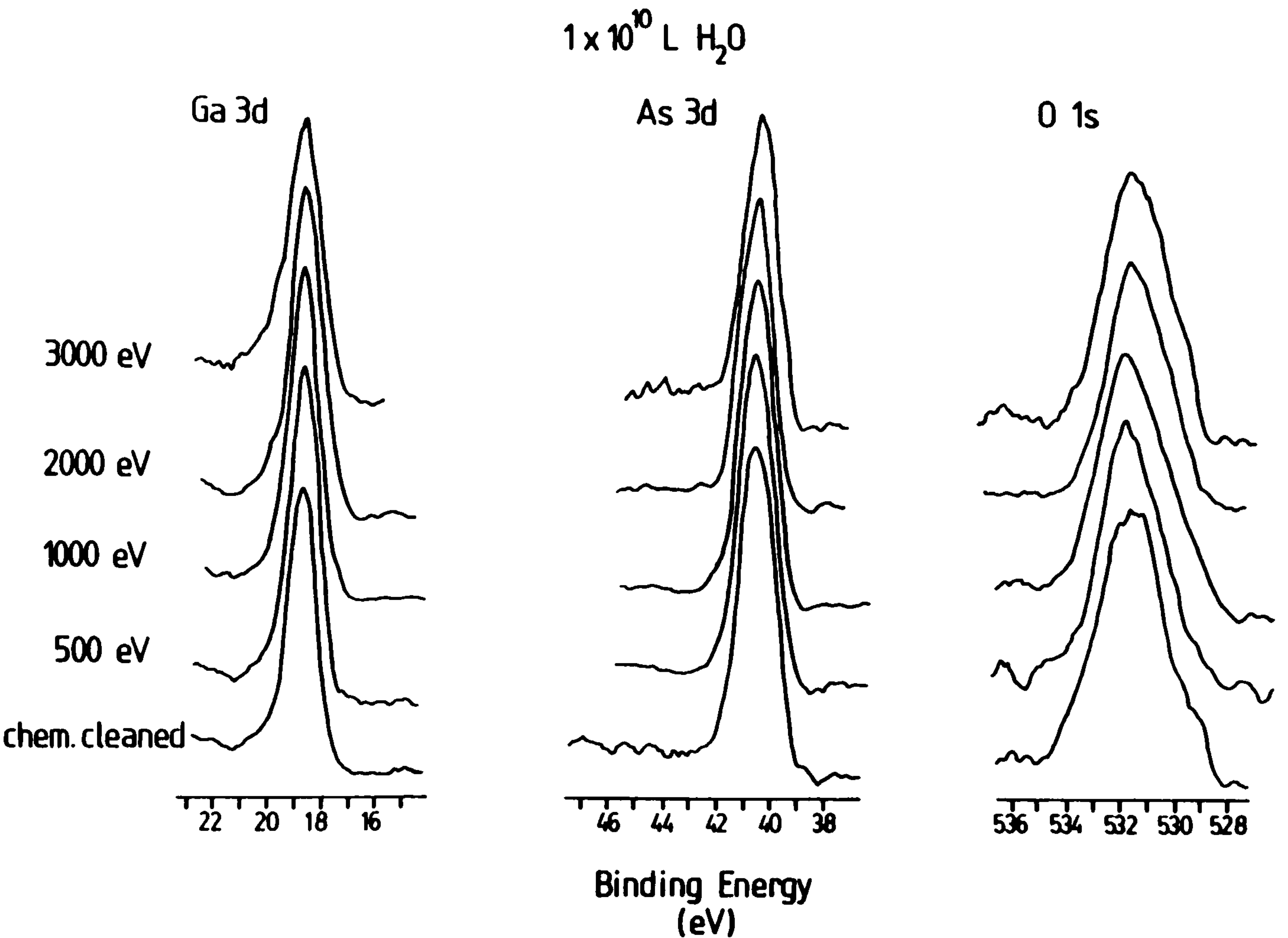


**Figure 4.7** XPS spectra for chemically cleaned and $Ar^+$ ion-bombarded GaAs exposed to $1x10^{10}$ L $H_2O$.

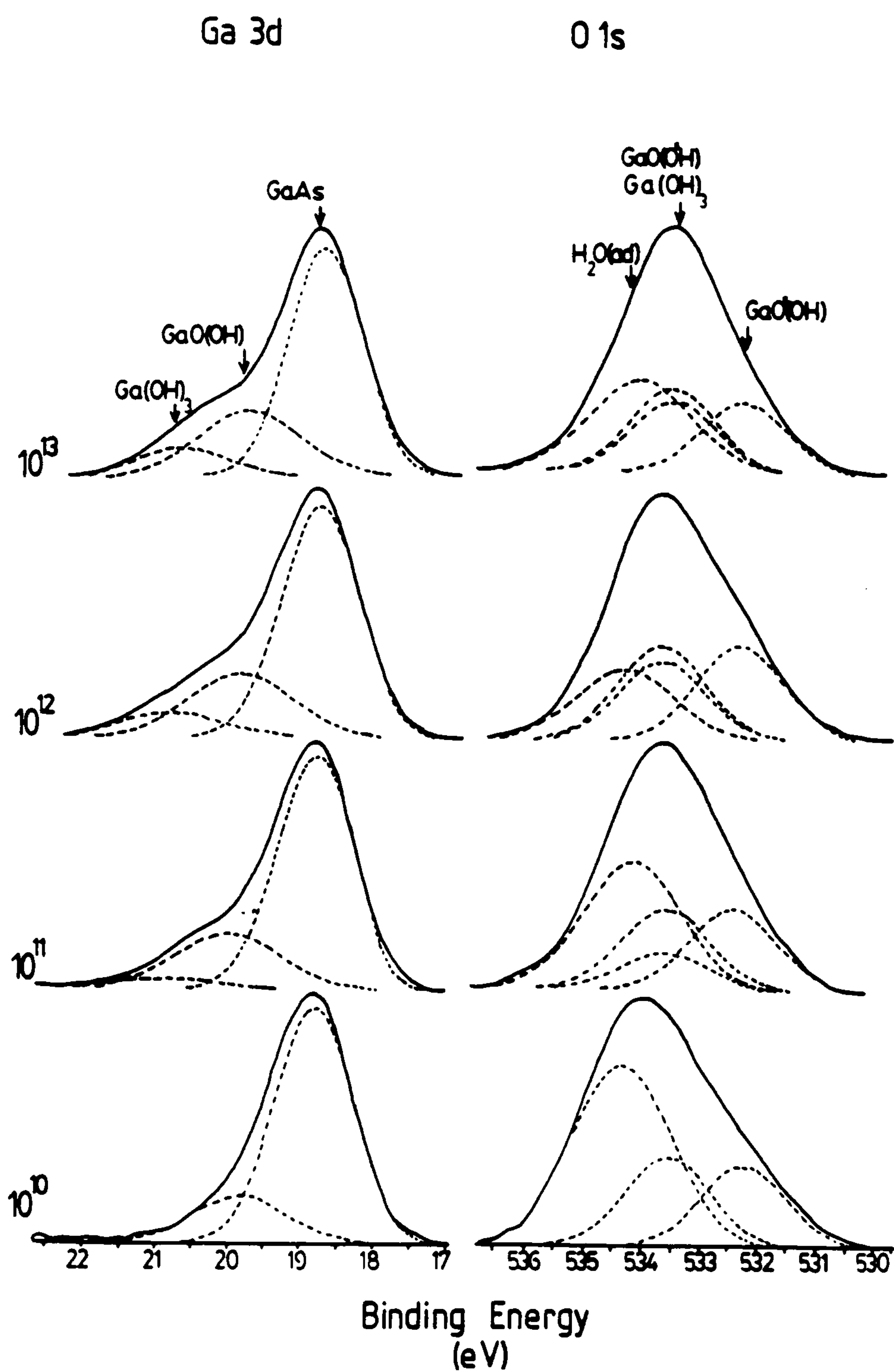


**Figure 4.8** Curve-resolved spectra for 3 KeV $Ar^+$ ion-bombarded GaAs exposed to $10^{10}$, $10^{11}$, $10^{12}$, and $10^{13}$ L $H_2O$.

this reason the Ga 3d and O 1s photopeaks ($10^{10}$ L $H_2O$) were curve resolved to include $Ga_2O_3$, GaO(OH), or different combinations of each. From the results of these curve resolutions, the best possible fits were obtained when GaO(OH) was assumed to be the species present following $H_2O$ exposure. The spectra shown in Figure 4.8 are characterized by photopeaks due to Ga(GaAs), Ga(GaO(OH)), O(Ga**O***(OH)), O(GaO(**O***H)), and O($H_2O$ ad) using the peak positions and FWHM that were determined from measurements on standard materials. The experimental peak positions as well as those obtained for the standard materials are summarized in Table 4.2 (p. 65).

For exposures above $10^{10}$ L $H_2O$, including a single photopeak in the Ga 3d region for GaO(OH) is no longer sufficient. A new photopeak, shifted 0.7-1.0 eV higher than that for GaO(OH), is needed to complete the curve fit as shown in Figure 4.8. This broadening may indicate the formation of another gallium-containing species, possibly $Ga(OH)_3$ [79,173]. For $10^{10}$ L $H_2O$ exposures described above, the photopeaks were first curve resolved by including $Ga_2O_3$, GaO(OH), or $Ga(OH)_3$ as well as possible combinations of all three species. Besides the peak positions and FWHM, one of the main considerations used in curve-fitting the photopeaks following $H_2O$ exposure was the relationship between the ratio Ga 3d/$\sigma$ : O 1s/$\sigma$ ($\sigma$ is the appropriate sensitivity factor) for each of the species $Ga_2O_3$, GaOOH, and $Ga(OH)_3$. The atomic ratios Ga : O for $Ga_2O_3$, GaOOH, and $Ga(OH)_3$ are 1:1.5, 1:2, 1:3, respectively. The curve-fitting procedure consists of obtaining a good fit in the Ga 3d region for the peaks being considered, followed by placing the appropriate peaks in the O 1s region based on the atomic ratios of the species and re-adjusting the peaks in the O 1s and Ga 3d regions until reasonable fits are obtained. From the Ga : O ratio and the known peak positions, it became evident that $Ga_2O_3$ was not one of the species present following $H_2O$ exposure. Its presence was ruled out from curve-fitting the O 1s photopeak. If only GaOOH and $Ga_2O_3$ are included, the O 1s photopeak is shifted to a lower binding energy than the experimental peak and the broadening on the higher binding energy side of

the Ga 3d peak cannot be explained. If only $Ga_2O_3$ (instead of GaOOH) is included along with $Ga(OH)_3$, a reasonable fit is obtained for the Ga 3d photopeak; however, not enough oxygen can be accounted for in the O 1s region. The best possible results were obtained using combinations of GaO(OH) and $Ga(OH)_3$. Even though good fits were obtained, there still is oxygen unaccounted for in the O 1s region at higher binding energy (≈533 eV). This was attributed to chemisorbed $H_2O$. Therefore, the photopeaks in Figure 4.8 for exposures above $10^{10}$ L are curve fit to include GaO(OH) and $Ga(OH)_3$ as well as the respective contributions to the O 1s photopeaks for these species. The -OH of $Ga(OH)_3$ was assumed to have an O 1s peak position similar to -OH in GaO(OH) [174]. The O($H_2O$ ad) peak position was taken from the literature [174,175].

The formation of $Ga(OH)_3$ occurs only for 2 and 3 KeV ion-bombarded GaAs exposed to $H_2O$ above $10^{10}$ L and the amount of $Ga(OH)_3$ produced increases with increasing $H_2O$ exposure. The relative amount of GaO(OH) and $Ga(OH)_3$ formed following $H_2O$ exposure is presented in Figure 4.9 for exposures of $10^{10}$ and $10^{11}$ L as a function of $Ar^+$ ion-bombardment energy. The trend is similar to that found for GaAs exposed to $O_2$ in that the relative amount of oxidized Ga increases with increasing ion bombardment energy up to 2 KeV. Also, the reaction of ion bombarded material is greater than that for chemically cleaned GaAs. The adsorption of $H_2O$ onto ion bombarded GaAs also produces peaks in the O 1s region due to O from GaO(OH), $Ga(OH)_3$, and that due to chemisorbed $H_2O$.

These results are similar to those of Webb and Lichtensteiger [79] and Childs *et al.* [35] who found that $H_2O$ predominantly bonds to Ga sites. Webb and Lichtensteiger [79] also observed the dissociative adsorption of $H_2O$ in the formation of Ga-OH bonds for exposures above $10^9$ L (from UPS and SIMS results). GaAs exposed to $H_2O$ has been shown to adsorb $H_2O$ in a two-step process: an initial step of molecular adsorption onto Ga sites [79,111,112] followed by a physisorbed or condensed $H_2O$ layer [79,112] for exposures greater than $10^6$ L. Above $10^6$ L, $H_2O$ dissociates to form $Ga(OH)_x$ species. The results of

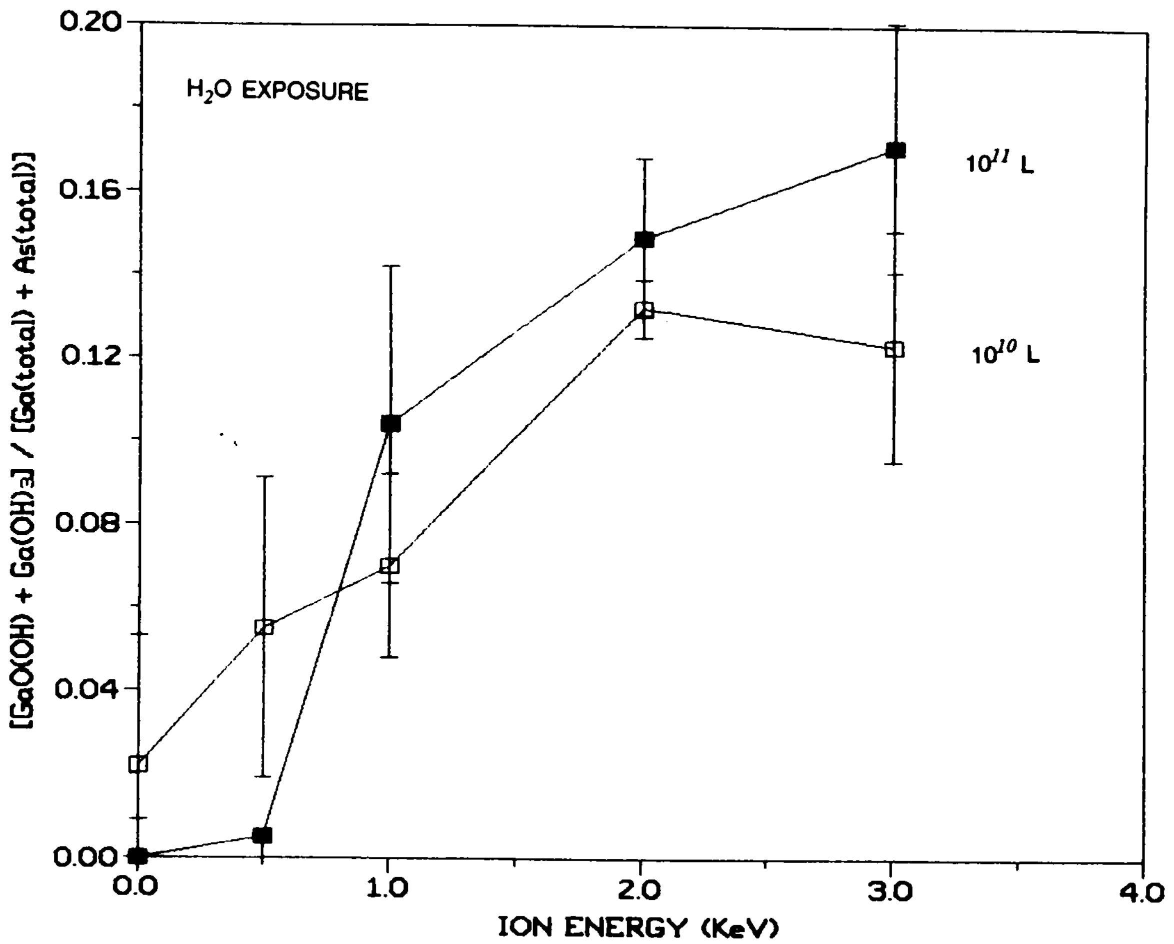


**Figure 4.9** Relative amounts of GaO(OH) and $Ga(OH)_3$ for $H_2O$ exposure of $Ar^+$ ion-bombarded GaAs.

this study suggest that water dissociatively reacts to form GaO(OH) and $Ga(OH)_3$ and is also molecularly adsorbed (chemisorbed) on the surface for ion bombarded GaAs exposed to $H_2O$. GaO(OH) is the predominant species for exposures below $10^{11}$ L $H_2O$. Above $10^{11}$ L exposure, further broadening of the Ga 3d photopeak is observed and is attributed to $Ga(OH)_3$ formation. These two different species have not been observed on chemically cleaned or annealed GaAs exposed to $H_2O$ [79]. Water dissociatively adsorbs on Si forming SiOH and SiH bonds [109]. It is reasonable to suggest that upon dissociative adsorption on ion bombarded GaAs, water forms GaOH and AsH bonds. A reaction of $H_2O$ with GaAs could include

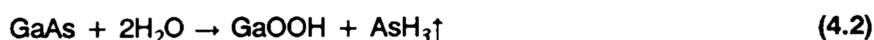

$$GaAs + 2H_2O \rightarrow GaOOH + AsH_3\uparrow \quad (4.2)$$

when only GaOOH is formed, and

$$2GaAs + 5H_2O \rightarrow GaOOH + Ga(OH)_3 + 2AsH_3\uparrow \quad (4.3)$$

when both GaOOH and $Ga(OH)_3$ are formed. It is not known whether AsH bonds form or whether $AsH_3$ is formed and released in the process. An alternate explanation offered by Childs *et al.* [109] is that $H_2O$ adsorbs dissociatively into chemisorbed O and $H_2$, which would be evolved from the surface during the reaction. However, if dissociation into O and $H_2$ were to occur, the hydroxide species would not be formed.

The total atomic concentration of oxygen determined from data taken at a 15° toa is presented in Table 4.3. Indicated in Figure 4.10 are the relative distributions of GaOOH and $Ga(OH)_3$ as a function of $H_2O$ exposure. The atomic concentration of oxygen does not increase with increasing $H_2O$ exposure. This would indicate that an intial amount of $H_2O$ is adsorbed upon the first $H_2O$ exposure at $10^{10}$ L. The adsorbed layer does not consist of

**Table 4.3** Atomic concentration of oxygen for 3 KeV $Ar^+$ ion-bombarded GaAs exposed to $H_2O$.

| Exposure (L) | Oxygen (atomic%) |
|---|---|
| $1 \times 10^{10}$ | $34 \pm 2$ |
| $4 \times 10^{11}$ | $43 \pm 4$ |
| $2 \times 10^{12}$ | $39 \pm 4$ |
| $1 \times 10^{13}$ | $43 \pm 4$ |

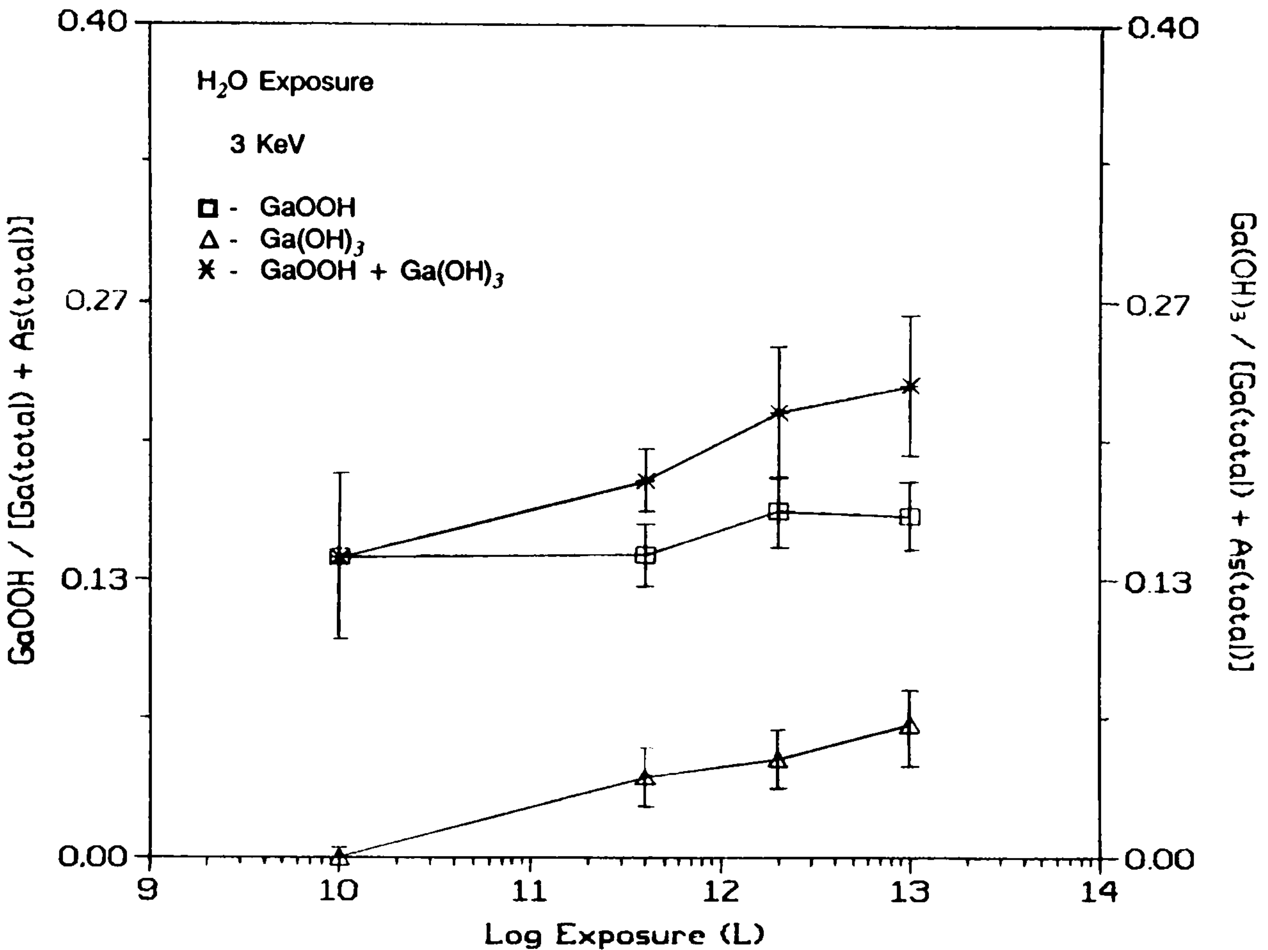


**Figure 4.10** Relative amounts of GaOOH and $Ga(OH)_3$ formed following $H_2O$ exposure for 3 KeV $Ar^+$ ion-bombarded GaAs.

only adsorbed $H_2O$; some dissociative adsorption takes place at this initial exposure to form GaOOH ($10^{10}$ L, Fig. 4.10). Since the total amount of oxygen does not change with increasing exposure, this would suggest that the initially adsorbed $H_2O$ layer dissociatively reacts to form GaOOH and $Ga(OH)_3$, and the increasing amounts of these species are not due to increasing $H_2O$ exposure, but to the dissociation of the initially adsorbed $H_2O$ layer over time. Both GaOOH and $Ga(OH)_3$ increase, but the concentration of GaOOH is always greater than $Ga(OH)_3$.

## 4.2 Effect of Varying Bombarding Ion

McGuire [13] and Holloway [58,170] stated that the surface composition is dependent on both the energy and mass of the incident bombarding ion. The mass of the primary bombarding ion determines the maximum amount of energy that can be transferred to an atom in the target at a given $E_o$ (equation 2.1). The penetration depth of the primary ion into the target is also determined by size. Lighter ions are expected to transfer less energy to the substrate upon collision, but can penetrate deeper into the target due to their size. Also, because a lighter ion loses less of its initial energy upon collision with the surface atoms, it is able to penetrate deeper into the surface because it is not stopped as quickly as a heavier ion. Table 4.4 summarizes the atomic radii and projected ranges for several primary ions. The initial transfer of energy and penetration depth are responsible for setting the collision cascade into motion which in turn determines how much damage and how deep is the damage layer (see Figure 2.9). The amount of surface damage and the depth of the damage could affect the chemical reactivity of a material as was already discussed in section 4.1. The dependence of the surface composition as a function of energy for a primary ion of fixed mass was discussed in section 4.1.1. In this section the effect of the incident bombarding ion mass on the surface composition will be examined and the effect of the variation in energy will be discussed.

**Table 4.4** Atomic radii and projected ranges for primary ions.

| ATOMIC RADIUS (Å)[a] | | PROJECTED RANGE (Å)[b] |
|---|---|---|
| He | 0.5 | --- |
| Ne | 0.7 | 56.8 |
| Ar | 0.9 | 43.6 |
| Xe | 1.3 | 28.4 |

Projected range is an average of 2.0 and 5.0 KeV projectiles and Ge target

a) Reference 182.

b) Reference 54.

### 4.2.1 *Ion Bombardment Effects on GaAs Surface Composition*

Chemically cleaned GaAs was ion bombarded with $^{3}He^{+}$, $^{20}Ne^{+}$ (referred to as $Ne^{+}$), $Ar^{+}$, and $Xe^{+}$ at 3 KeV ($10^{17}$ ions/cm$^{2}$) and at 1 KeV ($10^{17}$ ions/cm$^{2}$) for $Ar^{+}$ and $Xe^{+}$ to determine what effect varying the incident bombarding ion mass would have on the surface composition and reactivity. The relative amounts of Ga(GaAs) and As(GaAs) on the surface following ion bombardment with different mass ions as determined from XPS measurements taken at various take-off angles are summarized in Table 4.5 and Figures 4.11a and 4.11b. Ion bombardment of GaAs removes residual oxygen from the chemically cleaned surface, with more oxygen being removed with increasing ion bombardment energy. For the surfaces bombarded with different ions at an energy of 3 KeV, no residual oxygen (<2 at.%) was detected and therefore, only the Ga/As atomic ratio is reported.

Figures 4.11a and 4.11b compare the Ga/As atomic ratios following ion bombardment as a function of toa. Arsenic is preferentially sputtered from the GaAs surface in all cases as indicated by the Ga/As atomic ratios that are all greater than one. The extent of As depletion is greater for the heavier ions (at fixed energy) and the trend is the same as discussed previously for As depletion as a function of energy. For $^{3}He^{+}$ ion-bombardment at 3 KeV, preferential sputtering of As still occurs but not to the extent that is found for the heavier ions.

From equation 2.1, the maximum energy transfer equation, it can be predicted that more "damage" will be produced on a surface with increasing mass of the bombarding ion. The word "damage" is used in this context to mean sputtering or a disruption in the surface composition compared to the bulk. Table 4.6 lists values for $T_{max}$, the maximum energy transferred to an individual Ga or As atom, calculated from equation 2.1 for each of the bombarding ions at 1 and 3 KeV. From these values, it can be seen that the heavier ions transfer more energy to a Ga or As atom than do the lighter ions and since the equation is directly proportional to the bombarding ion energy, $E_o$, it is clear that more energy is

**Table 4.5** Ga/As atomic ratios for GaAs bombarded with various ions.

| | Ga/As | | | | | |
|---|---|---|---|---|---|---|
| Take-off Angle | 15 | 30 | 45 | 60 | 75 | 90 |
| Ion | | | | | | |
| 3 KeV $Xe^+$ | 1.73 | 1.79 | 1.80 | 1.76 | 1.70 | 1.73 |
| 3 KeV $Ar^+$ | 1.50 | 1.54 | 1.50 | 1.47 | 1.52 | 1.53 |
| 3 KeV $^{20}Ne^+$ | 1.32 | 1.42 | 1.28 | 1.12 | --- | 1.36 |
| 3 KeV $^{3}He^+$ | 1.16 | --- | --- | --- | --- | 1.22 |
| 1 KeV $Xe^+$ | 1.27 | 1.23 | 1.17 | 1.15 | --- | 1.29 |
| 1 KeV $Ar^+$ | 1.37 | --- | --- | --- | --- | 1.30 |

---- not measured

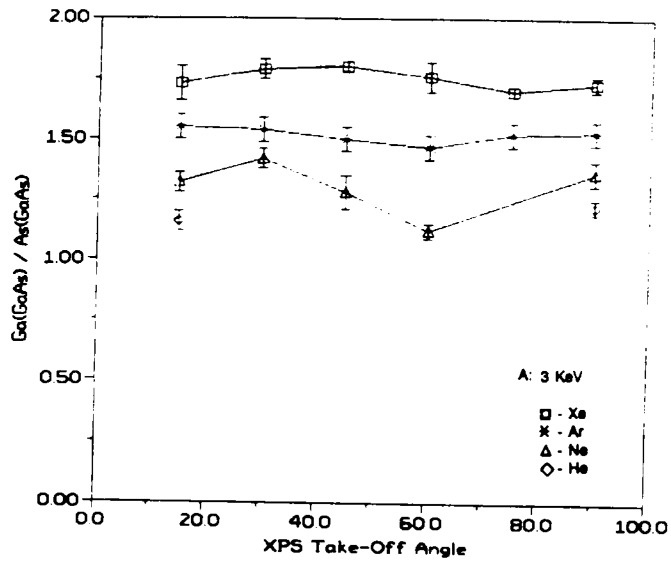


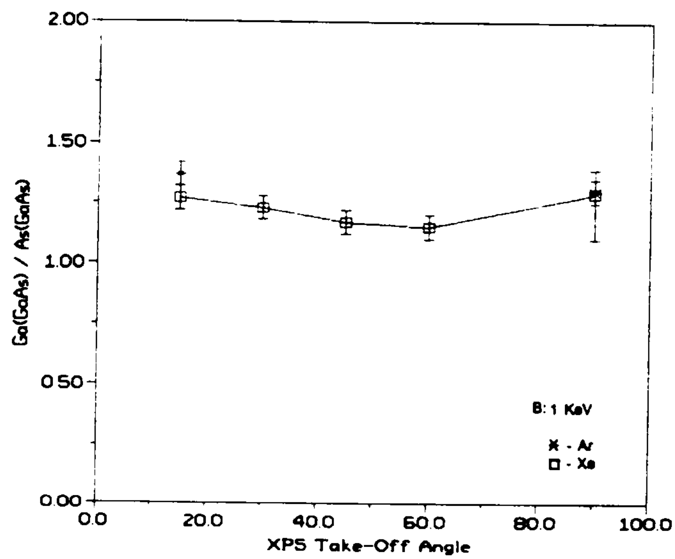


**Figure 4.11** Ga/As atomic ratios as a function of take-off angle.

**Table 4.6** $T_{max}$ values.

| | 1 KeV | | 3 KeV | |
|---|---|---|---|---|
| | Ga | As | Ga | As |
| $^{3}He^{+}$ | 0.158 | 0.144 | 0.474 | 0.432 |
| $^{20}Ne^{+}$ | 0.697 | 0.669 | 2.09 | 2.01 |
| $^{40}Ar^{+}$ | 0.926 | 0.907 | 2.78 | 2.72 |
| $^{131}Xe^{+}$ | 0.906 | 0.925 | 2.72 | 2.78 |

transferred if $E_o$ is greater.

However, $T_{max}$ values are not sufficient when trying to explain the As depletion following ion bombardment. The values for $T_{max}$ indicate no real preference for a greater energy transfer to either Ga or As. It is almost always the general case that the lighter atom is preferentially ejected from the surface during sputtering [57]. However, for GaAs this is not the case. Kelly [57] has proposed a chemical bonding model for preferential sputtering that predicts a higher sputtering yield for the more weakly bound surface species in a binary alloy, AB. From this model, there are two possible ways to account for the preferential sputtering of As from GaAs.

One model, which is proposed by Kelly [57] and discussed by Singer *et al.* [11], suggests that the preferentially sputtered species would have the lowest heat of atomization $\Delta H^a$ of the pair. Table 4.7 lists the heats of sublimation $\Delta H^\nu$, a measure of $\Delta H^a$, for three species sputtered from GaAs [11]. Assuming that only atomic Ga or As is sputtered from a surface, then Kelly's model would predict that Ga would be the preferentially sputtered species. However, Szymonski and Bhattacharya [177] have monitored the sputtered neutral particles ejected from GaAs (6 KeV $Ar^+$, 500 $\mu A \cdot cm^{-2}$) and observed $As_2$ as a significant fraction of sputtered particles (~28%). $As_2$ has a lower $\Delta H^\nu$ value than As in atomic form, and the formation of $As_2$ species during ion bombardment may account for the preferential sputtering of As as predicted by Kelly's model, since it would be the more weakly bound surface species.

Another model, which may be the more likely reason for preferential sputtering, involves thermal sputtering. Kelly's model predicts that thermal sputtering will be significant with any substance that exhibits a vapor pressure at a temperature, T, that exceeds a critical value which was estimated to be $10^{2\pm1}$ atm. In other words, the more volatile element will be preferentially sputtered from the surface. Elemental As and elemental Ga develop a vapor pressure of 133 Pa at 380 °C and 1350 °C, respectively [178]. Most ion bombardment

**Table 4.7** Heats of sublimation [176].

| Species | $\Delta H^{\nu}$(eV/atom) |
|---|---|
| $As(s) \rightarrow As(g)$ | 3.13 |
| $Ga(s) \rightarrow Ga(g)$ | 2.87 |
| $2As(s) \rightarrow As_2(g)$ | 2.30 |

experiments, as well as those in this work, are not carried out with any temperature control during the ion bombardment process. Local heating at the surface most likely occurs and since As is more volatile than Ga, this would also contribute to the preferential sputtering of As.

As discussed in section 4.1.1, the Ga/As atomic ratios at different toas can be used to evaluate the depth of damage caused by the different masses of bombarding ions. For each of the ions, the extent of As depletion is fairly uniform over the depth examined (~60Å). The endpoints given for $^{3}He^{+}$ in Figure 4.11a also indicate the same trend. However, the data for $Ne^{+}$ indicate a slight non-uniformity in the As depletion with depth, although it is just outside the experimental error of the measurement. Even though As depletion of an ion-bombarded surface is unanimously reported in the literature, the uniformity of the damaged surface layer is not agreed upon.

For GaAs sputtered with 1.5, 3, and 5 KeV $Ar^{+}$, Bussing *et al.* [180] observed composition depth profiles that show a surface composition near the bulk ratio, a subsurface As depletion, the extent of which increases with increasing ion energy and then a return to the bulk composition at a greater depth. They suggest that the disturbed layer is coincident with the penetration range of ions and their results support "the mechanism of preferential sputtering due to Gibbsian surface segregation, the As on the surface being replenished by diffusion from the disturbed layer with a diffusion rate enhanced by the higher defect density in the bombarded region." Wang and Holloway [48] observed the usual As depletion (1-5 KeV $Ar^{+}$/100-300 $\mu A \cdot cm^{-2}$) and the extent of depletion increased with increasing ion energy. However, the outer most surface was As depleted for low energy $Ar^{+}$ ion bombardment ($\leq$1 KeV); but for 3 and 5 KeV $Ar^{+}$ ion-bombardment the surface showed an As enrichment.

Neither of the above results was observed in this study. The differences from laboratory to laboratory could be due to the different ion bombardment conditions. Bussing *et al.* [180] used an ion beam oriented at 20° from the sample surface with no statement as to the

ion currents or ion bombardment time. Wang and Holloway [48] used an ion beam oriented at 15° with ion currents in the range 100-300 $\mu A \cdot cm^{-2}$. In this study, an ion beam oriented at 45° to the sample normal with beam currents $\leq 40$ $\mu \cdot cm^{-2}$ was used. The bombardment conditions could account for some of the differences since sputter yields and ion implantation depths are dependent on the incidence angle of the ion beam (see equation 2.3).

Another fact that could account for differences in the results of different groups could be in the treatment and composition of the initial surfaces before ion bombardment. The surface of chemically cleaned GaAs used in this study before ion bombardment was initially As-rich; however, no mention is made of the initial composition of the surfaces in any of the studies mentioned above. Most GaAs surface preparation involves some type of chemical etch, usually some mixture of $H_2SO_4$ : $H_2O_2$ : $H_2O$ before ion bombardment. This etch usually leaves a small amount of oxide on the surface. The chemical cleaning used in this study leaves no oxide on the GaAs(100) surface. The crystal surface orientation could also be important in determining the final surface composition. The results mentioned above were for GaAs(110), not GaAs(100), which could possibly react differently to the sputter conditions used by the various groups. A GaAs(110) crystal was sputtered with 3 KeV $Ar^+$ ions (under conditions used in this study) for a comparison and the Ga/As atomic ratio and depth of As depletion measured by XPS were not different from that observed for GaAs(100).

To summarize the results in this study, ion bombardment of GaAs(100) under the present experimental conditions produces a surface that is depleted in As. The extent of depletion is a function of the ion energy (fixed mass) and a function of the ion mass (fixed energy). The resulting surface shows a nearly uniform As depletion to a depth of at least 60Å (as measured by XPS).

### *4.2.2 Depth and Composition of Damaged Layer*

Among the questions that arise for ion bombarded GaAs materials are: 1) in what state (amorphous/crystalline) is the ion bombarded GaAs surface, 2) what is the depth of the damaged layer, and 3) in what form are Ga and As? These questions will be addressed in the following paragraphs.

The crystalline character of GaAs can be evaluated from optical measurements made in the visible and near ultraviolet region (E ranging from 1.6-5.6 eV). Crystalline GaAs exhibits a characteristic spectrum in this energy range and any decrease in the ordered structure towards one that is amorphous will alter the appearance of the spectrum [183,185]. In the energy range (1.5-5.6 eV), the optical penetration depth is of the order of 100Å (see Figure 4.12) and therefore, the type of damage and the depth of damage to the crystal structure caused by ion bombardment can be evaluated for a depth that is a little deeper than what could be probed by XPS.

Figure 4.13 shows a series of ultraviolet reflectivity spectra acquired for $Ar^+$ ion-bombarded GaAs at various energies. Also shown for comparison are those spectra obtained for crystalline and completely amorphous GaAs [181]. The reflectivity spectra in the photon energy region indicated in Figure 4.13 reflects the direct (k-vector conserved) interband electronic transitions. The three main peaks in the spectrum for crystalline GaAs are commonly denoted as $E_1$(2.9 eV), $E_1+\Delta_1$(3.1 eV, which is the spin-orbit split component of $E_1$) and $E_2$(5.0 eV, the interband transition) [185]. What is important to note when comparing these spectra is the shape and intensity of the three main peaks.

Figure 4.13 shows that $Ar^+$ ion-bombardment as low as 1 KeV begins to destroy the local crystalline order in the GaAs surface. Ion bombardment causes a decrease in the intensity of the $E_2$ peak, broadening of both the $E_1$ and $E_2$ peaks, and destruction of the $E_1$ splitting. These effects increase with increasing $Ar^+$ ion-bombardment energy and it is found that the crystal surface structure approaches that of amorphous GaAs. Feng *et al.*

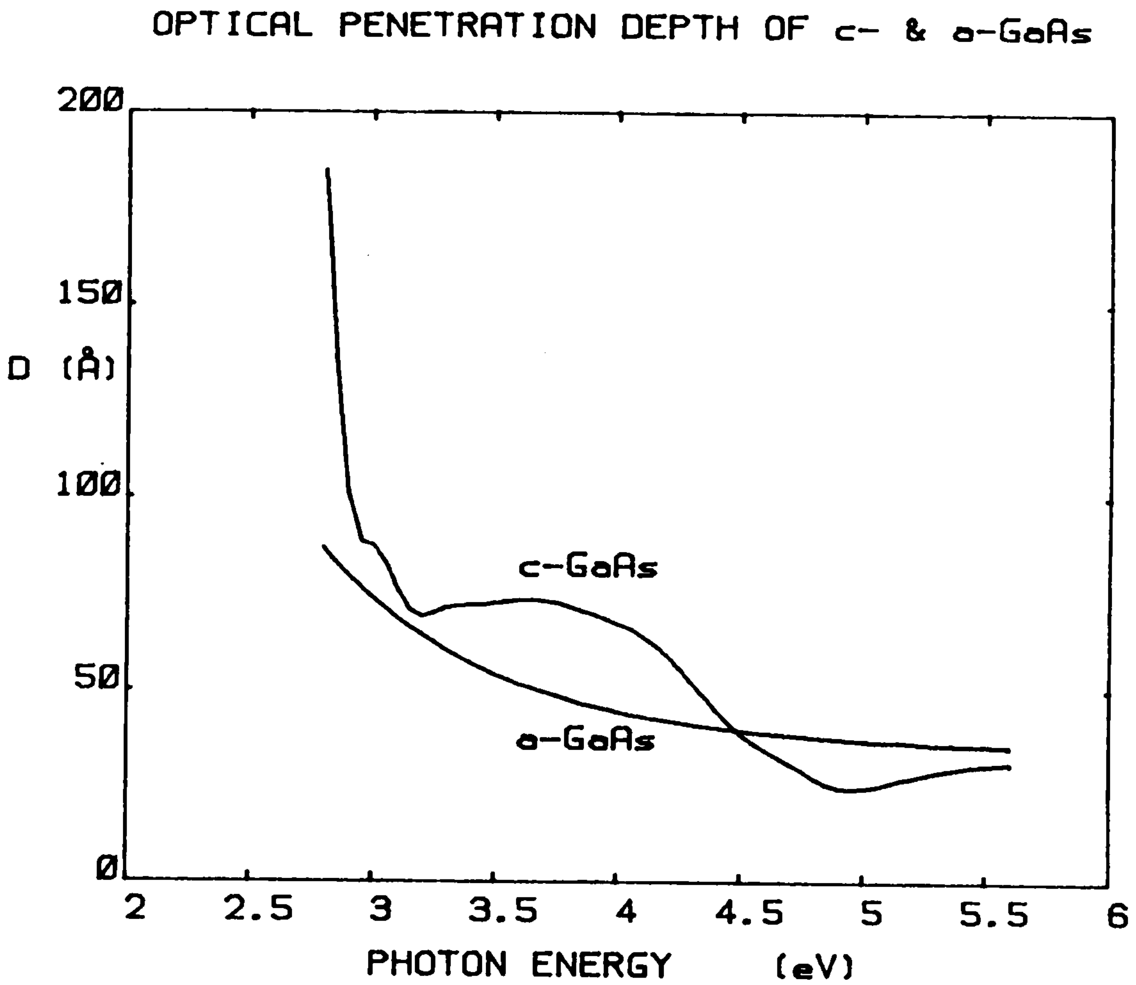


**Figure 4.12** Optical penetration depth for crystalline and amorphous GaAs [167].

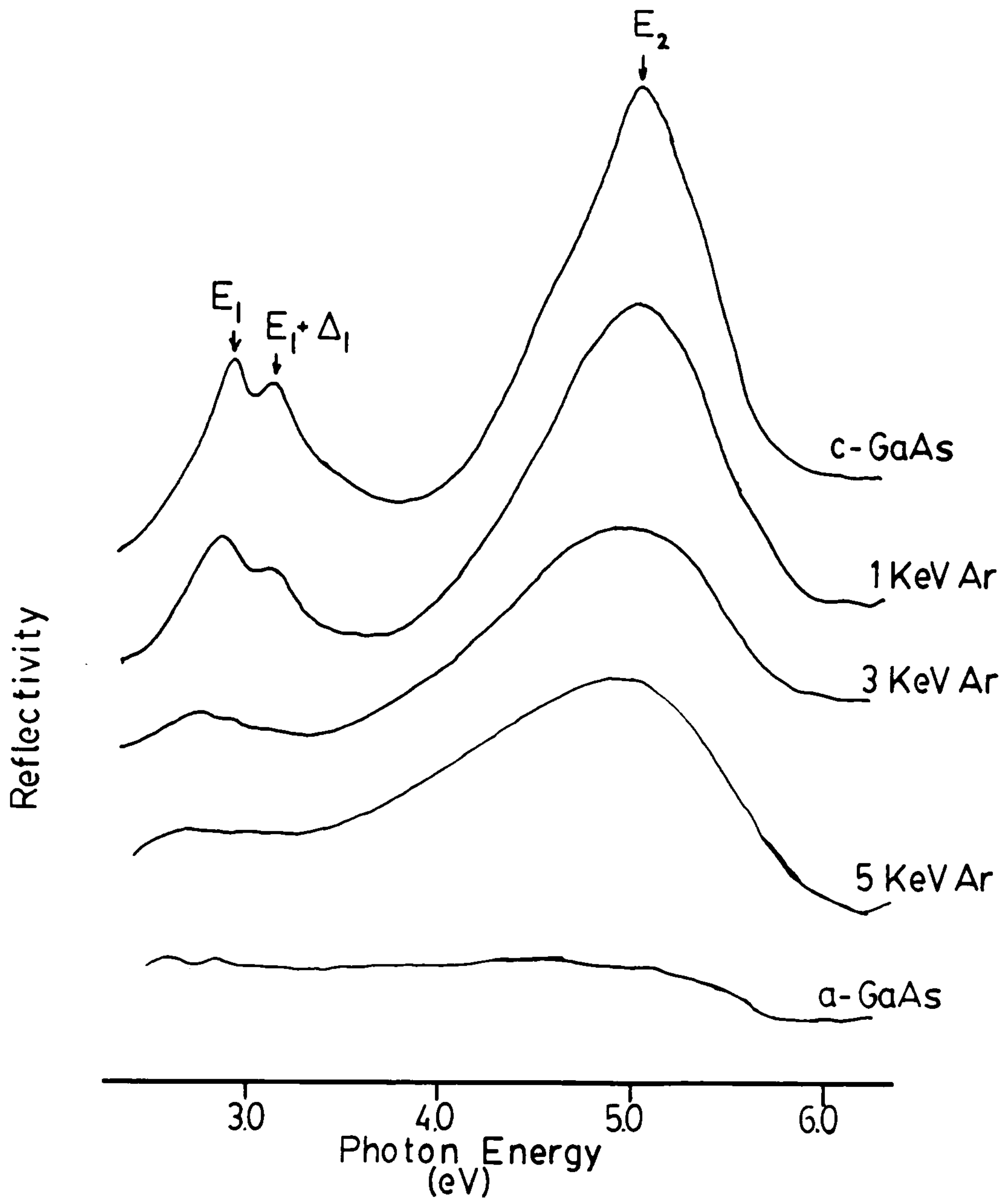


**Figure 4.13** Reflectivity spectra obtained for crystalline, amorphous [181], and $Ar^{+}$ ion-bombarded GaAs.

[185] obtained the complex dielectric function by the Lorentzian oscillator analysis for the series of spectra in Figure 4.13 and compared it with that of crystalline and amorphous GaAs. They determined that for 4 KeV $Ar^+$ ion-bombarded GaAs, about 45% of the near-surface region has been transformed to amorphous GaAs [186]. Also from the combination of the results from the reflectivity, Raman, and chemical etching studies of Feng *et al.* [185], it was found that the $Ar^+$ ion-bombarded surface structure can be viewed as a two-phase mixture consisting of crystalline and amorphous phases, the amounts of either are dependent on the ion bombardment energy. The damage distribution is Gaussian-like and the depth of damage is also dependent on ion energy (fixed mass). The damage depths determined for $Ar^+$ ion-bombarded GaAs for various energies are summarized in Table 4.8.

Figure 4.14 shows the reflectivity spectra acquired for GaAs bombarded with $Xe^+$ and $Ne^+$ ions at 3 KeV with crystalline GaAs included as a reference. Figure 4.15 shows the Raman spectra acquired for crystalline GaAs and GaAs ion bombarded with $^3He^+$, $Ne^+$, and $Xe^+$ at 3 KeV. Figure 4.16 shows the capacitance-voltage characteristics obtained for GaAs ion bombarded with $Ne^+$, $Ar^+$, and $Xe^+$ ions at 3 KeV. A more complete picture of the type and depth of damage caused by different ions at one energy is obtained by examining the results from Figures 4.14, 4.15, and 4.16.

An estimate of the depth of damage caused by different ions at one energy can be obtained by examining the Raman spectra in Figure 4.15 and the capacitance-voltage measurements in Figure 4.16. The absorption coefficient, $\alpha$, is smaller for amorphous GaAs than crystalline GaAs so that the laser beam probing depth, $1/(2\alpha)$, at the photon energy 2.71 eV (Ar-ion laser, 4579Å) is about 250Å for crystalline GaAs and 100Å for amorphous GaAs [167]. The probing depth for ion bombarded GaAs falls in between those values. The sharp, intense peak shown in the Raman spectra at 292 $cm^{-1}$ corresponds to the first-order LO Raman mode (a longitudinal optical mode [187]) in crystalline GaAs. The peaks in the area of 500-580 $cm^{-1}$ correspond to the second-order LO Raman mode (2LO) [167]. The

**Table 4.8** Damage depths obtained from reflectivity and Raman measurements for $Ar^+$ ion-bombarded GaAs [185].

| ENERGY (eV) | DAMAGE DEPTH (Å)* |
|---|---|
| 500 | 100 |
| 1000 | 200 |
| 2000 | 400 |
| 4000 | 500 |

* All values are approximate (±20%)

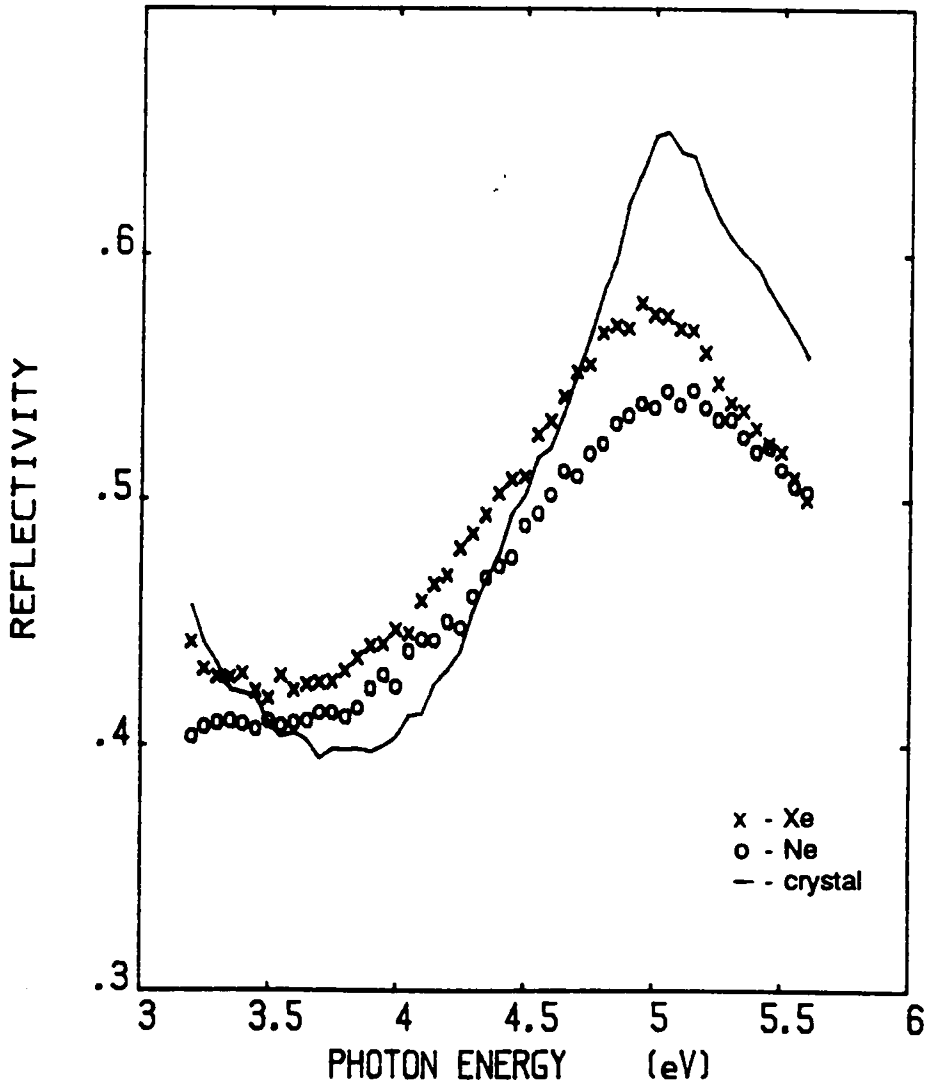


**Figure 4.14** Reflectivity spectra obtained for crystalline, 3 KeV $Ne^+$, and $Xe^+$ ion-bombarded GaAs.

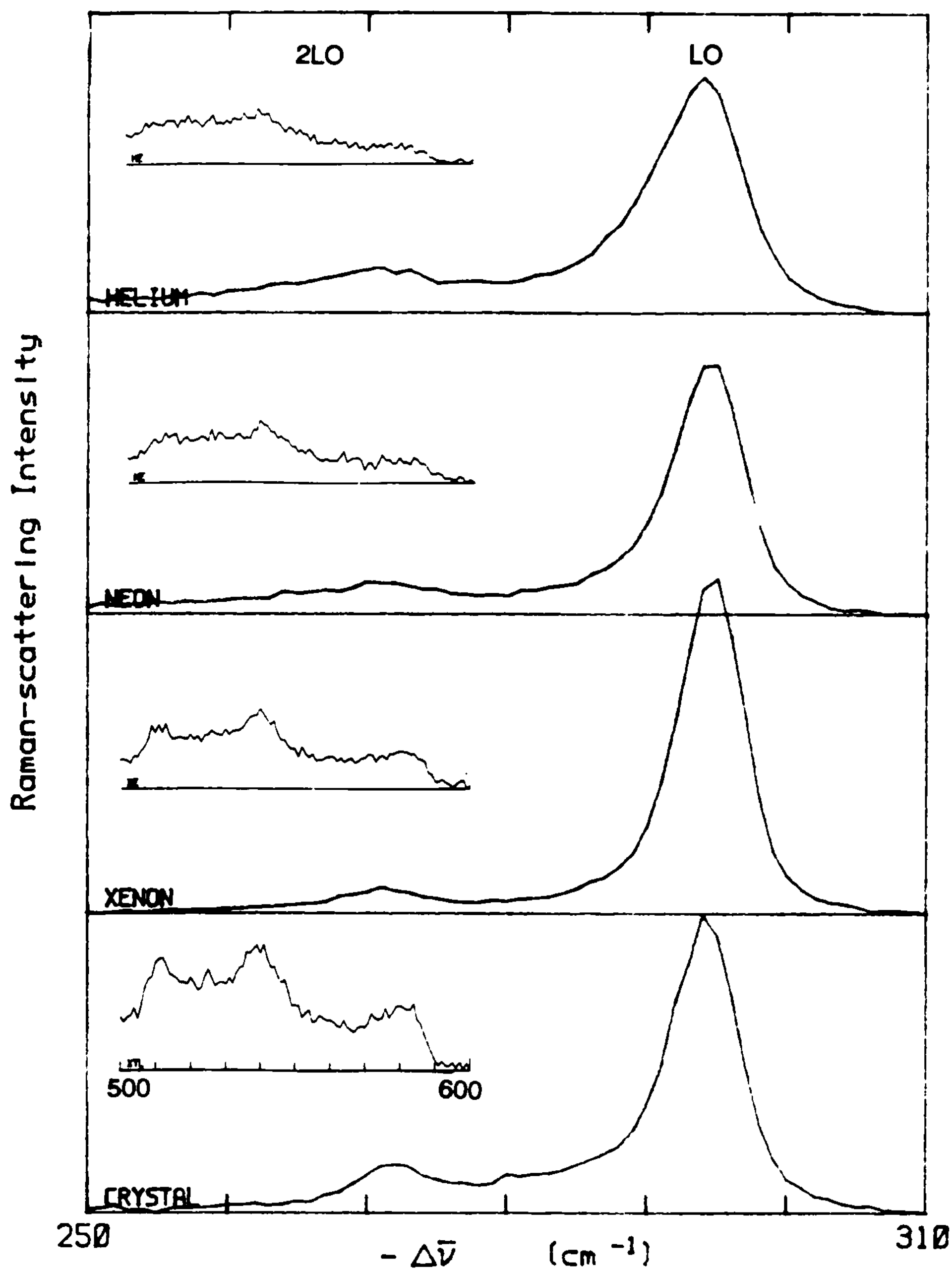


**Figure 4.15** Raman spectra obtained for crystalline, 3 KeV $^{3}He^{+}$, $Ne^{+}$, and $Xe^{+}$ ion-bombarded GaAs.

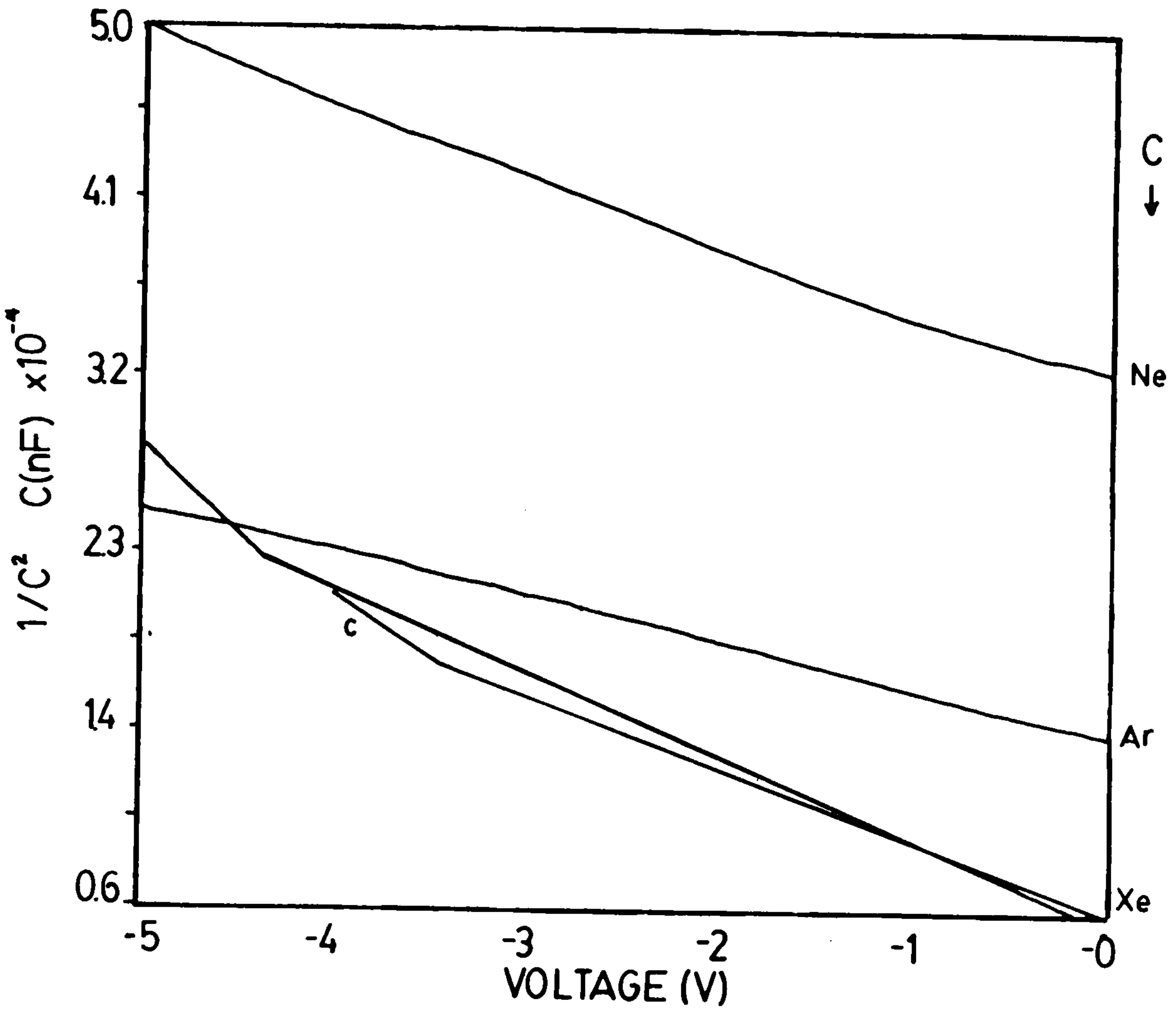


**Figure 4.16** Capacitance-Voltage characteristics for crystalline, 3 KeV $Ne^{+}$, $Ar^{+}$, and $Xe^{+}$ ion-bombarded GaAs.

LO and 2LO peaks are sensitive to the crystalline order in GaAs. Broadening and a decrease in the intensity of the LO peak indicates a disruption of the order and crystalline quality of the material. Indicated in Figure 4.15 are the ratios of the LO peak intensities for ion bombarded GaAs to that for crystalline GaAs. The decrease in intensity and broadening of the LO peak are noted for the ion bombarded samples shown in Figure 4.15 where the effect is greatest for the lightest ion, $^{3}He^{+}$, as indicated by the decrease in the ratio of LO(ion bombarded) to LO(crystalline), ratio = 0.79. GaAs ion bombarded with 3 KeV $Xe^{+}$ does not exhibit this effect. In fact it exhibits an enhancement of the LO mode compared to crystalline GaAs. $Xe^{+}$ ion-bombardment was carried out several times and the analysis was carefully examined for any systematic errors that might have caused this effect. Since damage caused by $Xe^{+}$ ion-bombardment is concentrated primarily at the surface (50Å) compared with other ion bombardments, it is possible that the surface temperature could increase enough to create crystalline regions near the surface by a "self-annealing" process [188]. "Self-annealing" could possibly explain the enhancement of the LO mode.

The LO line is not as sensitive to the amorphous changes caused by ion bombardment if less than 20% of the probed area is changed to amorphous material [188]. The 2LO lines are more sensitive to the degradation of surface crystallinity. The 2LO lines (500-580 $cm^{-1}$), inset in Figure 4.15, lose their sharpness for 3 KeV $Xe^{+}$ ion-bombarded GaAs compared to the crystalline material indicating that there is some amorphous material present very near the surface in the $Xe^{+}$ ion-bombarded material.

The reflectivity spectra shown in Figure 4.14 are not shown for the full photon energy range as in Figure 4.13, but the interpretation of the spectra is the same and the results support those obtained from the Raman spectra. The $E_2$ peak shows broadening and a decreased intensity for the ion bombarded material. This indicates a decrease in the order of the surface and a shift towards a degree of amorphicity. However, the amount of damage is inversely related to the ion mass, with the lighter ion, $Ne^{+}$, doing more damage

to the crystal than $Xe^+$. It is not absolutely conclusive due to the fact that the spectra were not acquired for the full photon energy range, but the depth of damage can be estimated to be between 50-100Å for 3 KeV $Xe^+$ and >100Å for 3 KeV $Ne^+$. The depth of damage was estimated from Figures 4.12 and 4.14. For $Xe^+$ ion-bombarded GaAs, the reflectivity curve in Figure 4.14 begins to follow the crystalline curve very closely beginning at ~3.5 eV. The optical penetration depth at 3.5 eV as determined from Figure 4.12, is ~50Å, so the depth of damage can be estimated to be ~50Å for 3 KeV $Xe^+$.

From the results of Feng *et al.* [185], 3 KeV $Ar^+$ ion-bombarded GaAs can be estimated to have a damaged layer between 400-500Å. Using this result and following the trends observed in the reflectivity (Figure 4.14) and Raman spectra (Figure 4.15) for ion bombarded GaAs, the depth of damage for 3 KeV $Ne^+$ ion-bombarded GaAs can be expected to be at least as deep as the damage in $Ar^+$ ion-bombarded GaAs. The damage to $^3He^+$ ion-bombarded GaAs can be estimated to be even deeper; at least 10 or 20 times deeper than 3 KeV $Xe^+$. Therefore, the damage depths follow a trend that is inversely proportional to the mass of the bombarding ion.

The electrical results for the capacitance-voltage measurements shown in Figure 4.16 qualitatively support the above results. Figure 4.17 schematically explains what can be determined from the C-V measurements. When a metal, such as Al, is placed on a semiconductor, a Schottky barrier results and a region under the Schottky metal contact is depleted of carriers (electrons for n-type GaAs). This region is called the depletion region (Figure 4.17a). The distance that this region extends into the material is a function of the voltage applied between the metal and the semiconductor as noted in Figure 4.17a. The absence of carriers in the depletion region causes it to act as an insulator between the metal on the surface and the conductive material beginning at the depletion zone edge. Therefore, the depletion region represents a parallel plate capacitor having a separation $w$ between the plates and a permittivity $\epsilon$:

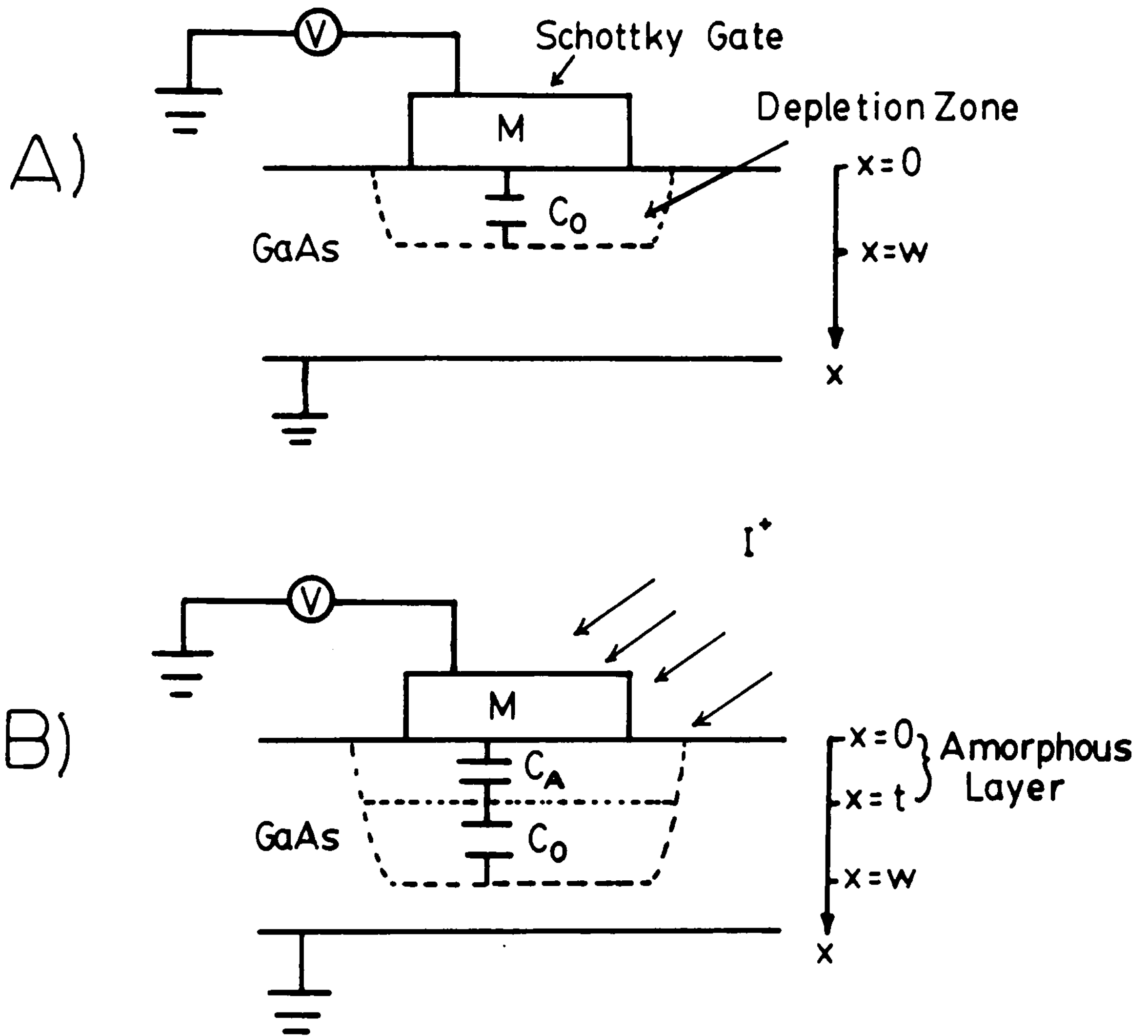


**Figure 4.17** Schematic of a) depletion region under a metal contact on a semiconductor and b) ion-bombarded [184].

$$C_o = \frac{\epsilon A}{w} \quad (4.4)$$

where A is the metal plate area. Ion bombardment causes an amorphous surface layer to form that is a certain thickness $t$ (Figure 4.17b). The electrical measurement probes much deeper (a few thousand angstroms) into GaAs than the amorphous layer extends. The amorphous layer will have a different capacitance than the crystalline substrate due to the disruption in the crystal order. Thus, one is essentially measuring two capacitors in series - capacitance $C_A$ with an amorphous layer of thickness $t$ and capacitance $C_o$ with a crystalline substrate of thickness $w$-$t$ (Figure 4.17b). For capacitors in series the equivalent capacitance C is

$$1/C = 1/C_A + 1/C_o \quad (4.5)$$

Therefore, increasing the thickness of an amorphous layer would decrease the overall measured capacitance of the diode. The capacitance at zero bias (right side of Figure 4.16) for ion-bombarded GaAs is lower than that of crystalline GaAs and the capacitance decreases with decreasing ion bombarding mass. This implies that an amorphous (damaged) layer is formed by ion bombardment and the depth of damage is greater for decreasing ion mass. The capacitance was not measure for 3 KeV $^3He^+$ ion-bombarded GaAs; however, from the trends indicated by the Raman spectra, it would be expected to show a lower capacitance than for 3 KeV $Ne^+$ ion-bombarded GaAs. The capacitance measured for 3 KeV $Xe^+$ is very close to the crystalline material value indicating that $Xe^+$ ion bombardment forms a very thin damaged layer. Sen [163] also showed from capacitance-voltage measurements that the damage layer increases with increasing ion bombardment energy for $Ar^+$ ion-bombarded GaAs.

### *4.2.3 The Chemical State of Ga and As in the Damaged Layer*

The chemical state of the Ga and As in the ion-bombarded material can be obtained from XPS data. Elemental Ga and As have different binding energies than Ga or As combined in GaAs. One way to learn how the As depletion is accommodated in ion-bombarded GaAs is to examine the energy differences between the Ga 3d and As 3d photopeaks. Binding energy differences are used because discrepancies exist in the literature for the absolute binding energies of Ga and As in different chemical states. Although the absolute values differ, binding energy differences measured on the same analytical instrument should be consistent. The energy differences are summarized in Table 4.9.

It is not evident from the differences in the binding energies of the photopeaks that a change in the chemical state of either As or Ga occurs as a result of ion bombardment. It can be concluded that the resulting surface is not a combination of both Ga and As in elemental form, because of the much larger $\Delta E(Ga^{\circ}\text{-}As^{\circ})$ [157].

Childs and Lagally [35] suggested the formation of elemental Ga on an ion bombarded surface and that Ga "beads" would appear as a second phase that are of the order of $1\mu m$ in diameter or smaller, covering about 20% of the ion bombarded surface. They observed an increase in the intensity at the top of the valence band and an overall broadening in the line-shape of the Ga LMM Auger peak due to the disorder introduced in the GaAs phase. It was suggested that the spectrum was a superposition of elemental Ga and Ga(GaAs). Su *et al.* [66] did not observe Ga droplets.

In this study a change in binding energy was not noted for either Ga or As upon ion bombardment; however, there is a slight broadening in the Ga 3d photopeak following ion bombardment. The FWHM of chemically cleaned GaAs is $1.0\pm0.1$ eV and the FWHM of ion bombarded GaAs is consistently wider at $1.2\pm0.1$ eV. Since the peak broadening is so small, it is difficult to determine whether the broadening is caused by elemental Ga

**Table 4.9** Energy differences ΔE between Ga 3d and As 3d photopeaks for various bonding states.

| Condition | ΔE(eV) |
|---|---|
| GaAs[a] | 22±0.2 |
| Ga° and As°[a] | 23.4±0.2 |
| Ga° and As(GaAs)[a] | 22.8±0.2 |
| As° and Ga(GaAs)[a] | 22.6±0.2 |
| Chemically cleaned[b] | 21.9±0.2 |
| Ion bombarded[b] | 22.0±0.2 |

a) From reference 75,157,192

b) From this work

formation. The slight peak broadening could possibly be due to increased disorder in the surface and that stronger Ga-Ga bonds and weaker As-Ga bonds are present in an ion bombarded surface [11,66]. The As deficiency created by ion bombardment would suggest that a substantial number of Ga atoms in the surface region have other Ga atoms as nearest neighbors. It is not evident from the XPS data whether the Ga atoms remain unbonded producing dangling bonds or whether the As deficiencies are replaced by Ga-Ga "wrong" bonds [190]. Bonds between like atoms destroy the chemical order and could account for the broadening observed in the Ga 3d photopeak for ion bombarded GaAs. It is also possible that broadening could be produced by Ga atoms having many other Ga atoms as nearest neighbors without being bonded to them since the lack of As atoms next to Ga atoms would change the chemical (electrostatic) environment around the Ga atoms compared to the original GaAs environment. The binding energy of the Ga atoms with other Ga atoms as nearest neighbors, whether bound or not, could be reduced; Ga metal has a lower binding energy than Ga of GaAs. No changes in the shape or width of the As 3d photopeak were observed following ion bombardment.

### *4.2.4 Ion Implantation*

The results discussed in the previous section show that varying the mass of the bombarding ion causes changes in the composition and the depth of the resulting damage layer, which is most likely caused by two things. The first is that more energy is initially transferred from a heavy ion to the surface atoms so that the majority of its energy is expended immediately at the surface and is involved in sputtering. Therefore less energy is transferred to a second and third, etc., atom to set the cascade motion in progress and the bombarding ion comes to rest very near the surface. The second is that a lighter atom is usually smaller and can penetrate deeper into the surface and it transfers less energy to the atoms in the lattice and is therefore not stopped as quickly. Thus a lighter atom leaves

behind a trail of damage that extends further into the surface.

Bombarding the GaAs surface with energetic ions is almost always accompanied by the implantation of the bombarding ions into the surface. There are several parameters which determine the profile of the implanted atoms which build up in the solid, a few of which are listed below [191]:

- sputtering yield
- mobility of implanted atoms in target
- flux of incident ions
- density of trapping sites in lattice
- chemical interaction between implanted species and target
- target temperature

The concentration of implanted ions is largely determined by the sputtering yield and if there is no chemical interaction between the incident ion and the target, the concentration of the implanted atoms saturates in most materials at about 0.3-1 gas atoms per target atom.

Due to the relatively large XPS sensitivity factors for the Xe $3d_{5/2}$ and Ne 1s photo-electrons (see Table 3.1), it was possible to detect these atoms in GaAs following ion bombardment. The atomic concentrations for 3KeV $Ne^+$ and $Xe^+$ and 1 KeV $Xe^+$ implanted in GaAs as a function of depth (determined from different toas) are shown in Figure 4.18. The amount of implanted atoms is not a function of the energy since the amount of Xe detected is equivalent for GaAs bombarded with both 1 and 3 KeV $Xe^+$. The bombarding ions become implanted in GaAs at least as deep as can be detected by XPS (limited by the mean free path of either Xe or Ne). The amount of Ne implanted is greater than that of Xe at 35Å, and it becomes even greater (1.5 at.%) for Ne at 50Å. This build-up could be controlled by the sputter rate and the penetration depth. The sputter yield for $Xe^+$/GaAs would be expected to be greater than that for $Ne^+$/GaAs ($T_{max}$ values in Table 4.6) and $Ne^+$ is expected to have a deeper penetration into GaAs (Table 4.4). Thus a build-up of Ne

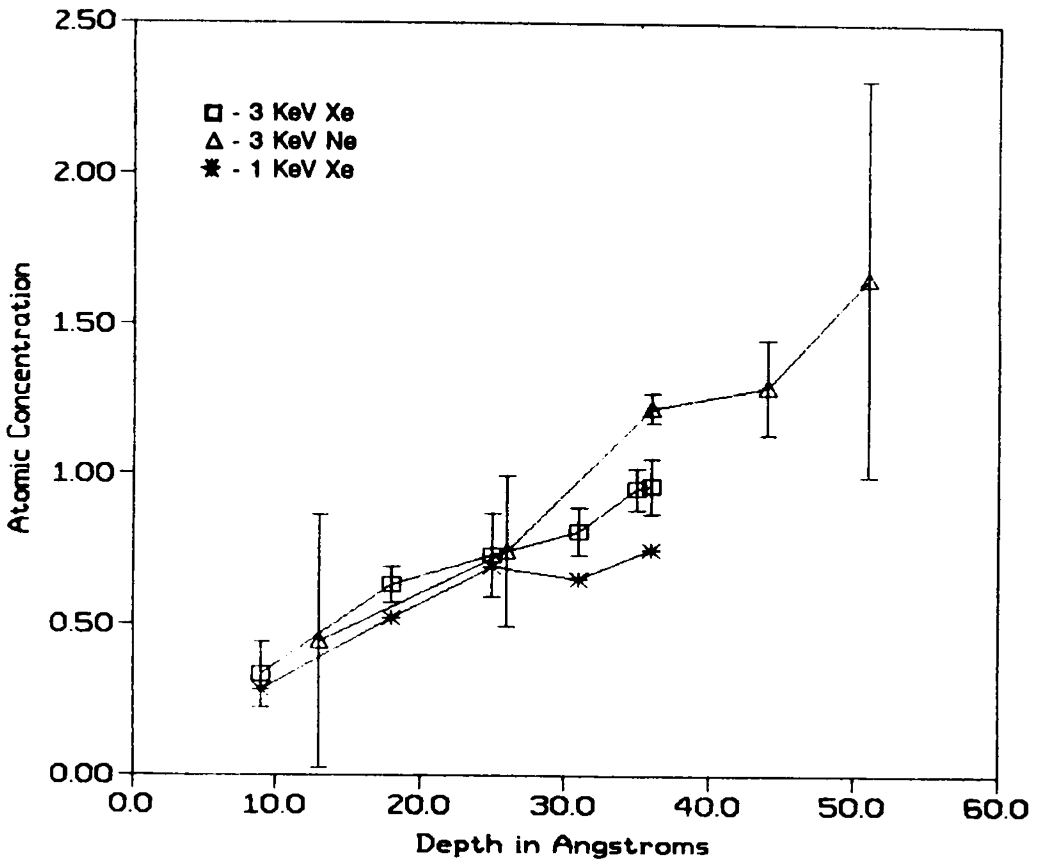


**Figure 4.18** Atomic Concentration of Xe and Ne found in GaAs following ion bombardment.

would be expected. If XPS could probe deeper than 50Å for Xe and Ne, Xe would not be expected to be implanted much deeper than what is already observed because of the factors stated above and from the shallow damage depth results of the uv-vis, Raman, and electrical studies. From previous trends, the depth of $Ar^+$ ion implantation would be expected to lie between that of $Xe^+$ and $Ne^+$, and $^3He^+$ would be even deeper than $Ne^+$, since the sputter rate of $^3He^+$ would be expected to be smaller than $Ne^+$. The binding energies of Xe and Ne implanted in GaAs are 669.7±0.2 eV and 863.6±0.2 eV, respectively. These binding energies are the same as those obtained for Ne and Xe implanted in other materials such as C, Fe, and Cu [192,193] and indicate that they are interstitial gas atoms and do not interact chemically with the GaAs lattice.

## 4.3 Effect of Varying Bombarding Ion on Reactivity

### *4.3.1 $O_2$ Exposure*

Chemically cleaned GaAs was ion bombarded with 3 KeV $^3He^+$, $Ne^+$, $Ar^+$, and $Xe^+$ ions ($10^{17}$ ions/cm$^2$) and subsequently exposed to $1x10^7$, $1x10^8$, and $2x10^{11}$ L $O_2$. XPS spectra obtained at a 15° toa for each of the $O_2$ exposures are presented in Figures 4.19 ($^3He^+$), 4.20 ($Ne^+$), 4.21 ($Ar^+$), and 4.22 ($Xe^+$). The relative quantities of gallium and arsenic oxides produced following $O_2$ exposure were determined from curve-resolved spectra and are shown in Figure 4.23 for the various ion bombarded samples as a function of $O_2$ exposure. Exposure of ion bombarded GaAs to $O_2$ produces $Ga_2O_3$, $As_2O_3$, and $As_2O_5$, with preferential formation of $Ga_2O_3$. All of the ion bombarded surfaces, regardless of the bombarding ion, produce approximately the same quantity of arsenic oxides and this quantity is also the same as that found for chemically cleaned and IHT GaAs exposed to $O_2$ (see Figure 4.5).

It can be seen from the relative amount of oxide formed that there is a relationship between the mass of the bombarding ion and the relative amount of oxide formed. The relative amount of $Ga_2O_3$ increases with increasing mass of the bombarding ion, with the amount of $Ga_2O_3$ formed being the greatest for the 3 KeV $Xe^+$ bombarded samples. This is most likely due to the increasing number of defect sites that are left in the surface layer with the increasing mass of the bombarding ion. It was shown previously (sect. 4.1) that ion bombardment had an effect on the chemical reactivity of GaAs, with $Ga_2O_3$ being the dominant species. The amount of $Ga_2O_3$ formed was shown not to be dependent on the Ga/As ratio by comparing the $O_2$ exposure results of ion bombarded GaAs to those of IHT prepared GaAs (Figure 4.5). This point can be reinforced once again by examining the data for of $^3He^+$ ion-bombarded GaAs exposed to $O_2$. The Ga/As atomic ratio of GaAs bombarded with $^3He^+$ ions was 1.16 (15° toa from Table 4.5) and 1.23 for IHT GaAs. Compar-

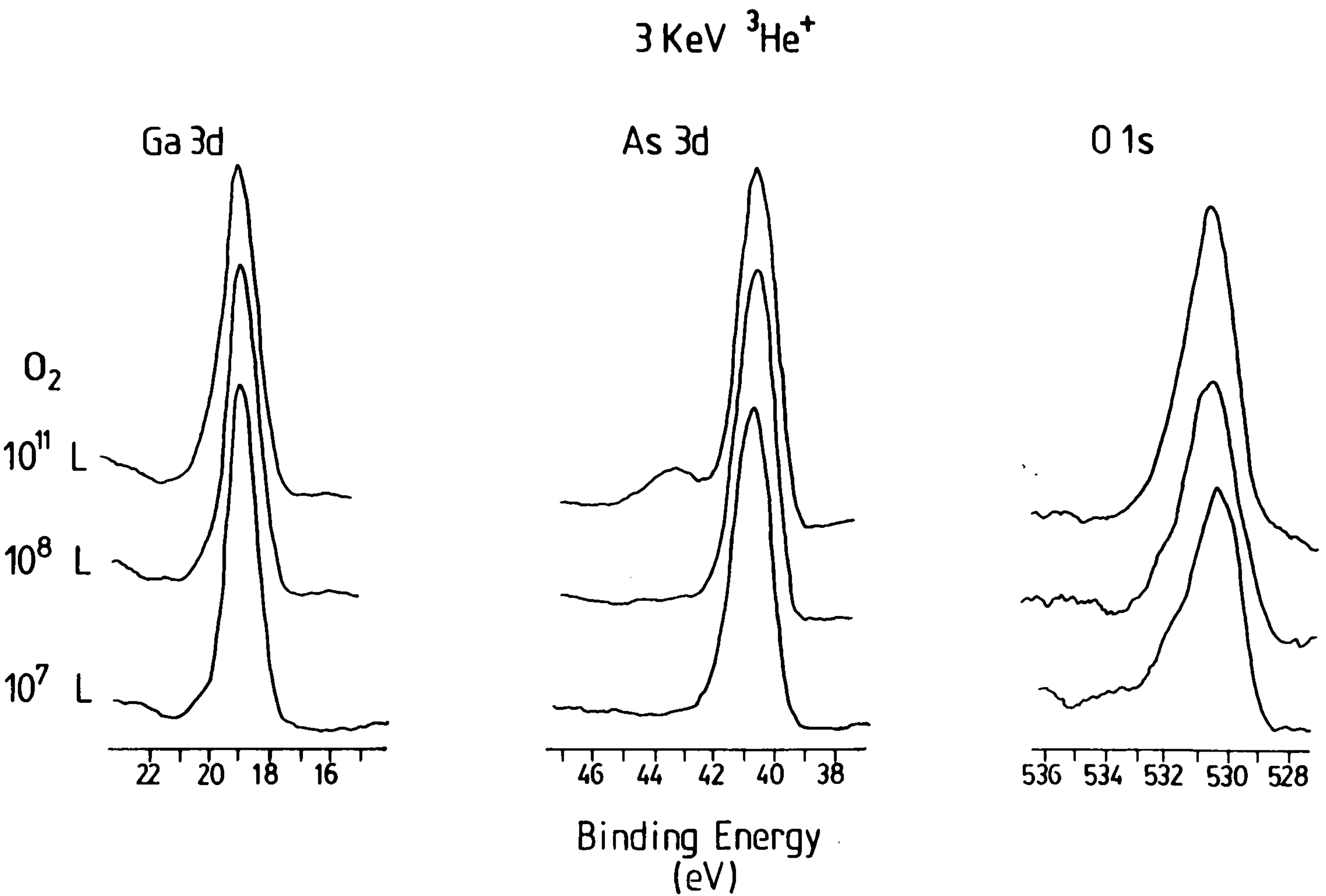


**Figure 4.19** XPS spectra for 3 KeV $^{3}He^{+}$ ion-bombarded GaAs exposed to $1 \times 10^{7}$, $1 \times 10^{8}$, and $2 \times 10^{11}$ L $O_2$.

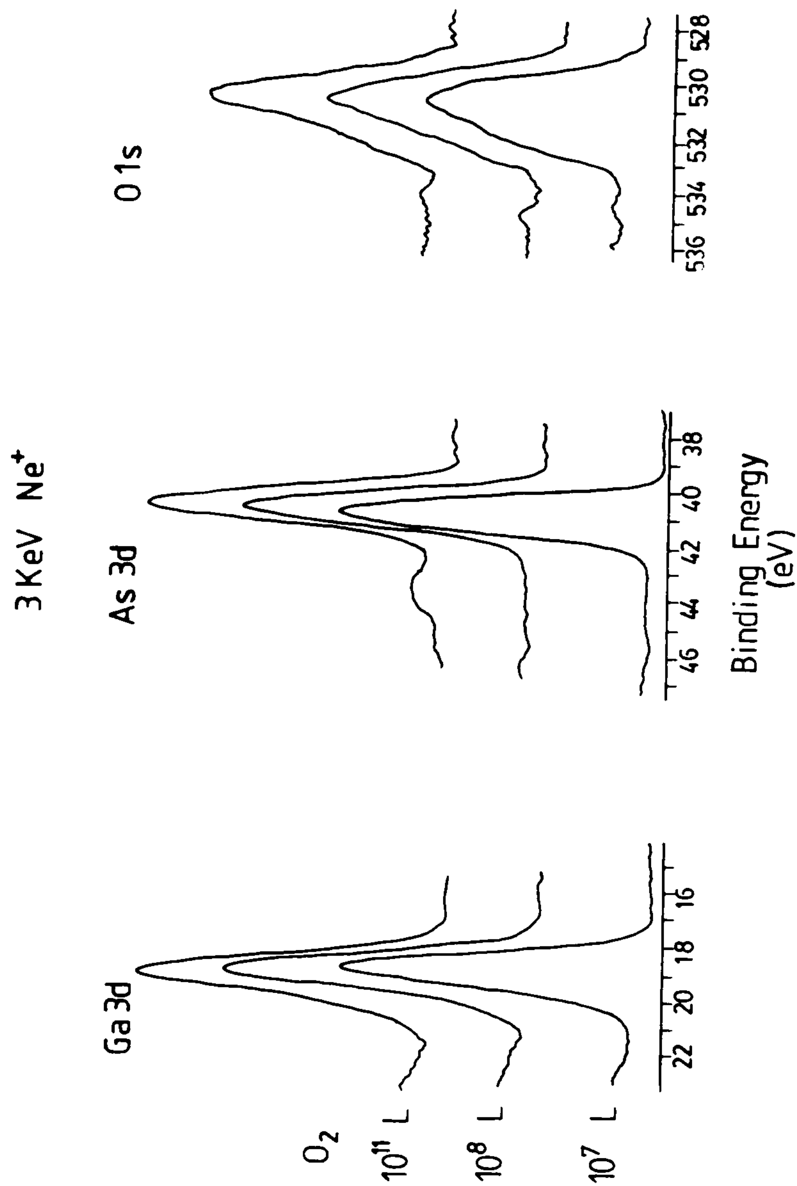


**Figure 4.20** XPS spectra for 3KeV $Ne^+$ ion-bombarded GaAs exposed to $1x10^7$, $1x10^8$, and $2x10^{11}$ L $O_2$.

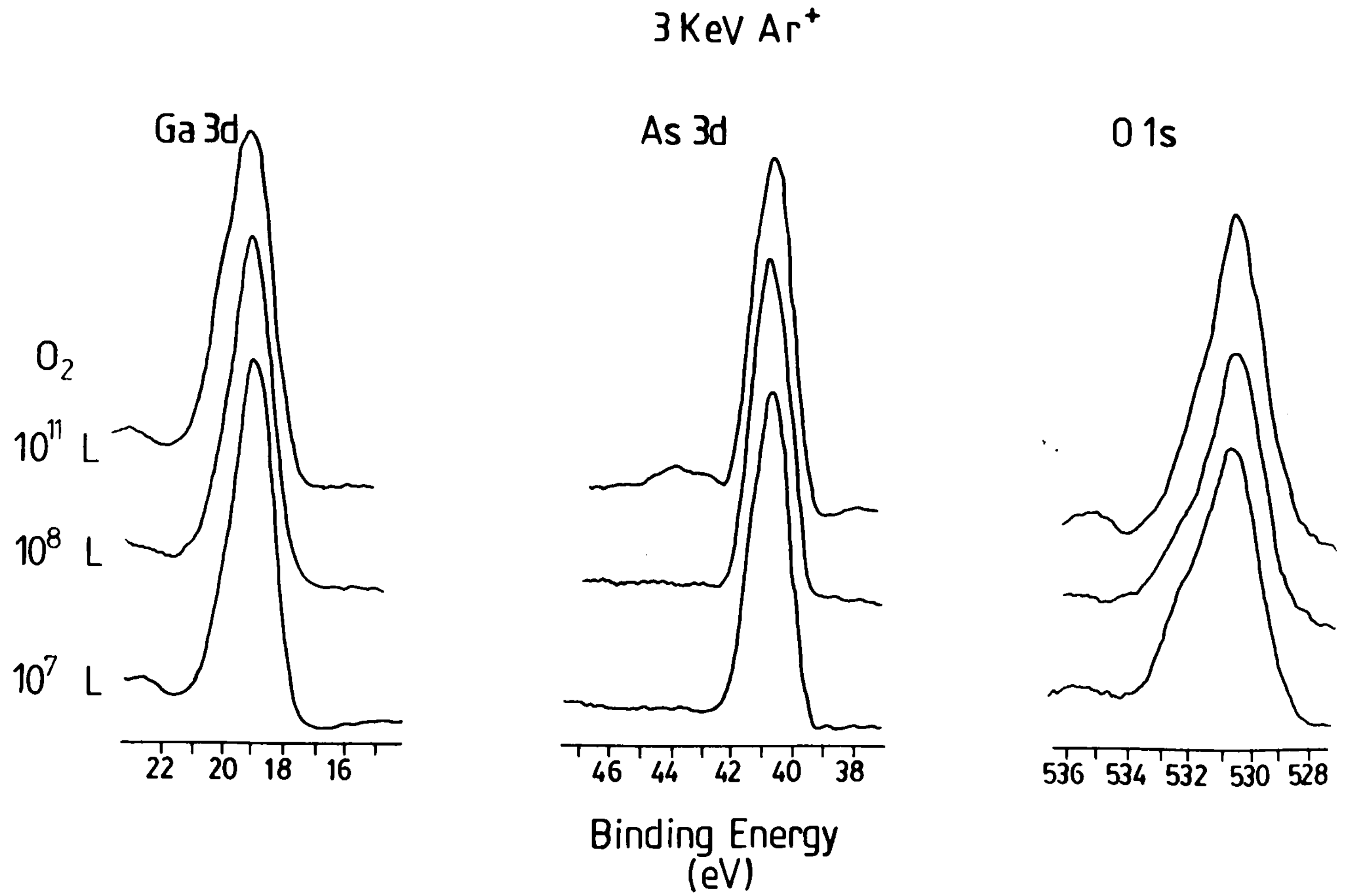


**Figure 4.21** XPS spectra for 3 KeV $Ar^+$ ion-bombarded GaAs exposed to $1x10^7$, $1x10^8$, and $2x10^{11}$ L $O_2$.

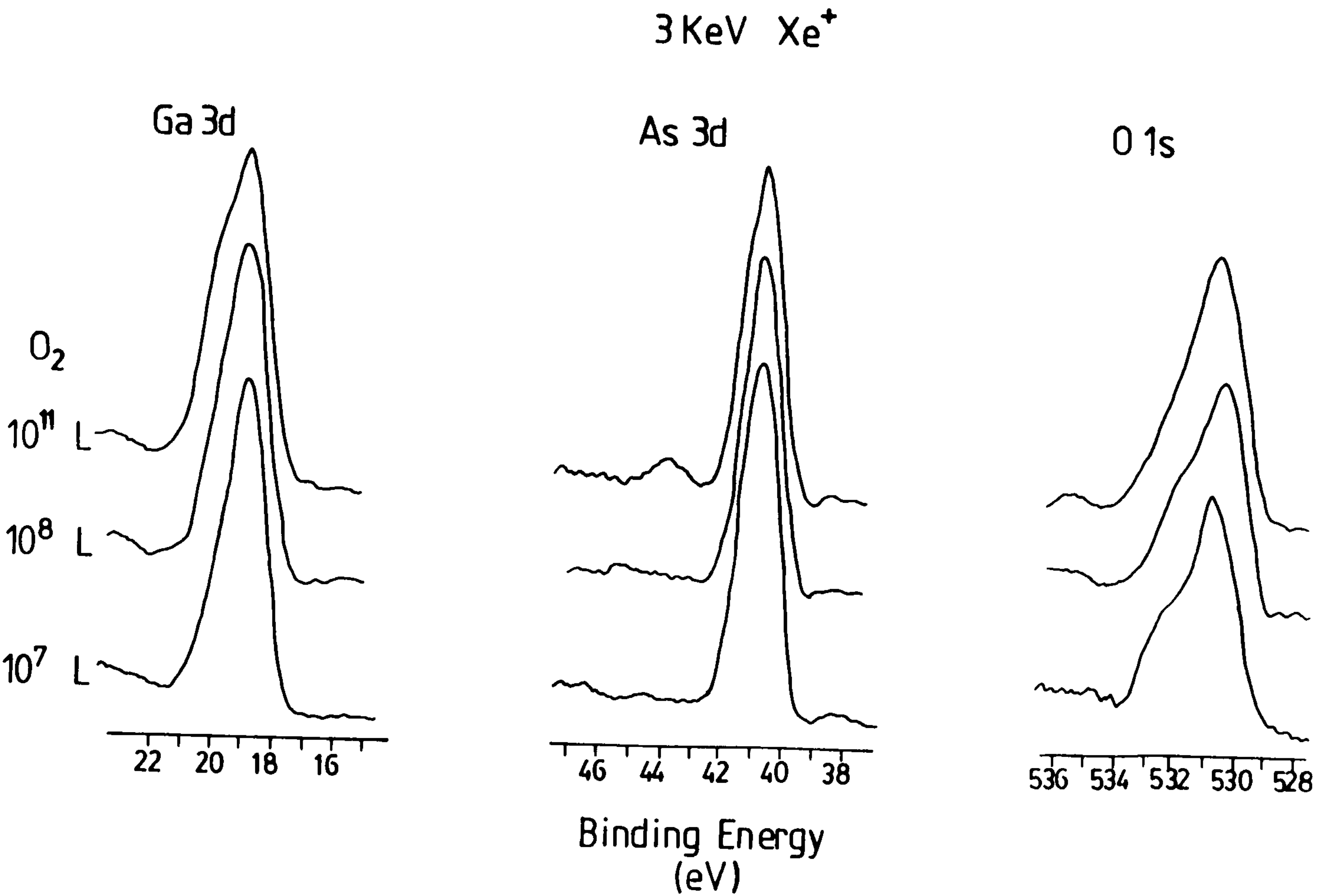


**Figure 4.22** XPS spectra for 3 KeV $Xe^+$ ion-bombarded GaAs exposed to $1x10^7$, $1x10^8$, and $2x10^{11}$ L $O_2$.

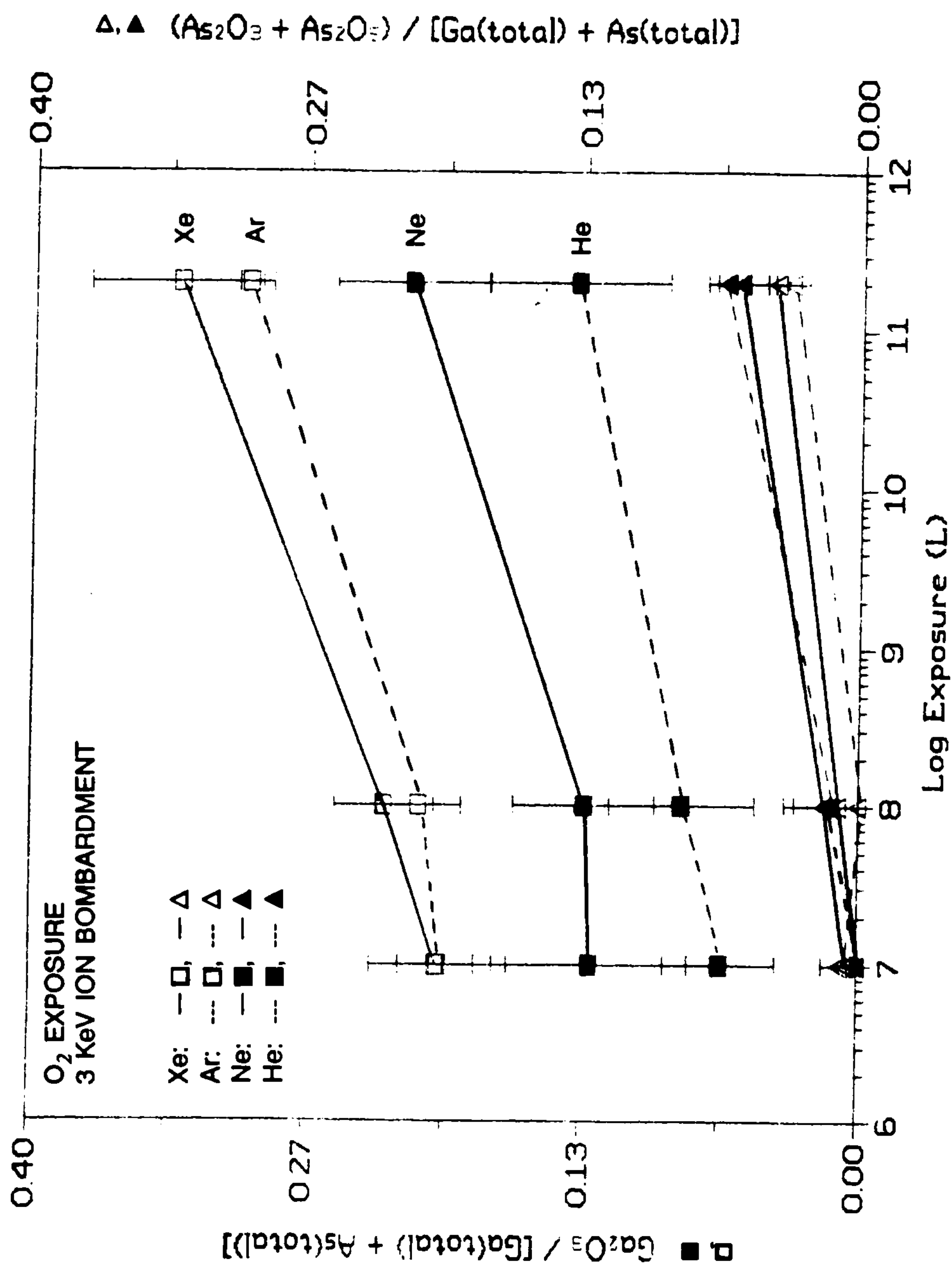


**Figure 4.23** Relative amounts of gallium and arsenic oxides formed for 3 KeV $^{3}He^{+}$, $Ne^{+}$, $Ar^{+}$, and $Xe^{+}$ ion-bombarded GaAs as a function of $O_2$ exposure.

ing Figures 4.5 and 4.23, the average amount of $Ga_2O_3$ formed upon $O_2$ exposure at $2x10^{11}$ L is greater for $^3He^+$ than for IHT GaAs (0.13, 0.08, respectively), even though the Ga/As atomic ratios are almost the same. An important difference to note is not only the amount of $Ga_2O_3$ formed but the relative amounts of both gallium and arsenic oxides formed. IHT exhibits equal formation of both gallium and arsenic oxides, whereas the $^3He^+$ ion-bombarded GaAs exhibits the usual behavior of ion bombarded material exposed to $O_2$; preferential formation of $Ga_2O_3$. Therefore, it can be concluded that the Ga/As ratio does not control the amount of oxide formed and these results support the earlier conclusions suggesting that reactions take place at defect sites which are formed by ion bombardment.

From the results for $O_2$ exposure of GaAs bombarded with different ions, it can be concluded that surface defects definitely play a role in the reactivity and the concentration of defects can be controlled by the mass of the bombarding ion. It was shown (section 4.2) that the depth of the damaged (amorphous) layer in GaAs caused by ion bombardment, was greater for lighter ions. If a surface is bombarded with the same flux of ions of different masses, then the same number of defects should be imparted to the surface, only the depth distribution is different (assuming equivalent sputter rates). However, to assume equivalent sputter rates when comparing the series of bombarding ions is not entirely correct. The entire ion bombardment process is influenced by the sputter yield, penetration range of the ions into the solid, and by the amount of energy initially transferred to the surface ($T_{max}$) which sets the collision cascade into motion. The lighter ions would spread the defects through a layer which is deeper into the sample and would sputter away less of the surface atoms. The heaviest ion would leave the highest number of defects concentrated at the surface because it does not penetrate very deeply into the crystal and it is continually eroding away more of the surface than the lighter ions, thereby affecting the reactivity at the surface to the greatest extent.

Xenon ion bombardment only causes a damaged layer approximately 50Å deep. The

damage it causes is confined mainly to the surface atoms, therefore imparting more defects at the surface - more broken Ga-As bonds, more As deficiencies and more disorder. The disorder caused by $^3He^+$ is spread throughout the lattice (greater than 100Å) and damage at the surface is less. Initial oxidation occurs at surface defect sites [14,35,36,40,41, 43,70,72,77,83,102,127,171] and since $Xe^+$ ion bombardment will cause the concentration of defects to be greatest at the surface, it will show the greatest effect on the reactivity, i.e. enhanced oxidation. Lighter ions impart defects deep into the crystal, which never come into contact with oxygen molecules during the reaction (at least under the present exposure conditions) and therefore do not affect the reaction to as great an extent. Also any damage present deeper into the crystal away from the surface atoms (the first few atomic layers), may be of a different form. Defects on the surface may be composed mainly of broken Ga-As bonds with many dangling Ga bonds. Deeper defects may have a chance to reform bonds in the crystal (away from the first layer of atoms) to form a random network of Ga-Ga wrong bonds [183], which would be less reactive than the Ga dangling bonds. Figure 4.24 presents the structure of the GaAs(100) surface before ion bombardment and some possiblities for configurations of the surface after ion bombardment that contain As deficiencies, Ga dangling bonds, and Ga-Ga "wrong" bonds [183].

Relative amounts of oxide formed on $O_2$ exposed 1 KeV $Xe^+$ and $Ar^+$ ion-bombarded GaAs are presented in Figure 4.25. One KeV $Xe^+$ or $Ar^+$ ion-bombarded GaAs exposed to $O_2$ forms less $Ga_2O_3$ than the respective 3 KeV samples, reinforcing that the effect of the energy of the bombarding ion still holds for different masses. Also 1 KeV $Xe^+$ forms more oxide than 1 KeV $Ar^+$, illustrating the effect of ion mass on reactivity.

#### 4.3.2 $H_2O$ Exposure

In the previous section, it was found that increasing the mass of the bombarding ion resulted in increased reactivity of ion bombarded GaAs. This effect is also observed for ion

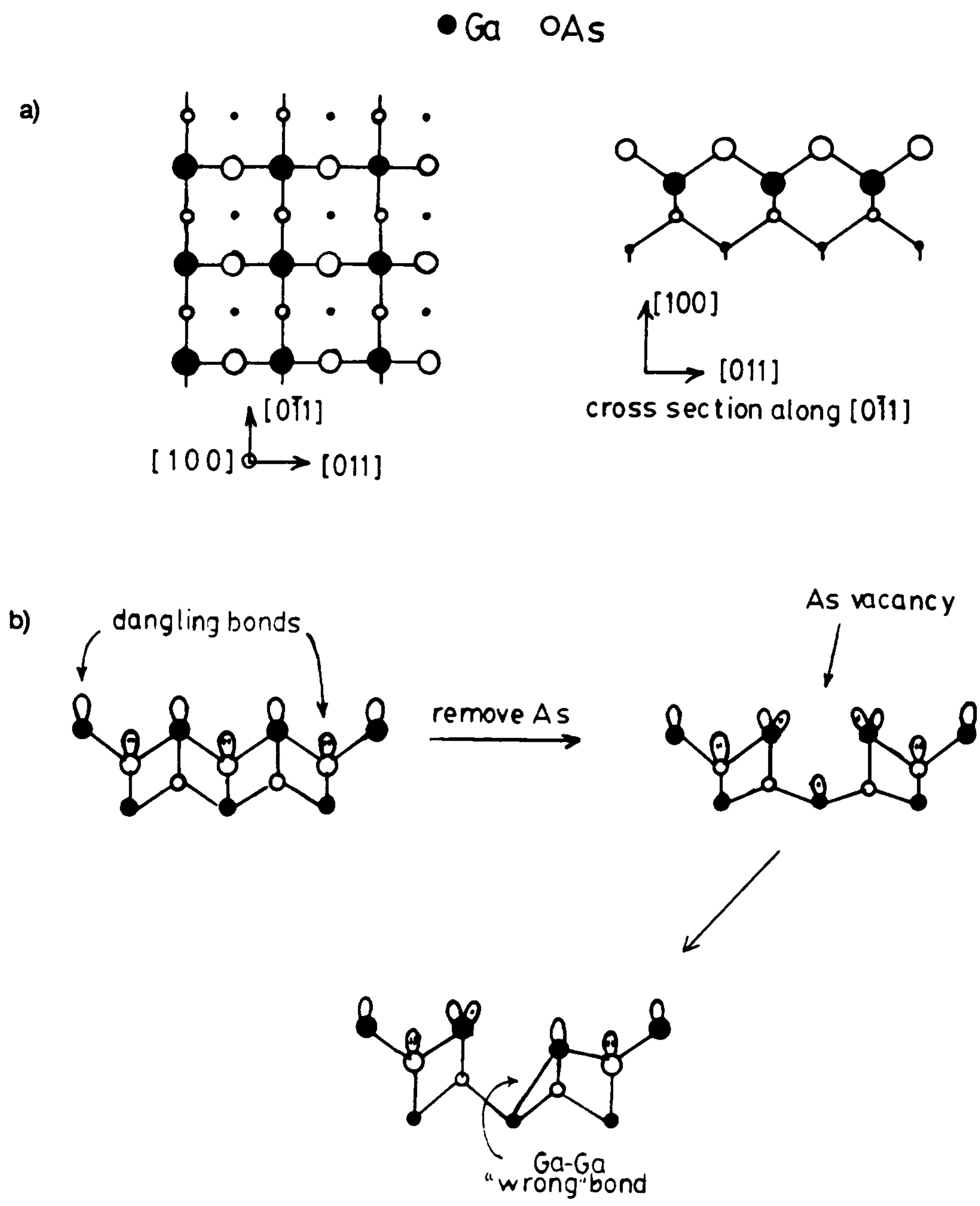


**Figure 4.24** GaAs(100) surface before and after ion bombardment.
a) GaAs(100) surface before ion bombardment [5].
b) Possible surface configurations after ion bombardment.

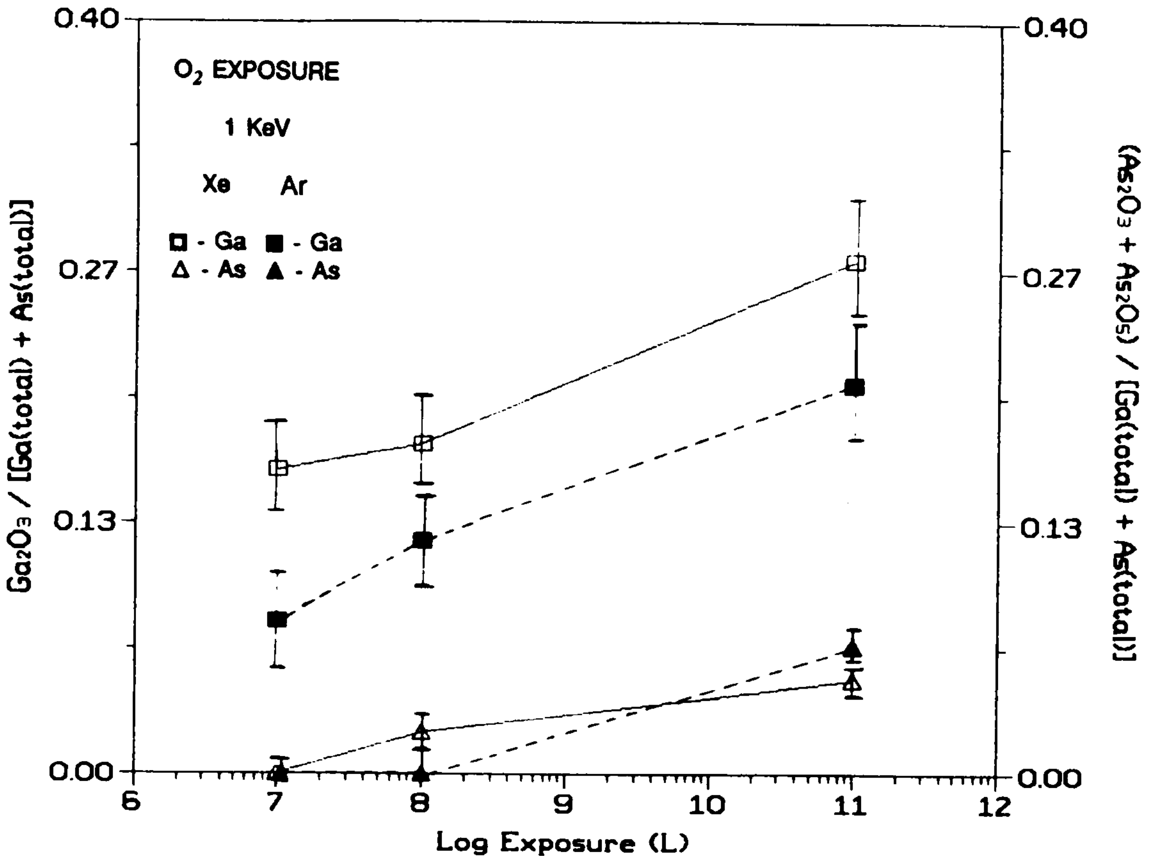


**Figure 4.25** Relative amounts of gallium and arsenic oxides formed for 1 KeV $Ar^+$ and $Xe^+$ ion-bombarded GaAs exposed to $O_2$.

bombarded GaAs exposed to $H_2O$. The XPS spectra for the curve-resolved Ga 3d and O 1s photopeaks (15° toa) for 3 KeV $Xe^+$ and $Ar^+$ ion-bombarded GaAs exposed to $10^{13}$ L $H_2O$ are shown in Figure 4.26. The relative amounts of oxidized gallium species (GaOOH and $Ga(OH)_3$) produced following $H_2O$ exposure are presented in Table 4.10 along with the atomic percent of $H_2O$(ads) and total oxygen content.

It was mentioned in section 4.1.5 that the total concentration of oxygen did not increase with increasing $H_2O$ exposure. The total amount of oxygen for 3 KeV $Xe^+$ ion-bombarded GaAs exposed to $10^{13}$ L $H_2O$ is the same as that for 3 KeV $Ar^+$ ion-bombarded GaAs exposed to $10^{13}$ L $H_2O$. What differs is that the total amount of oxidized gallium species is greater for the $Xe^+$ ion-bombarded sample and the distribution of species is different (see Table 4.10). The relative amount of GaOOH is approximately the same for the two samples; however, the amount of $Ga(OH)_3$ is greater for the $Xe^+$ ion-bombarded sample. This suggests that the different ion bombardment conditions have an effect on the dissociation of the adsorbed $H_2O$ layer.

### *4.3.3 NO Exposure*

The results of Bertness *et al.* [115] for $N_2O$ and $O_2$ adsorption and Bermudez *et al.* [118] for NO and $O_2$ adsorption on GaAs(110) suggest that dissociative adsorption is dependent upon the bond energies of the molecules. Nitrous oxide with the weakest bond energy shows the greatest reactivity with GaAs(110) [115]. Bermudez *et al.* also observed that NO reacted more slowly with GaAs than $O_2$ in the exposure range $10^4$ - $10^7$ L where defects are thought to play an important role in the dissociation process on cleaved or annealed material. For the present study, it was reasoned that if defects on ion bombarded GaAs are responsible for providing initial reaction sites, then the differences between $O_2$ and NO reactions would be more pronounced for ion bombarded GaAs than cleaved GaAs(110)

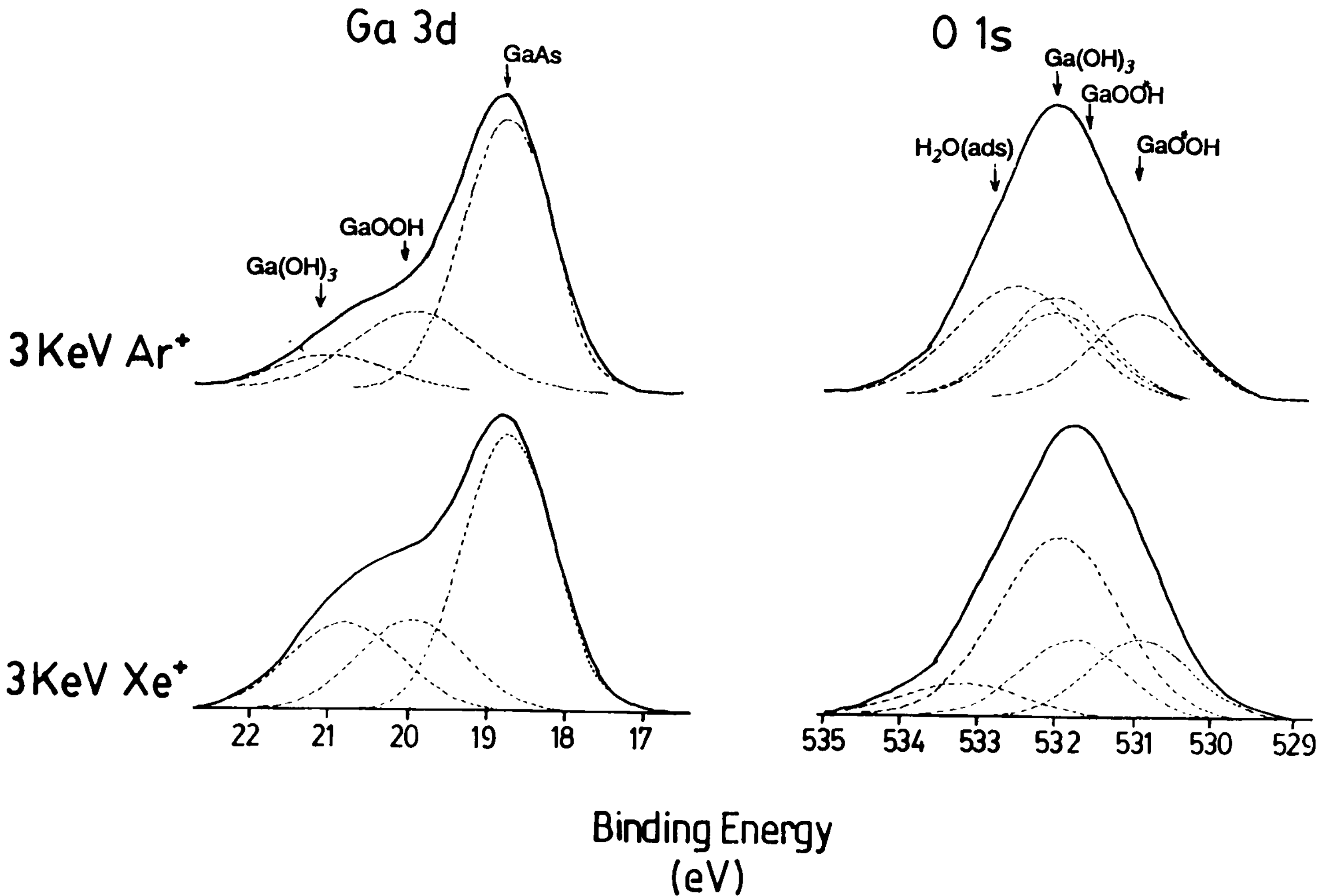


**Figure 4.26** Curve-resolved XPS spectra for 3 KeV $Xe^+$ and $Ar^+$ ion-bombarded GaAs exposed to $10^{13}$ L $H_2O$.

**Table 4.10** 3 KeV $Xe^+$ and $Ar^+$ ion-bombarded GaAs exposed to $10^{13}$ L $H_2O$.

| Ion | Total Oxide[a] | $Ga(OH)_3$[b] | GaOOH[b] | $O(H_2O_{ads})$ (% at.) | O(total) (% at.) |
|---|---|---|---|---|---|
| $Xe^+$ | 0.340 | 0.172 | 0.168 | 4 ± 2 | 46 ± 5 |
| $Ar^+$ | 0.228 | 0.064 | 0.164 | 14 ± 5 | 43 ± 5 |

a) [$Ga(OH)_3$ + GaOOH] / [Ga(total) + As(total)], ±10%.

b) $Ga(OH)_3$ or GaOOH / [Ga(total) + As(total)], ±10%.

which should have a lower number of surface defects. Since NO, $N_2O$, and $O_2$ exhibited different reactivities with GaAs(110) and have different bond strengths, it was thought that more insight into the nature of the ion bombarded surface and the mechanisms of reaction could be gained by examining NO and $N_2O$ reactions.

The XPS spectra obtained at a 15° toa are presented in Figure 4.27 for the Ga 3d, As 3d, and O1s levels for 3 KeV $Xe^+$ and $Ne^+$ ion-bombarded GaAs following $3x10^6$, $1x10^7$, and $1x10^8$ L NO exposures. Representative curve-resolved spectra are shown in Figure 4.28 for 3 KeV $Xe^+$ and $Ne^+$ ion-bombarded GaAs exposed to $10^8$ L NO. No signal from the N 1s level (<2 at.%) was observed for any of the NO exposures nor was any detected by Auger analysis. Chemically cleaned GaAs, upon exposure to $10^8$ L NO, exhibited no changes in the XPS spectra following exposure. The relative amounts of gallium and arsenic oxides are shown in Figure 4.29 for 3 KeV $Xe^+$ and $Ne^+$ ion-bombarded GaAs as a function of NO exposure.

The curve-resolved spectra shown in Figure 4.28 identify the chemical species formed on ion-bombarded GaAs following NO exposure. Following NO exposure at $3x10^6$ L, only $Ga_2O_3$ was formed on ion-bombarded GaAs. At $10^7$ and $10^8$ L NO exposures, both gallium and arsenic oxides were produced, with $Ga_2O_3$ being the major component. The relative amount of $Ga_2O_3$ formed following NO exposure is greater for 3 KeV $Xe^+$ ion-bombarded samples than the amount formed for 3 KeV $Ne^+$ ion-bombarded samples. This supports previous conclusions that the reactivity increases with increasing mass of the bombarding ion, where the reactivity is directly related to the increased number of surface defects.

The O 1s photopeak exhibits two distinct peaks separated by approximately 2 eV. The lower binding energy photopeak corresponds to oxygen from gallium and arsenic oxides. The higher binding energy photopeak at ~532.4 ± 0.3 eV exhibits the same binding energy that was attributed to molecularly adsorbed oxygen for ion bombarded GaAs exposed to $O_2$. This higher binding energy photopeak is in the area where molecularly adsorbed NO would

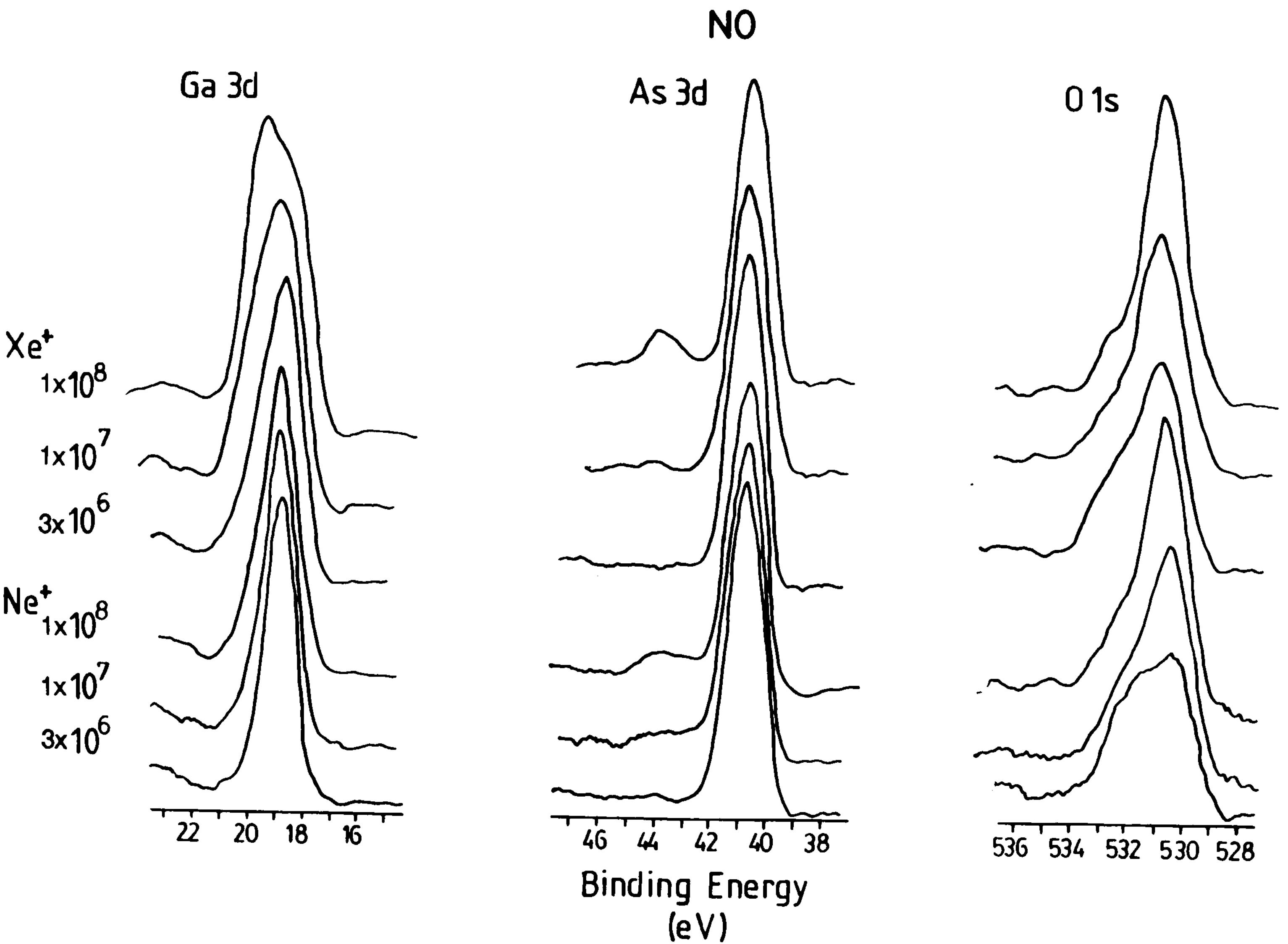


**Figure 4.27** XPS spectra for 3 KeV $Xe^+$ and $Ne^+$ exposed to $3x10^6$, $1x10^7$, and $1x10^8$ L NO.

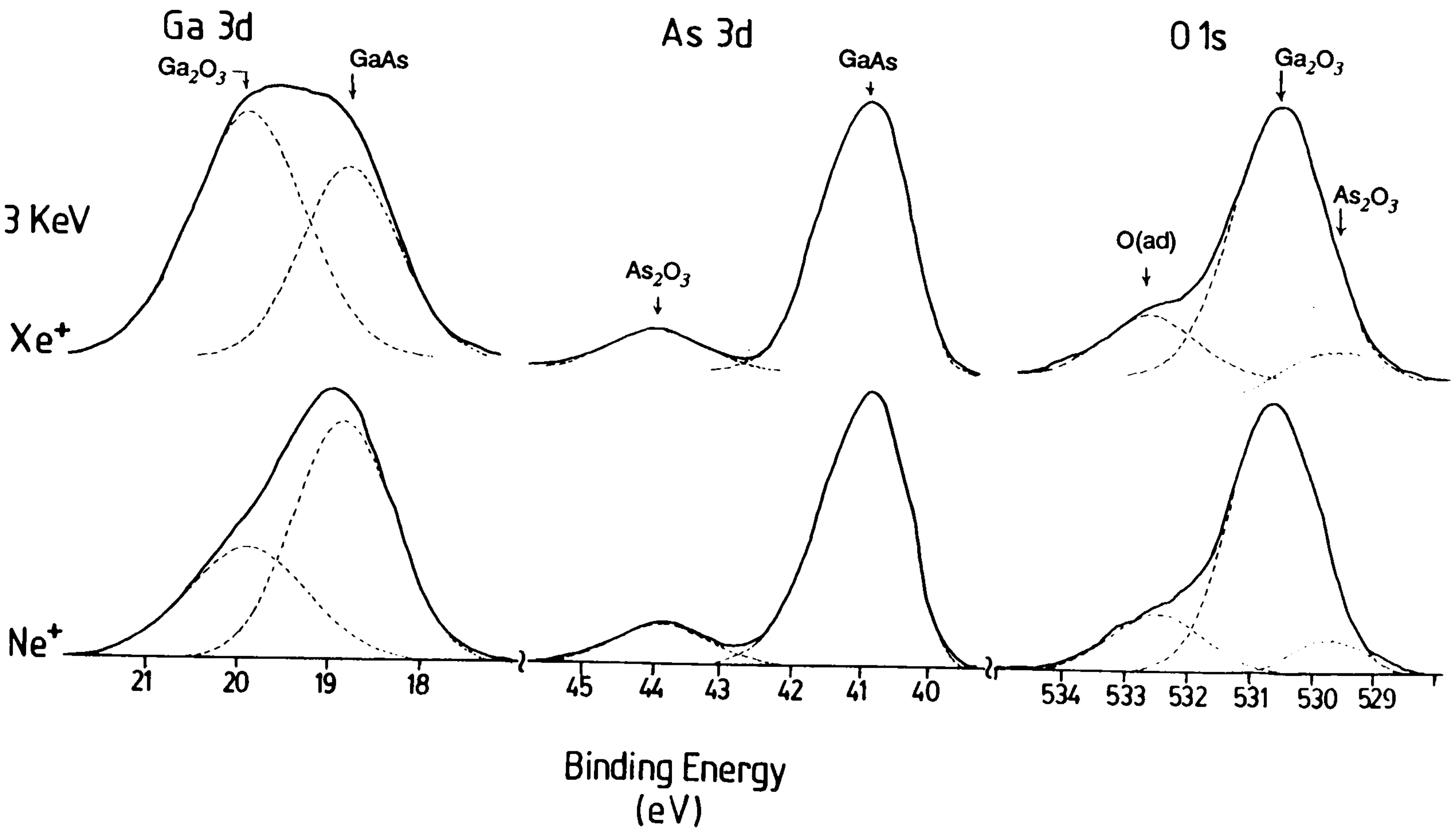


Figure 4.28 Curve-resolved XPS spectra for 3 KeV $Xe^+$ and $Ne^+$ exposed to $10^8$ L NO.

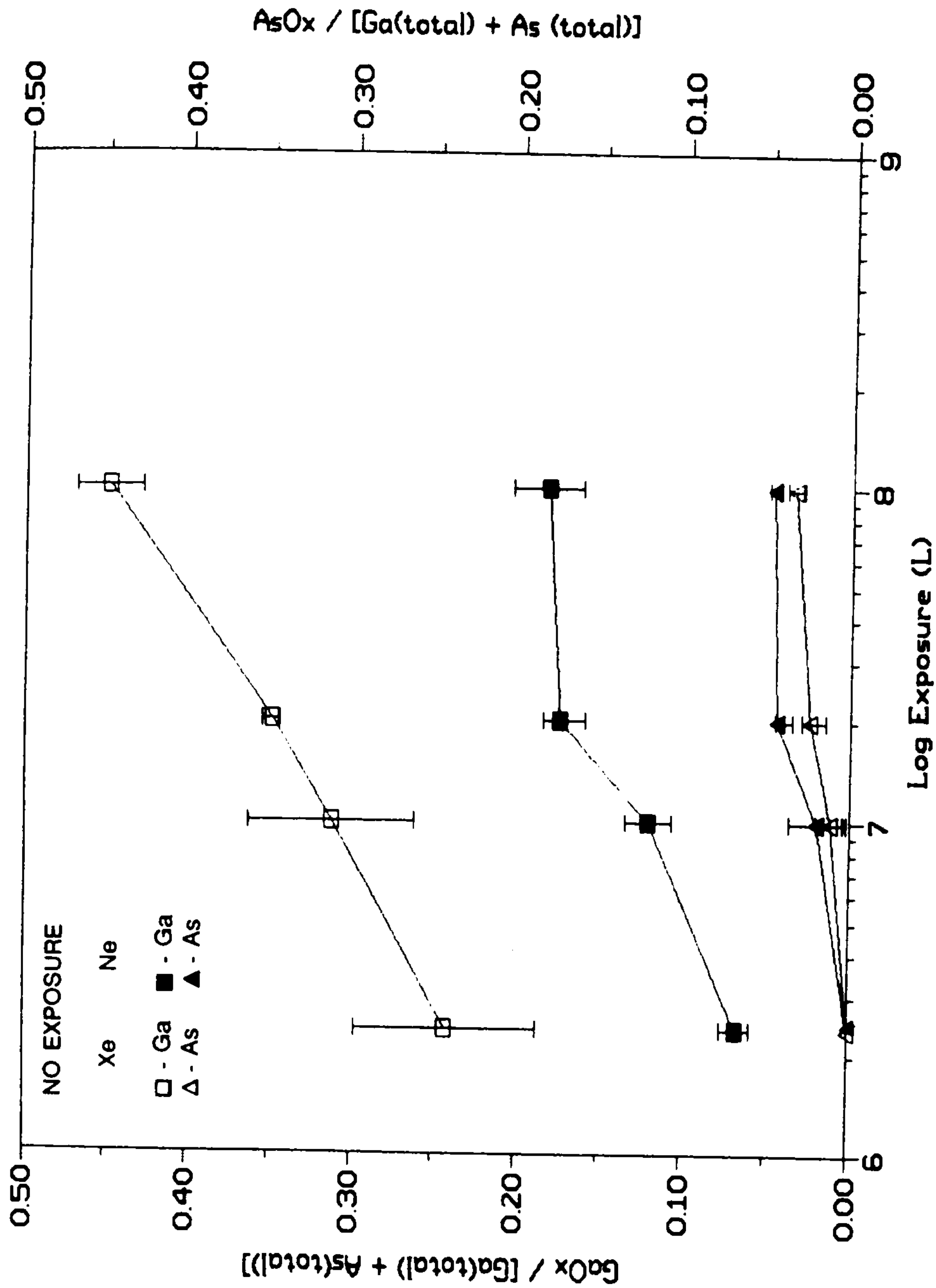


**Figure 4.29** Relative amounts of oxide produced for 3 KeV $Xe^{+}$ and $Ne^{+}$ ion-bombarded GaAs as a function of NO exposure.

be expected [194]; however, this peak cannot be attributed to NO due to the lack of a corresponding N 1s signal. The intensity of the O 1s photopeak at 532.4 eV is definitely strong enough (5-10 at.%) to produce a corresponding N 1s signal since the sensitivity factors for N 1s and O 1s are approximately the same (see Table 3.1). The molecularly adsorbed oxygen peak is formed upon initial exposure to NO ($3x10^6$ L) and the intensity does not appear to grow with increasing exposure as does the peak due to the oxides.

The lack of a signal from the N 1s region suggests that room temperature adsorption of NO on ion bombarded GaAs is dissociative. Dissociative adsorption was also observed by Bermudez *et al.* [118] on $Ar^+$ sputtered/annealed, clean GaAs(110). The adsorption of NO on $Ne^+$ sputtered/annealed GaAs(110) at 90 K resulted in molecular adsorption of NO with the possibility of some dissociative adsorption [119]. So and Ho [119] observed vibrational bands in the HREELS (high resolution electron energy loss spectroscopy) spectra that provided evidence for the presence of GaO, AsO, and AsN species on the surface following NO adsorption (2.0 L). They observed some reaction of adsorbed NO with GaAs which produced a small amount of $N_2O$.

When comparing equivalent NO and $O_2$ exposures for 3 KeV $Xe^+$ ion-bombarded GaAs samples, the relative amount of oxide formed following exposure to NO is greater than the equivalent $O_2$ exposure (compare Figures 4.9 and 4.23). For either NO or $O_2$ exposure, approximately the same amount of arsenic oxide is produced. However, at $10^8$ L NO or $O_2$ exposure (3 KeV $Xe^+$), the relative amount of gallium oxide produced following an NO exposure is almost twice that for an equivalent $O_2$ exposure. At $10^8$ L NO exposure, the relative amount of gallium oxide is greater than the amount produced following a $10^{11}$ L $O_2$ exposure. The differences observed in the amounts of oxides produced following NO and $O_2$ reactions can help to provide an explanation for a possible reaction pathway and also provide evidence for the nature of the ion bombarded GaAs surface. This will be discussed in section 4.4.

When the NO gas was not properly purified, $NO_2$ was observed as a contaminant (<10%, determined from mass spectral analysis) and the reaction with GaAs was quite different. The results were not reproducible when compared to those results obtained from pure NO exposures. The NO results presented previously were all obtained using purified NO.

Spectra are shown in Figure 4.30 for ion bombarded GaAs exposed to NO contaminated with $NO_2$. Differences were observed in the amount of oxidation of both Ga and As and a weak N 1s photopeak signal was detected. Following NO(contaminated) exposures, greater amounts of gallium and arsenic oxides were produced than for equal exposures using pure NO. In one case (3 KeV $Xe^+/10^8$ L NO(contaminated)) the exposure yielded almost identical results as a lower exposure of pure NO (3 KeV $Xe^+/10^7$ L NO). A N 1s peak was detected at ~404 eV, which is in the area expected for nitrogen bonded to oxygen [194]. $N_2O$ exhibits two N 1s photopeaks at 402 and 406 eV. Thus the presence of $N_2O$ can be ruled out. There is evidence for the presence of $NO_2$ in the O 1s photopeak following NO(contaminated) exposure. Figure 4.31 shows the curve-resolved spectra for the O 1s photopeaks corresponding those in Figure 4.30. The oxygen peak due to adsorbed oxygen is broader than expected and another peak can be included in the spectra at ~533 eV, which provides evidence for adsorbed $NO_2$ [194]. The N:O atomic ratio is close to 1:2. The important fact is that N is found on the surface following exposures using contaminated NO and it is not observed for adsorption with purified NO.

#### *4.3.4 $N_2O$ Exposure*

The XPS spectra obtained at a 15° toa are presented in Figure 4.32 for the Ga 3d, As 3d, and O 1s levels for 3 KeV $Xe^+$ and $Ne^+$ ion-bombarded GaAs following $1x10^7$, $1x10^8$, and $2x10^{11}$ L $N_2O$ exposures. No signal from the N 1s level was observed for any of the

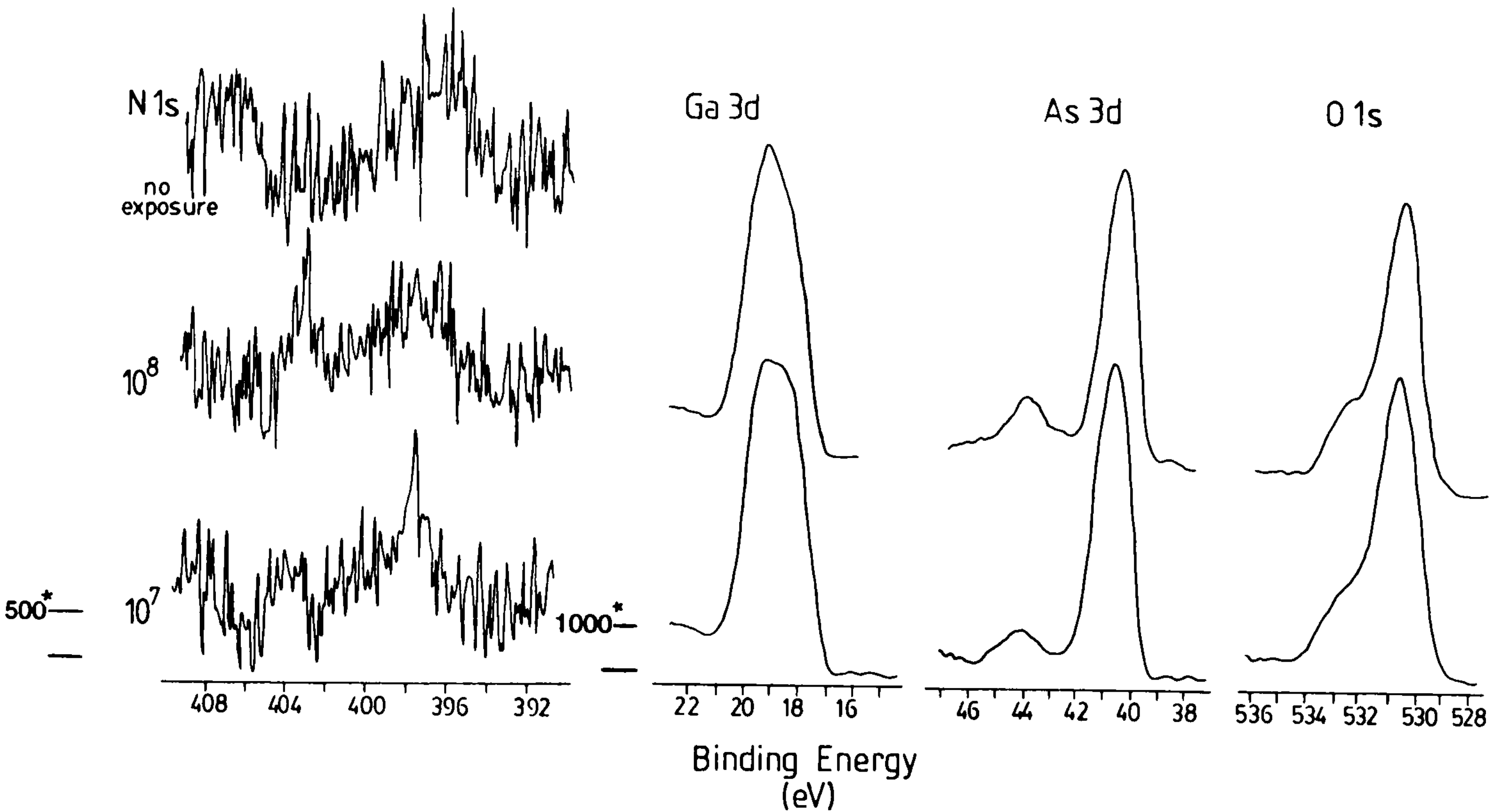


**Figure 4.30 XPS spectra for 3 KeV $Xe^+$ ion-bombarded GaAs exposed to contaminated NO.**

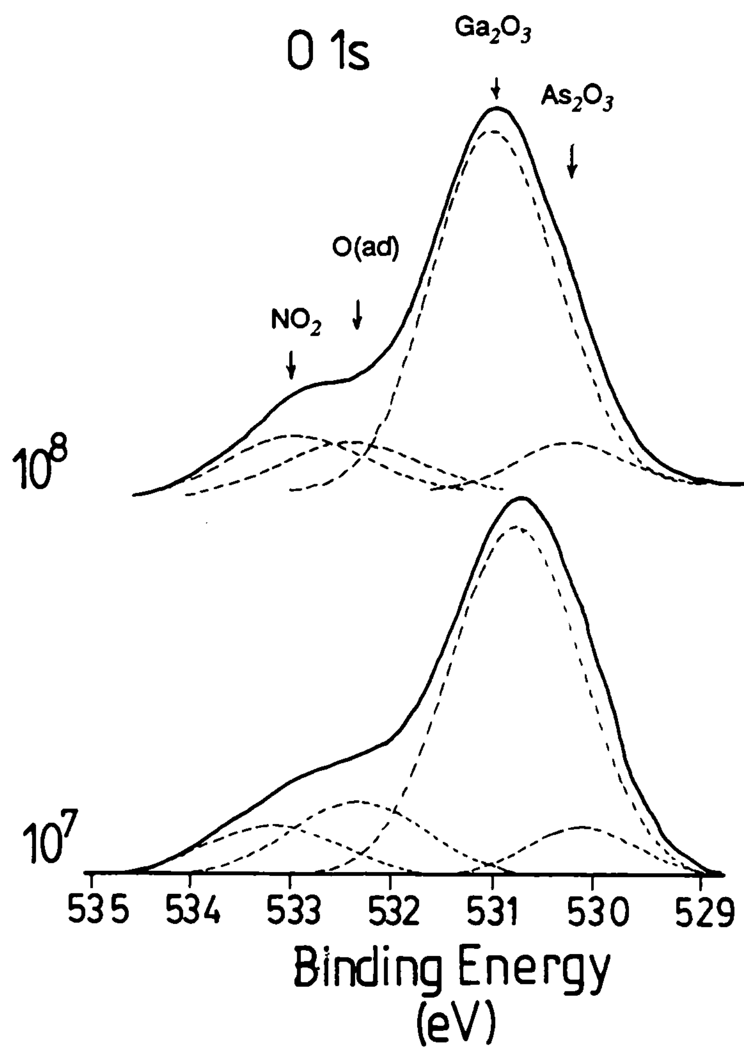


**Figure 4.31** Curve-resolved O 1s spectra for contaminated NO exposure.

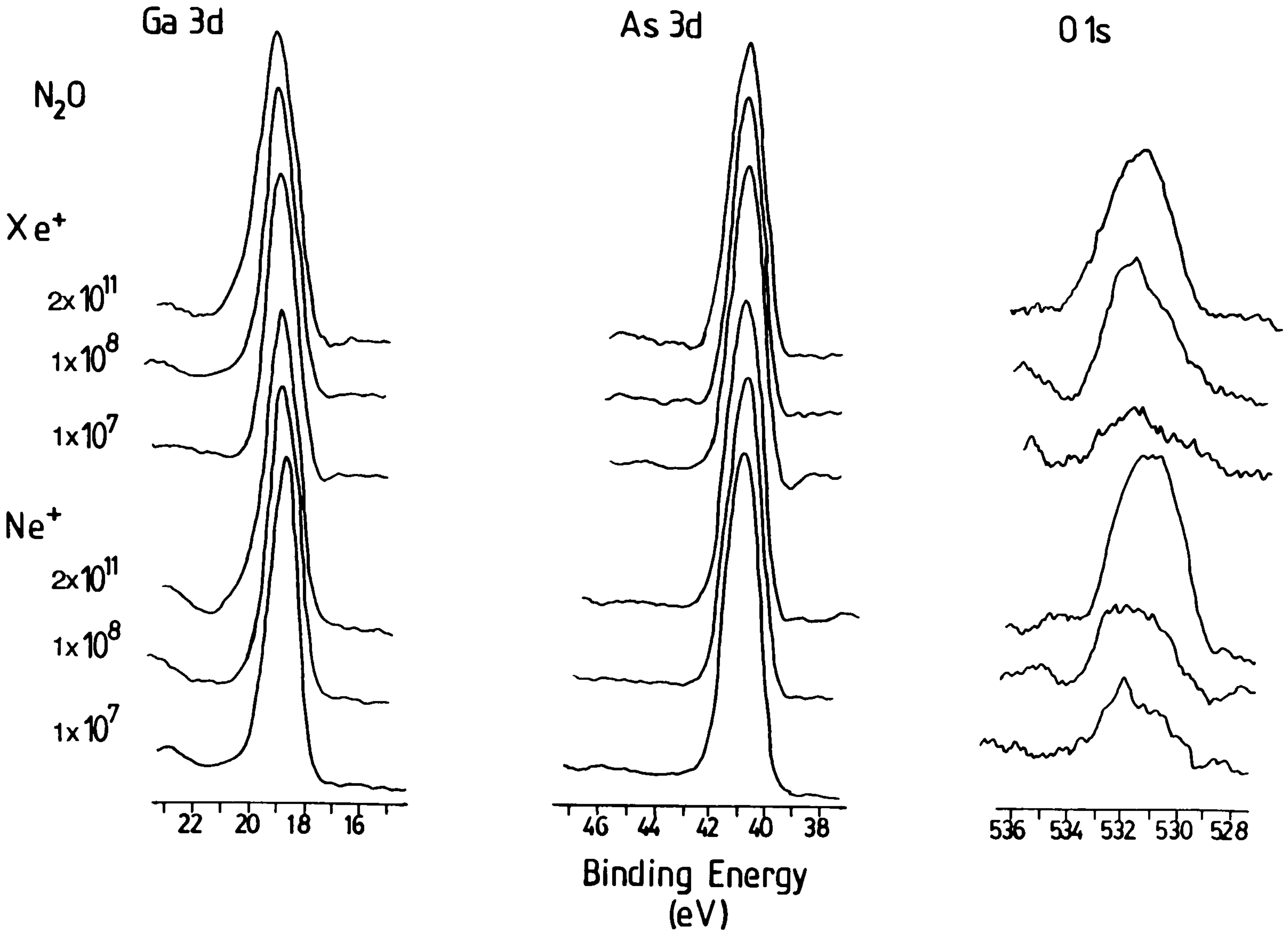


**Figure 4.32** XPS spectra taken at 15° toa for 3 KeV $Xe^+$ and $Ne^+$ ion-bombarded GaAs following $1x10^7$, $1x10^8$, and $2x10^{11}$ L $N_2O$ exposures.

$N_2O$ exposures, which suggests that the dissociation of $N_2O$ into $N_2$ (which desorbs) and atomic oxygen occurs [115]. The relative amount of oxide produced as a function of $N_2O$ exposure is presented in Figure 4.33. Ion bombarded GaAs exposed to $N_2O$ at the exposure levels indicated produces only $Ga_2O_3$ and the amount of $Ga_2O_3$ is equivalent for both 3 KeV $Xe^+$ and $Ne^+$ ion-bombarded samples for $N_2O$ exposures below $10^{11}$ L. At $10^{11}$ L $N_2O$ exposure, 3 KeV $Xe^+$ ion-bombarded GaAs produces more $Ga_2O_3$ than 3 KeV $Ne^+$ ion-bombarded GaAs. The O 1s photopeak exhibits the two characteristic oxygen peaks; one due to the oxygen from $Ga_2O_3$ (~531 eV) and the other due to adsorbed molecular oxygen (532.6 eV).

These results are quite unlike those presented by Bertness *et al.* [115] for cleaved GaAs(110) exposed to $N_2O$, except that they also observed no nitrogen on the surface. One difference is that they found oxidation below $10^6$ L $N_2O$ exposure, with As being the predominantly oxidized species. In this study, oxidation is barely discernable below $10^{11}$ L $N_2O$ exposure. Another difference is that the extent of oxidation for GaAs(110) exposed to $N_2O$ was greater than for an equivalent $O_2$ exposure. The opposite is found in this study. The amount of oxide formed is much greater for an $O_2$ exposed surface than for an $N_2O$ exposed surface (at equal exposures).

## 4.4 Possible Reaction Mechanisms with Ion Bombarded GaAs and a Model for the Ion Bombarded GaAs Surface

It was shown in previous sections that ion bombardment enhanced the reactivity of GaAs and that enhancement was related to the energy and mass of the bombarding ion. It was also suggested that enhanced reactivity was related to the presence of defects on the surface of ion bombarded GaAs. However, when comparing the reactivity of an ion bombarded surface exposed to a series of different gases (i.e. 3 KeV $Xe^+$ exposed to NO, $O_2$, and $N_2O$), distinct differences were observed in the relative amounts of oxides produced.

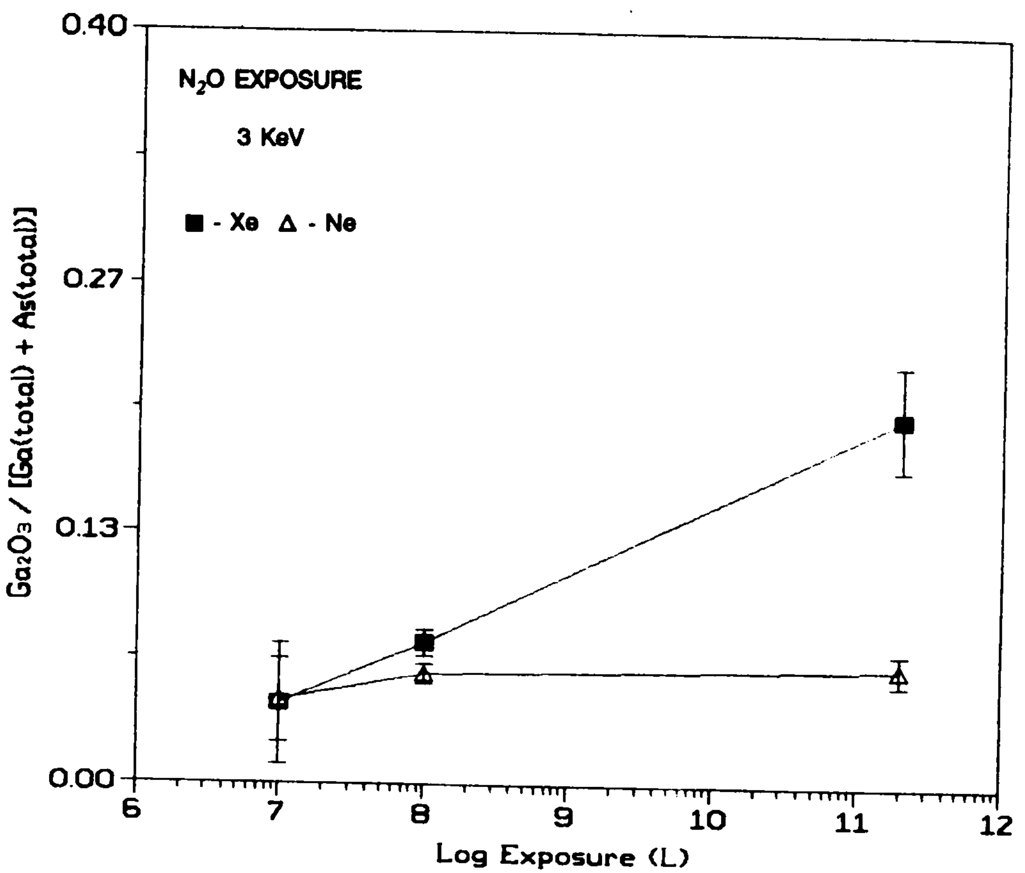


**Figure 4.33** Relative amounts of oxide formed as a function of $N_2O$ exposure for 3 KeV $Xe^+$ and $Ne^+$ ion-bombarded GaAs.

NO was shown to be the most reactive and $N_2O$ the least reactive. For 3 KeV $Xe^+$ ion-bombarded GaAs, NO exposure yielded the greatest amount of $Ga_2O_3$. Differences were also noted between the results obtained for ion bombarded GaAs and results reported for GaAs(110) by Bermudez *et al.* [118] (NO exposure) and Bertness *et al.* [115] ($N_2O$ and $O_2$ exposures). These differences provide some insight for possible models of the ion bombarded GaAs surface and the pathway of the reactions.

In the study of $O_2$ and $N_2O$ reactions with cleaved GaAs(110) [115], break-up of the reacting molecules upon adsorption was the limiting step in the chemisorption reaction. The X-O bond strengths (X = N-, O-, and $N_2$-) for NO, $O_2$, and $N_2O$ are 6.5, 5.1, and 1.7 eV, respectively. Bertness *et al.* observed more oxidation following $N_2O$ adsorption than for $O_2$ adsorption. In this study just the opposite trend in reactivity is observed for $N_2O$ versus $O_2$ adsorption reactions. Therefore, the conclusion that dissociation of the reactant molecule is the determining factor in the reaction with ion bombarded GaAs can be eliminated. Other factors, such as sticking coefficients, the structure of the ion bombarded surface, the interaction of the reactant molecule with the ion bombarded surface, and the reaction pathways most likely control the reactions.

The trends in reactivity noted for ion bombarded GaAs exposed to the various gases (reactivity: NO> $O_2$> $N_2O$) are very similar to the results observed by others [115,118,119, 195] for ***photoenhanced*** chemical reactions on GaAs. Reactions that exhibit an enhancement in reactivity (in this case produce more oxide) when illuminated with light are designated as photoenhanced chemical reactions. Usually a wavelength of light is chosen that is known not to excite the reacting molecules. The references cited here [115,118,119,195] utilized visible and near uv irradiation ($<10$ W/cm$^2$). $O_2$ [115,195] and NO [118] exhibited photoenhancement and $N_2O$ [115] exhibited no photoenhancement. Photon-induced enhancements in reactivity are usually attributed to interactions of the adsorbed molecule with photogenerated carriers; electron-hole pairs that are created in the bulk by the

interaction of photons with the semiconductor. The pairs migrate to the surface and react with the adsorbate-surface complex, and induce reactions [196]. Ion bombardment results in a disruption of the surface structure and an increased number of electrons could be present at the surface in the form of singly occupied dangling bonds, which are referred to as defects. If defects are in the form just described, the increased reactivity of ion bombarded GaAs exposed to $O_2$ and NO suggests that an increased number of carriers (electrons) on the surface may be involved. The extent to which the different gases interact with surface electrons (defects) results in the differences observed in the relative amount of oxides produced following exposure of an ion bombarded surface to the different gases.

From the XPS results, it was found that the ion bombarded surface was As deficient and evidence was also presented for disorder (breaking of Ga-As bonds) in the surface (broadening of the Ga 3d photopeak). Evidence for disorder was also obtained from Raman and uv-reflectivity spectra, and electrical measurements. Therefore, the trend found in the reactivities under the conditions used suggests that defects are present on an ion bombarded surface. The defects may be single electron Ga dangling bonds and/or Ga-Ga "wrong" bonds both of which result in an increase in the concentration of electrons at the surface (see Figure 4.24). The presence of defects at the surface could aid in the adsorption or dissociation of reactant molecules depending on the extent that each reactant molecule interacts with the defect. For singly occupied dangling bonds the reactivity might be controlled by the initial formation of a negative complex:

$$X(g) + e^{-}(s) \rightarrow X^{-}(ad) \quad (4.6)$$

where X represents NO, $O_2$ or $N_2O$ and $e^{-}(s)$ denotes an electron in a surface Ga dangling bond. It has been suggested by others [66,115,195] that the dissociation of the reactant molecule takes place through a negative complex and Barton *et al.* [41] noted that this dissociation could take place at defect sites. Therefore, the relative reactivity observed,

NO > $O_2$ > $N_2O$, for ion bombarded GaAs should be directly related to the electron affinity of the molecules. The electron affinities (gas-phase) for NO, $O_2$, and $N_2O$ are 0.024, 0.44, and <1.465 eV, respectively [179]. Since the electron affinity of NO is the smallest but it showed the greatest reactivity with GaAs, the formation of the negative complex appears not to be the controlling factor in the reactions (based on the electronegativity values).

The sticking coefficients of the reactant gases may be partly responsible for the observed reactivities. The sticking coefficient, which is the probability of an incident molecule sticking to the surface is defined by [198]

$$s = \frac{\text{rate of adsorption of gas}}{\text{rate of collision with surface}} \tag{4.7}$$

as a function of the fractional coverage $\theta$ defined by

$$\theta = \frac{\text{number of molecules adsorbed}}{\text{maximum uptake}} \tag{4.8}$$

Plots of s versus $\theta$ have an initial region ($\theta < 0.6$) in which s is nearly constant. As $\theta$ approaches 1, the sticking coefficient declines to zero. The value of s as $\theta \rightarrow 0$ is known as the initial sticking coefficient, $s_o$, the sticking coefficient on a clean surface. The initial sticking coefficients for $O_2$/GaAs have been reported for almost every GaAs surface and a complete listing is reported by Ranke *et al.* [199]. The sticking coefficients vary widely ($10^{-9}$ to $10^{-4}$) for different GaAs surfaces and depend on the crystallographic orientation and on how the surfaces were prepared (cleaved or ion bombarded and annealed) [43]. Generally, disordered surfaces exhibit a higher sticking coefficient for $O_2$ than for ordered surfaces. The initial sticking coefficients cannot be calculated from the data in this study due to the lack of data points at very low exposures and low coverages. However, an indication of what the trend might be for the sticking coefficients of $O_2$, NO, and $N_2O$ on ion bombarded

GaAs can be obtained. The magnitude of the initial sticking coefficient will be reflected in the amount of oxygen found on a sample following initial exposure (the first exposure of clean, ion bombarded GaAs). If the initial sticking coefficient for one gas is higher than that of another gas, then the atomic concentration of oxygen will be lower for the gas with the lower initial sticking coefficient. The lowest exposure obtained for $O_2$ and $N_2O$ was $10^7$ L and there was some data for NO where the initial exposure was carried out at $10^7$ L. The atomic percent of oxygen following $O_2$, NO, and $N_2O$ exposures were found to be 25 ± 5, 27 ± 5, and 7 ± 3, respectively. These values indicate that there should be no difference in the initial sticking coefficients for $O_2$ and NO, but that $N_2O$ would have the lowest sticking coefficient of the three.

At this point, however, an explanation can be offered for the low reaction results observed with $N_2O$ on ion bombarded GaAs. The low sticking coefficient (proposed from the oxygen concentration above) could be the limiting factor in the reaction of $N_2O$ with ion bombarded GaAs. Even if a reaction is favored (see equation 4.9), the molecules never get a chance to react with the surface if the sticking coefficient is very low, because they do not adsorb.

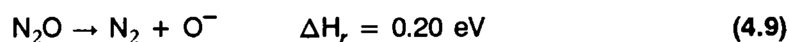

$$N_2O \rightarrow N_2 + O^- \qquad \Delta H_r = 0.20 \text{ eV} \qquad \textbf{(4.9)}$$

The sticking coefficients alone do not explain the enhanced reactivity observed for NO and $O_2$. In order to explain the differences in reactivity, it is important to examine first what is known about the surface bonding schemes of GaAs(110) and Si(111) and some conclusions presented by Goddard *et al.* [83] for the initial steps in the chemisorption of $O_2$ and the bonding of O atoms to the surface of GaAs(110) and Si(111). The GaAs(110) surface is important because most of the data presented in the literature deals with GaAs(110) and the interaction of O and $O_2$ with GaAs(110) have been well studied. GaAs(110) also possesses

a doubly occupied surface dangling bond (see Figure 4.34), a fact that will be useful in comparing ion bombardment results. Si(111) possesses a singly occupied dangling surface bond (see Figure 4.34) and it is suitable for comparing the interaction of O and $O_2$ with a singly occupied dangling bond. Si(111) also serves as a model surface for demonstrating the interaction of $O_2$ with ion bombarded GaAs.

### *4.4.1 GaAs(110) and Si(111) Surfaces*

Shown in Figure 4.34 are the bonding schemes for GaAs(110) and Si(111). The three electrons from surface Ga atoms participate in covalent bonding with three As neighbors and three of the five As valence electrons participate in bonding with Ga neighbors. The last two electrons from As occupy a nonbonding (dangling) orbital that projects out of the surface. This is probably why most of the reactions observed for the oxidation of cleaved GaAs(110) result in the preferential formation of arsenic oxides. The dangling bond on the surface As atom is the most accessible site for a reaction and the reactant molecule is forced to interact with the lone pair resulting in the oxidation of surface As atoms. The important point to note for the Si(111) surface is that Si atoms terminate at the surface with dangling bonds that are occupied by one electron. Because these two surfaces terminate differently - GaAs(110) with filled dangling bonds and Si(111) with singly occupied dangling bonds - the bonding of $O_2$ and O atoms may be expected to be different for the two surfaces.

### *4.4.2 Chemisorption of $O_2$ and O Atoms to GaAs(110) and Si(111)*

A complete review of the chemisorption of $O_2$ and O atoms to GaAs and Si was published by Goddard *et al.* [83]; presented here is only a short summary of the conclusions. Before discussing the conclusions, the symbols used for $O_2$ and O will be presented. Oxygen has the electron configuration $1s^2 2s^2 2p^4$, with 4 electrons in the three *p*

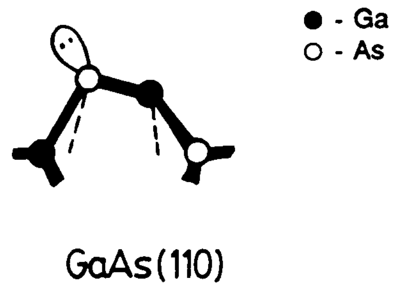


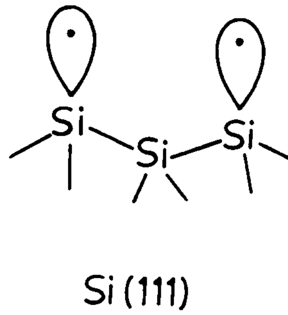


**Figure 4.34** Bonding schemes for GaAs(110) [197] and Si(111) [83].

orbitals. For simplicity, the s orbital will not be shown, but will be indicated as xx in subsequent Lewis-type congfigurations. If the *p* orbitals are represented with 8,∞, and o (*p* orbital out of the plane), and electrons represented with dots, then the ground state of the O atom and $O_2$ can be illustrated as [83]:

(4.10)

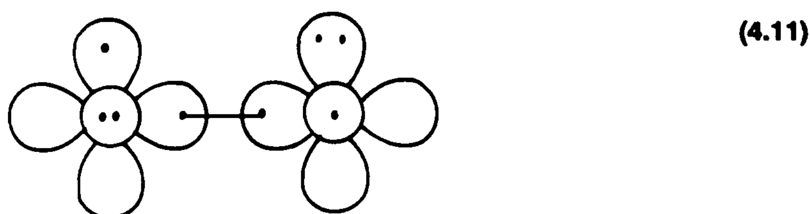

(4.11)

A summary of the conclusions presented by Goddard *et al.* for the interaction of $O_2$ and O with GaAs(110) and Si(111) are:

1) $O_2$ requires at least one singly occupied orbital on GaAs(110) or Si(111) that can be paired with the one of the singly occupied orbitals of $O_2$ to make a strong chemical bond. This singly occupied orbital is available on the Si(111) surface. The ground state of $O_2$ bonds to the Si(111) surface and leads to a peroxy radical (4.12) and the terminal O atom (excited state of peroxy radical (4.13a)) then may react with the surface by attacking an adjacent surface Si atom to form a bridged bond (4.13b) or two chemisorbed O atoms (4.14), which can then attack a Si-Si bond to form (4.15). Atomic O can also bond directly to the surface as in (4.16).

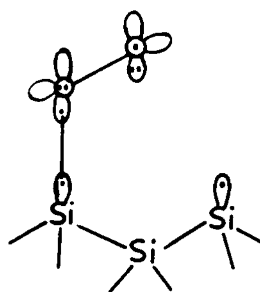

(4.12)

a)

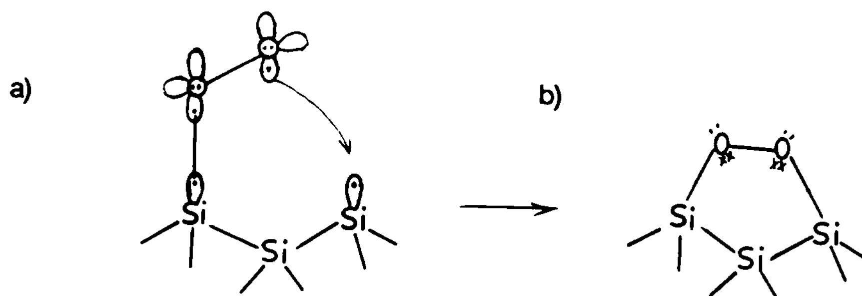


(4.13)

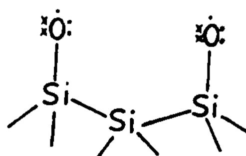

(4.14)

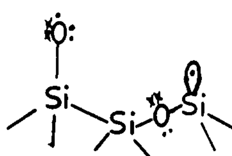

(4.15)

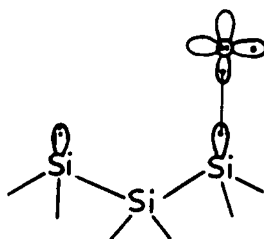

(4.16)

2) On the GaAs(110) surface there are no singly occupied orbitals to pair with $O_2$ and bonding with As is not favorable; however, O atom does make a strong bond with As (4.17b). The As lone pair delocalizes toward O and forces the O electrons to fill two of the three *p* orbitals forming an excited state of O (4.17a). An empty orbital on Ga is available for bonding but this cannot bond strongly to the lone pair orbital of O (4.18). Ga has no nonbonding electrons to donate to the O atom without disrupting one of the three other bonds to As and it is not favorable for O to donate electrons into the empty Ga orbital [41].

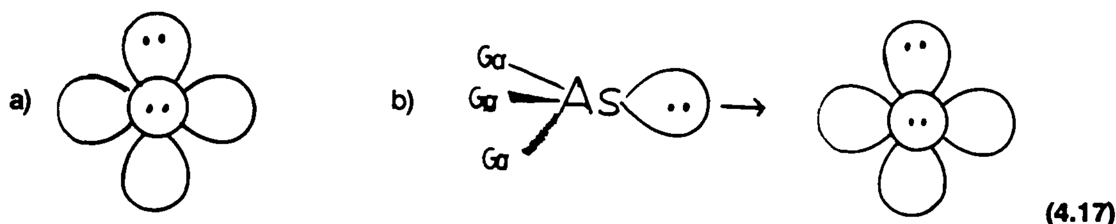


(4.17)

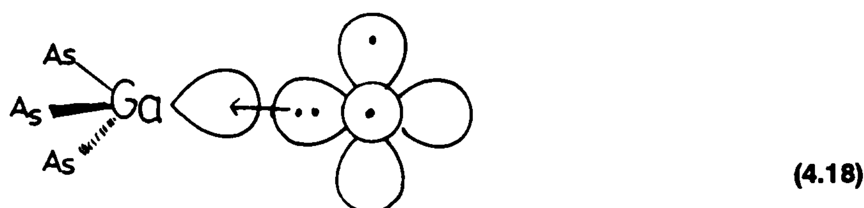


(4.18)

The most important conclusion made by Goddard *et al.* that is important in the present work is the following: "molecular $O_2$ bonds only weakly to the perfect GaAs(110) surface. In our view, defect sites with a broken Ga-As bond are required to form a strong bond to molecular $O_2$. Indeed, such sites may catalyze the dissociation of $O_2$ into chemisorbed O atoms. These O atoms may then attack nearby Ga or As atoms even though $O_2$ would not. This O atom may then bond to As atoms of the perfect surface...or may attack the AsGa bonds of the surface to form the oxide."

### 4.4.3 A Possible Surface Model for Ion Bombarded GaAs

It was previously proposed that ion bombardment disrupts the surface Ga-As bonds and that the surface is likely composed of Ga atoms terminated with singly occupied dangling bonds. The dangling bond model is supported by the results observed in this study for the oxidation of ion bombarded GaAs by $O_2$. The reaction of $O_2$ with ion bombarded GaAs was greater than with chemically cleaned and IHT prepared GaAs and it was also greater than the results for similar $O_2$ exposures for cleaved GaAs(110) [66]. $O_2$ does not interact strongly with As atoms on GaAs(110) because there are no singly occupied orbitals to pair with $O_2$ and the Ga atoms do not provide sites for strong bonds. However, if the ion bombarded GaAs surface were composed of singly occupied dangling bonds, the interaction of $O_2$ would be expected to be greater than that for a non-bombarded surface. The dangling bonds on an ion bombarded surface would provide more favorable conditions for $O_2$ chemisorption. The configuration of the ion bombarded surface and the interaction of $O_2$ with that surface may be similar to that shown for Si(111) and can be used as a model for demonstrating why the ion bombarded GaAs surface is considered to be composed of singly occupied Ga dangling bonds. Figure 4.24 illustrates possible structures for ion bombarded GaAs. Diatomic oxygen initially interacts with surface dangling bonds of Ga to form a peroxy radical (4.19) or two chemisorbed O atoms (4.20).

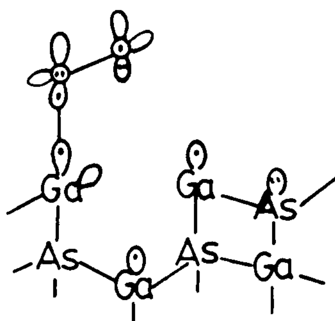


(4.19)

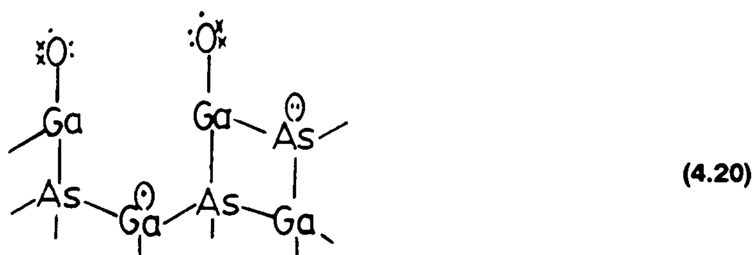


If there are Ga-Ga "wrong" bonds available as a result of ion bombardment, the terminal O atom in the peroxy radical structure could attack an adjacent Ga-Ga bond to form (4.21) rather than a Ga-As bond to form (4.22b). Attack at Ga-Ga is favored over attack of Ga-As bonds because less energy is required to break a Ga-Ga bond than a Ga-As bond (1.43, 2.17 eV, respectively [180]). Structure (4.20) with two chemisorbed O atoms could also form (4.22b).

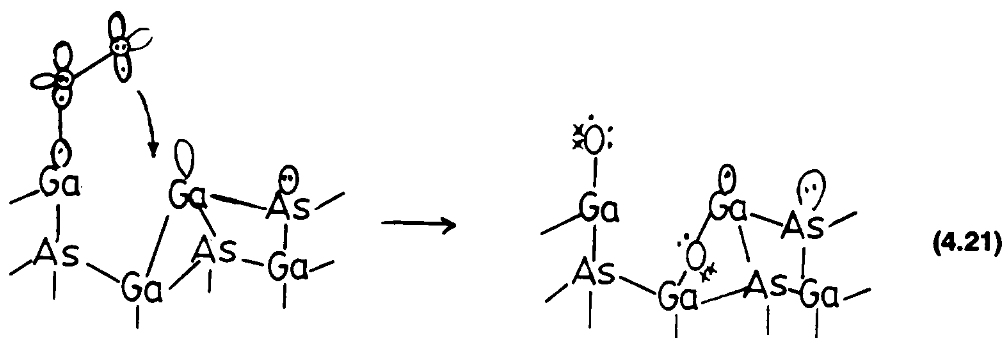


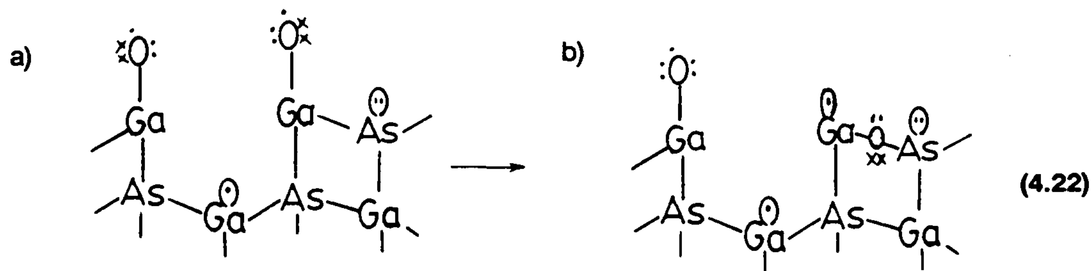

The model just proposed offers an explanation for why $O_2$ interacts more strongly with ion bombarded GaAs than non-ion bombarded GaAs. However, if the limiting factor was the interaction of the reactant molecule with the surface dangling bonds to form the adsorbed complex $O_2^-$, then it would be expected that there would be a relationship between the electron affinity and reactivity. There is no relationship between the electron affinity and the reactivity because the reactivity of $O_2$ is less than NO, but NO has the lower electron affinity. Therefore, some step in the reaction pathway that comes after the formation of the adsorbed complex must be controlling the reactions.

### *4.4.4 Possible Reaction Pathways for NO and $O_2$*

The reaction of NO with ion bombarded GaAs was even greater than that for $O_2$. As previously stated, the differences in the reaction do not appear to be the formation of an adsorbed complex. Therefore, limiting steps in the possible reaction pathways should be considered. The reactions for chemisorption of $O_2$ and NO are outlined below and the values for $\Delta H_r$ were calculated from those for the gaseous state [176] and are in electron volts (eV).

The reactions being considered for $O_2$ are:

$\Delta H_r$ (eV)

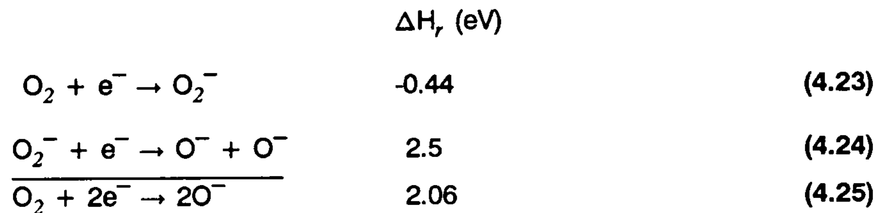

$$O_2 + e^- \rightarrow O_2^- \qquad -0.44 \qquad (4.23)$$

$$O_2^- + e^- \rightarrow O^- + O^- \qquad 2.5 \qquad (4.24)$$

$$O_2 + 2e^- \rightarrow 2O^- \qquad 2.06 \qquad (4.25)$$

and those for NO are:

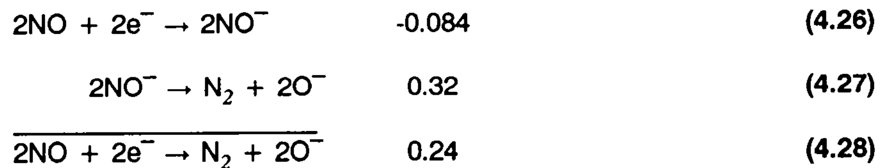

$$2NO + 2e^- \rightarrow 2NO^- \qquad -0.084 \qquad (4.26)$$

$$2NO^- \rightarrow N_2 + 2O^- \qquad 0.32 \qquad (4.27)$$

$$2NO + 2e^- \rightarrow N_2 + 2O^- \qquad 0.24 \qquad (4.28)$$

Reactions 4.23 and 4.26 involve formation of the adsorbed negative molecule. Stated previously, if this were the limiting factor, $O_2$ reactions would be preferred over NO reactions. Reaction step 4.24 involves the further addition of an electron to $O_2^-$, which is probably the interaction of the $O_2^-$(ads) with a dangling bond on a nearby Ga atom (see 4.20). Reaction 4.27 involves the formation of $N_2$ from two adsorbed $NO^-$ molecules. Clearly, reaction 4.27 is favored over 4.24 (based only on thermodynamics). The overall $\Delta H_r$ for $O_2 \rightarrow 2O^-$ is 2.06 eV and for $2NO \rightarrow N_2 + 2O^-$ is 0.24 eV, thus the reaction of NO with GaAs is thermodynamically favored over $O_2$. The formation of $N_2$ from the NO reaction is also supported by the XPS results. No N is detected following NO exposure, which suggests that $N_2$ is produced and desorbs from the surface during the reaction. Reactions 4.23 through 4.28 that have been shown up to this point involve the formation of two Ga-$O^-$ species on ion bombarded GaAs (see 4.20 for example). From these proposed reactions, both $O_2$ and NO would form the two $GaO^-$ species (with NO giving off $N_2$) and any reactions occurring after this point to form the more complex oxides ($Ga_2O_3$ or $As_2O_3$) would involve the same starting point (i.e. the Ga-$O^-$ surface species/two chemisorbed O atoms, structure (4.20)), where from this point the Ga-$O^-$ would go on to form the more complex oxides, $Ga_2O_3$ and $As_2O_3$, by breaking other Ga-Ga "wrong" bonds or Ga-As bonds (see 4.22); the energy required to break the bonds would be 1.43 and 2.17 eV, respectively. The formation of two chemisorbed $O^-$ species would most likely occur for NO adsorption, but $O_2$ adsorption to form $O_2^-$ could take a different pathway. Breaking of surface bonds (Ga-As or Ga-Ga) could occur if it is more favorable for the peroxy radical structure (4.19) to directly attack an adjacent bond (4.22) instead of dissociating into two chemisorbed $O^-$. Values for the Ga-As or Ga-Ga bond strengths and the $\Delta H_r$ (gas phase value) for equation 4.24, would lead one to suggest that direct attack is more favorable over dissociation; however, the NO reaction is still favored over either $O_2$ pathway.

It can be concluded that there are two factors that control reactions with ion bombarded

GaAs. The first is the sticking coefficient, which limited the reaction of $N_2O$ with ion bombarded GaAs. A molecule such as $N_2O$ could exhibit a low sticking coefficient as a result of the structure of the ion bombarded surface. Repulsion could occur between $N_2O$ and the ion bombarded surface due to the increased number of dangling bonds containing upaired electrons which would inhibit the adsorption of $N_2O$; whereas, NO and $O_2$ would prefer to interact with this kind of surface because of the unpaired electrons available to bond with. Therefore, NO and $O_2$ would exhibit increased sticking coefficients over that of $N_2O$.

If the sticking coefficient is high enough to allow adsorption of the reactant molecules, then a second factor comes into control. This factor is the preferred reaction pathway. Possible reaction pathways were presented above for $O_2$ and NO. The one step in the NO reaction (4.27) is thermodynamically more favorable than step 4.24 or 4.20 in the $O_2$ reaction, which leads to the suggestion that this step is the controlling step in the reaction with ion bombarded GaAs. Therefore, explanations can be suggested for the observed trend in reactivity NO $> O_2 > N_2O$ when considering the sticking coefficients and possible reaction pathways.

## 4.5 Composition of Oxide Layers

Shown in Figure 4.35 are the curve-resolved spectra taken at different toas for the Ga 3d, As 3d, and O 1s photopeaks for a 3 KeV $Ar^+$ ion-bombarded GaAs sample exposed to $10^{13}$ L $O_2$. Also shown in Figure 4.36 are the curve-resolved spectra taken at different toas for the Ga 3d and O 1s photpeaks for a 3 KeV $Xe^+$ ion-bombarded GaAs sample exposed to $10^{13}$ L $H_2O$. Figure 4.37a and 4.37b show the relative amount of oxide for each component as a function of toa. In this case, each of the oxide layers ($O_2$ and $H_2O$) is composed of at least two components. The intensity of each of these components

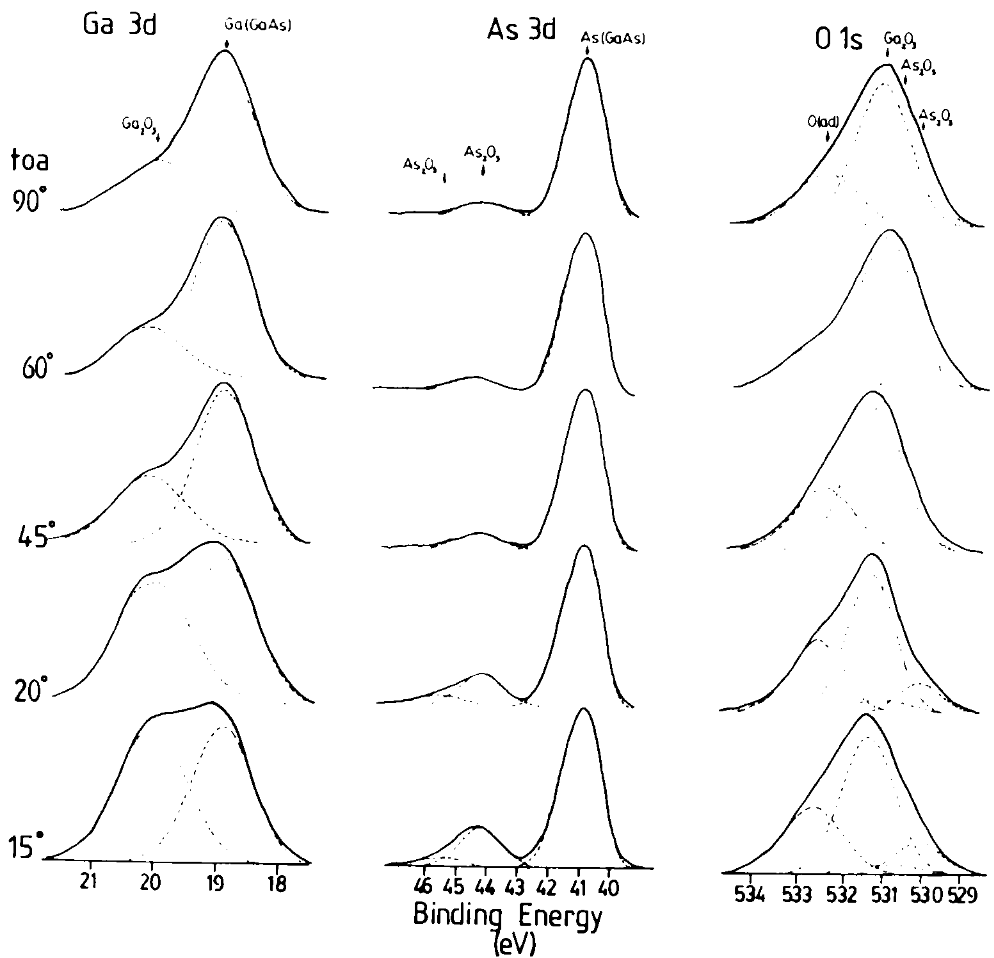


**Figure 4.35** Curve-resolved spectra at various take-off angles for 3 KeV $Ar^+$ ion-bombarded GaAs exposed to $10^{13}$ L $O_2$.

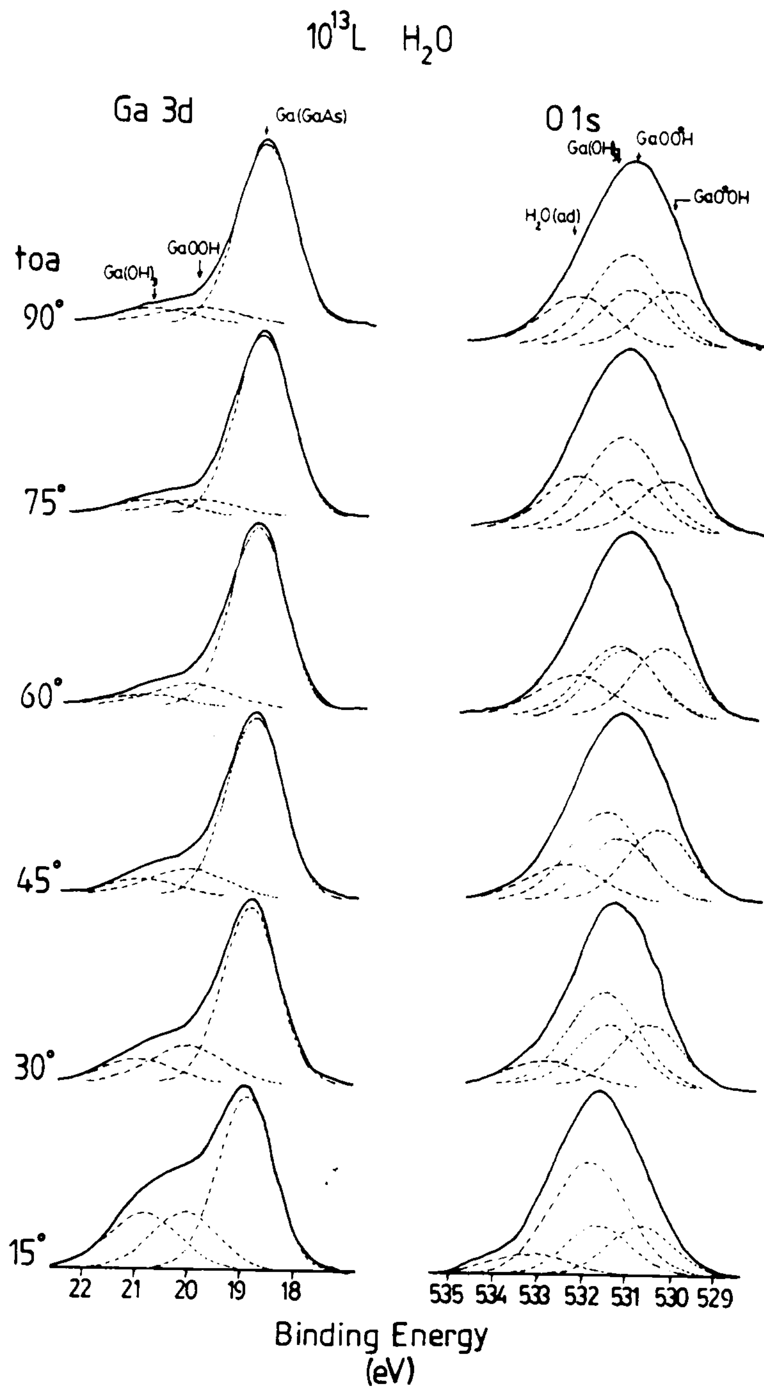


**Figure 4.36** Curve-resolved spectra at various take-off angles for 3 KeV $Xe^+$ ion-bombarded GaAs exposed to $10^{13}$ L $H_2O$.

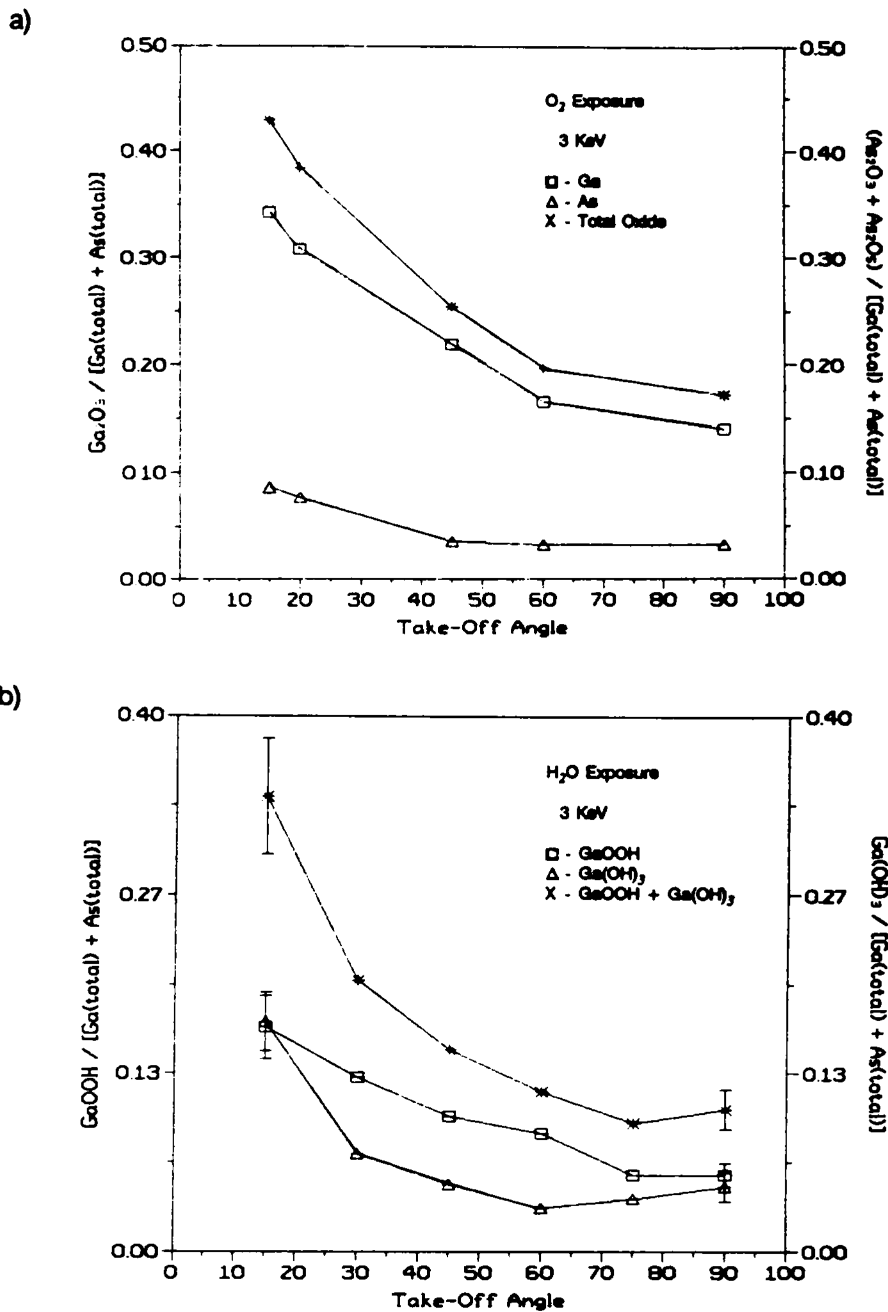


**Figure 4.37** Relative amounts of oxide formed for (a) 3 KeV $Ar^+$ ion-bombarded GaAs exposed to $10^{13}$ L $O_2$ and (b) 3 KeV $Xe^+$ ion-bombarded GaAs exposed to $10^{13}$ L $H_2O$ as a function of take-off angle.

decreases with increasing toa and each component decreases at about the same amount relative to the other component; i.e. $Ga_2O_3$ to ($As_2O_3$ and $As_2O_5$). Each component decreasing relative to the other as a function of toa, would indicate that the oxide layer formed is a homogeneous layer of the two components with neither of the components preferentially formed at the surface or interface. Many of the literature results for $O_2$ exposed GaAs report a build-up of arsenic oxides at the interface [5,108], but this is usually for much thicker oxide layers or oxides formed by anodization.

# Chapter V: Summary

In this study it was found that the reactivity of the GaAs surface could be increased by ion bombardment. The extent of increase was directly dependent upon the energy and mass of the bombarding ion. The oxidation results were compared to chemically cleaned (1:1 HCl(conc)/$H_2O$) GaAs(100) and IHT prepared GaAs(100) and to results from the literature for cleaved GaAs(110) and ion bombarded/annealed GaAs.

Chemical cleaning of GaAs(100) removes the oxides from GaAs and leaves a surface that is As-rich and contains adsorbed oxygen. IHT prepared GaAs(100) contains $<10$ at.% adsorbed oxygen and is slightly Ga-rich (Ga/As = $1.23\pm0.07$). Ion bombardment of chemically cleaned GaAs(100) results in the preferential sputtering of As, with the As depletion being greatest for 2 and 3 KeV $Ar^+$ and 3 KeV $Xe^+$ ion-bombardment. The As depletion was determined to be at least 60Å as measured by XPS. Ion bombardment causes the surface to become disordered as evidenced by the destruction of the peaks due to crystalline GaAs in uv-reflectivity spectra and Raman spectra. The depth of damage to the crystal could be estimated from the uv-reflectivity and Raman spectra. The damage depth increased with increasing $Ar^+$ ion bombardment energy and the damage depth was most shallow for 3 KeV $Xe^+$ ion bombardment ($\approx$50Å) and greatest for 3 KeV $^3He^+$ ion-bombardment ($>$500Å). The relative damage depth was also confirmed by capacitance-voltage measurements. The overall capacitance of the area sampled by the diode decreased with decreasing ion mass, which was caused by the increasing depth of an amorphous layer that was caused by ion bombardment.

The effect of increasing ion bombardment energy on reactivity was studied for $O_2$ and $H_2O$ exposures. Samples were bombarded with 0.5 - 3KeV $Ar^+$ ions. Exposure of ion-bombarded GaAs to $10^{11}$ - $10^{13}$ L $O_2$ resulted in the formation of $Ga_2O_3$, $As_2O_3$, and $As_2O_5$

with preferential formation of $Ga_2O_3$. Exposure to $10^9$ -$10^{13}$ L $H_2O$ resulted in the formation of GaOOH and $Ga(OH)_3$. Chemically cleaned GaAs produced equivalent amounts of $Ga_2O_3$ and $As_2O_3$ upon $O_2$ exposure. The chemical reactivity of ion bombarded GaAs increased with increasing $Ar^+$ ion-bombardment energy. The increased chemical reactivity was shown to be a result of the formation of defects. Comparison of oxidation results of ion bombarded material with IHT prepared material substantiated this result. If the amount of Ga present in the surface layer were controlling the preferential formation of $Ga_2O_3$, then the relative amount of oxides formed on IHT treated GaAs should have been similar to 1 KeV $Ar^+$ ion-bombarded GaAs which had a similar Ga/As atomic ratio. Instead, IHT prepared GaAs produced equivalent amounts of $Ga_2O_3$ and $As_2O_3$ even though the surface was Ga rich.

The relative concentration of defects imparted to the crystal surface that affect the chemical reactivity was changed by varying the mass of the bombarding ion while keeping the ion energy and fluence constant. The effect of the mass of the bombarding ion on chemical reactivity was investigated for 3 KeV $^3He^+$, $^{20}Ne$, $Ar^+$, and $Xe^+$ ions. Exposure of these ion bombarded surfaces to $10^7$ - $10^{11}$ L $O_2$ produced $Ga_2O_3$, $As_2O_3$, and $As_2O_5$ with preferential formation of $Ga_2O_3$. The greatest amount of $Ga_2O_3$ was produced following exposure of 3 KeV $Xe^+$ ion-bombarded GaAs to $O_2$. This suggests that the greatest concentration of defects is present on a surface bombarded with $Xe^+$ even though the depth of damage to the crystal was the most shallow.

Ion bombarded GaAs exposed to $10^6$ - $10^8$ L NO showed a greater reactivity than for the equivalent $O_2$ exposure. Nitrous oxide ($10^7$-$10^{11}$ L) was less reactive than $O_2$. Nitric oxide exposures resulted in the formation of $Ga_2O_3$ and $As_2O_3$, and $N_2O$ exposures yielded only $Ga_2O_3$. Comparison of the NO, $N_2O$, and $O_2$ exposures assissted in the development of a possible model for the ion bombarded GaAs surface.

Ion bombarded GaAs is more reactive towards $O_2$ and NO than a cleaved GaAs(110) surface. It was speculated that the configuration of the ion bombarded surface is the

reason for enhanced reactivity. Ion bombardment results in the formation of defects by breaking surface bonds. It was suggested that these surface bonds are present in the form of singly occupied dangling bonds. The singly occupied dangling bonds provide the proper environment for interaction with $O_2$. Therefore, the presence of these dangling bonds assists in the adsorption of $O_2$. The sticking coefficients for NO and $O_2$ on ion bombarded GaAs were found to be greater than that for $N_2O$. The ion bombarded surface does not provide the proper environment for $N_2O$ adsorption. It is not known why $N_2O$ shows the least reactivity other than the low sticking coefficient which is a measure of the interaction of the reactant molecule with the surface. A molecule such as $N_2O$ could exhibit a low sticking coefficient as a result of the structure of the ion bombarded surface. Repulsion could occur between $N_2O$ and the ion bombarded surface due to the increased number of dangling bonds containing unpaired electrons, whereas NO and $O_2$ would prefer to interact with a surface containing unpaired electrons.

Once NO and $O_2$ have adsorbed, the controlling factor appears to be the reaction pathway. It was suggested that the reaction pathway taken by NO to form $N_2$ and two adsorbed $O^-$ would be thermodynamically favored over the formation of two $O^-$ from $O_2$.

In conclusion it can be stated that ion bombardment results in the formation of defects on GaAs that are likely to be in the form of single electron dangling bonds and that the presence of defects has a great effect on the reactivity of GaAs at the surface. A greater reactivity at the surface is observed when the concentration of surface defects is greater, regardless of the amount of damage that extends deeper into the crystal (at least for the exposures in this study). An important point to note is that increased surface reactivity can be created by bombardment with heavy ions without causing a great amount of damage deep into the crystal lattice as is found with lighter ions.

The fact that the surface chemical reactivity can be enhanced without the generation of deep crystal damage (>50Å) could be used in the future for the selective control of

chemical reactions at the very surface of GaAs. Enhanced reactivity of the surface could be induced by heavy (mass) ion bombardment for the sole purpose of depositing materials right at the surface (dopants, thin oxide coatings, etc.) without further need to anneal out the damage in the crystal caused by ion bombardment, thus avoiding the destruction of the deposited layers by high annealing temperatures. Particular surface chemical reactions could be chosen that could control or aid in the selection of particular surface states that affect GaAs device performance.

# Literature Cited

1. Williams, R. E. *Gallium Arsenide Processing Techniques*; Artech House: Massachusetts, 1984; p 1.

2. Goldschmidt, V. M. *Trans. Faraday Soc.* **1929**, *25*, 253.

3. Welker, H. *Z. Naturforsch A* **1952**, *7*, 744.

4. Jordan, A. S.; Parsey, Jr., J. M. *MRS Bulletin* **1988**, 36.

5. Croydon, W. F.; Parker, E. H. C. *Dielectric Films on GaAs*; Gordon and Breach: New York, 1981; pp 1-10.

6. Williams, R. E. *Gallium Arsenide Processing Techniques*; Artech House: Massachusetts, 1984; p 20.

7. Ghandhi, S. K.; Kwan, P.; Bhat, K. N.; Borrego, J. M. *IEEE Electron Device Lett.* **1982**, *EDL-3*, 48.

8. Pang, S. W. *Solid State Technol.* **1984**, *27*, 249.

9. Oehrlein, G. S. *Physics Today* **1986**, *39(10)*, 26.

10. Pang, S. W.; Geis, M. W.; Efremow, N. N.; Lincoln, G. A. *J. Vac. Sci. Technol. B* **1985**, *3*, 398.

11. Singer, I. L.; Murday, J. S.; Comas, J. *J. Vac. Sci. Technol.* **1981**, *18*, 161.

12. Singer, I. L.; Murday, J. S.; Cooper, L. R. *Surf. Sci.* **1981**, *108*, 7.

13. McGuire, G. E. *Surf. Sci.* **1978**, *76*, 130.

14. Chye, P. W.; Su, C. Y.; Lindau, I.; Skeath, P.; Spicer, W. E. *J. Vac. Sci. Technol.* **1979**, *16*, 1191.

15. Chang, R. P. H.; Coleman, J. J.; Polak, A. J.; Feldman, L. C.; Chang, C. C. *Appl. Phys. Lett.* **1979**, *34*, 237.

16. Williams, R. E. *Gallium Arsenide Processing Techniques*; Artech House: Massachusetts, 1984; p 21.

17. Williams, R. E. *Gallium Arsenide Processing Techniques*; Artech House: Massachusetts, 1984; p 22.

18. Mande, C.; Sapre, V. B. *Indian J. Pure Appl. Phys.* **1979**, *17*, 331.

19. Blakemore, J. S. *J. Appl. Phys.* **1982**, *53*, R123.

20. Shur, M. *GaAs Devices and Circuits*; Plenum Press: New York, 1987; p 10.

21. Williams, R. E. *Gallium Arsenide Processing Techniques*; Artech House: Massachusetts, 1984; p 19.

22. Williams, R. E. *Gallium Arsenide Processing Techniques*; Artech House: Massachusetts, 1984; p 30.

23. Wight, D. R. In *Gallium Arsenide: Materials, Devices, and Circuits*; Howes, M. J., Morgan, D. V., Eds.; John Wiley and Sons: New York, 1985; p 8.

24. Williams, R. E. *Gallium Arsenide Processing Techniques*; Artech House: Massachusetts, 1984; p 31.

25. Williams, R. E. *Gallium Arsenide Processing Techniques*; Artech House: Massachusetts, 1984; pp 35-42.

26. Kirkpatrick, C. G.; Chen, R. T.; Holmes, D. E.; Elliot, K. R. In *Gallium Arsenide: Materials, Devices, and Circuits*; Howes, M. J., Morgan, D. V., Eds.; John Wiley and Sons: New York, 1985; pp 39-94.

27. Wight, D. R. In *Gallium Arsenide: Materials, Devices, and Circuits*; Howes, M. J., Morgan, D. V., Eds.; John Wiley and Sons: New York, 1985; p 3.

28. Mullin, J. B.; Heritage, R. J.; Holliday, C. H.; Straughan, B. W. *J. Cryst. Growth* **1968**, *34*.

29. Mullin, J. B.; Straughan, B. W.; Brickell, W. S. *J. Phys. Chem. Solids* **1965**, *26*, 782.

30. Dorrity, I. A.; Grange, J. D.; Wickenden, D. K. In *Gallium Arsenide: Materials, Devices, and Circuits*; Howes, M. J., Morgan, D. V., Eds.; John Wiley and Sons: New York, 1985.

31. Sherburne, R. K.; Farnsworth, H. E. *J. Chem. Phys.* **1951**, *19*, 387.

32. Ponpon, J. P. *Surf. Sci.* **1985**, *162*, 687.

33. Clement, A.; Fonash, S. J. *J. Appl. Phys.* **1984**, *56*, 1063.

34. Farnsworth, H. E.; Woodcock, R. F. *Adv. in Catal.* **1957**, *9*, 123.

35. Childs, K. D.; Lagally, M. G. *Phys. Rev. B* **1984**, *30*, 5742.

36. Brundle, C. R.; Seybold, D. *J. Vac. Sci. Technol.* **1979**, *16*, 1186.

37. Su, C. Y.; Lindau, I.; Skeath, P.; Chye, P. W.; Spicer, W. E. *J. Vac. Sci. Technol.* **1980**, *17*, 936.

38. Stöhr, J.; Bauer, R. S.; McMenamin, J. C.; Johansson, L. I.; Brennan, S. *J. Vac. Sci. Technol.* **1979**, *16*, 1195.

39. Kahn, A.; Kanani,; Mark, P.; Chye, P. W. *Surf. Sci.* **1979**, *87*, 325.

40. Mark, P.; So, E.; Bonn, M. *J. Vac. Sci. Technol.* **1977**, *14*, 865.

41. Barton, J. J.; Goddard III, W. A.; McGill, T. C. *J. Vac. Sci. Technol.* **1979**, *16*, 1178.

42. Lüth, H.; Büchel, M.; Dorn, R.; Liehr, M.; Matz, R. *Phys. Rev. B* **1977**, *15*, 865.

43. Mark, P.; Creighton, W. F. *Thin Solid Films* **1979**, *56*, 19.

44. Kawabe, M.; Kanzaki, N.; Masuda, K.; Namba, S. *Appl. Opt.* **1978**, *17*, 2556.

45. Kwan, P.; Bhat, K. N.; Borrego, J. M.; Ghandi, S. K. *Solid State Electronics* **1983**, *26*, 125.

46. Smith, P. J.; Allan, D. A. *Vacuum* **1984**, *34*, 209.

47. Ludeke, R.; Ley, L. *J. Vac. Sci. and Technol.* **1979**, *16*, 1300.

48. Wang, Y. X.; Holloway, P. H. *J. Vac. Sci. Technol. B* **1984**, *2*, 613.

49. Wight, D. R. In *Gallium Arsenide: Materials, Devices, and Circuits*; Howes, M. J., Morgan, D. V., Eds.; John Wiley and Sons: New York, 1985; p 20.

50. Johnson, S. T.; Williams, J. S.; Elliman, R. G.; Pogany, A. P.; Nygren, E.; Olson, G. L. *MRS Symp. Proc.* **1987**, *82*, 27.

51. Davis, G. D.; Savage, D. E.; Lagally, M. G. *J. Electron Spectrosc. Rel. Phenom.* **1981**, *23*, 25.

52. Carter, G.; Colligon, J. S. *Ion Bombardment of Solids*; Elsevier: New York, 1968.

53. Greene, J. E. *CRC Crit. Rev. Sol. St. Mater. Sci.* **1983**, *11*, 47.

54. Benninghoven, A.; Rüdenauer, F. G.; Werner, H. W. *Secondary Ion Mass Spectrometry: Basic Concepts, Instrumental Aspects, Applications, and Trends*; John Wiley: New York, 1987.

55. Sigmund, P. In *Sputtering by Particle Bombardment I: Physical Sputtering of Single-Element Solids*; Berisch, R., Ed.; Springer-Verlag: Berlin, 1981; p 10-70.

56. Sigmund, P. *Phys. Rev.* **1969**, *184*, 383.

57. Kelly, R. *Surf. Sci.* **1980**, *100*, 85.

58. Battacharya, R. S.; Holloway, P. H. *Appl. Phys. Lett.* **1981**, *38*, 85.

59. Miranda, R.; Rojo, J. M. *Vacuum* **1984**, *34*, 1070.

60. Navinsek, B. *Prog. Surf. Sci.* **1976**, *7*, 54.

61. Bhattacharya, R. S.; Ghose, D.; Basu, D.; Karmohapatro, S. B. *J. Vac. Sci. Technol.* **1987**, *5*, 179.

62. Greene, J. E.; Barnett, S. A. *J. Vac. Sci. Technol.* **1982**, *21*, 285.

63. Lee, W. W.; Oblas, D. *J. Appl. Phys.* **1975**, *46*, 1736.

64. Cuomo, J. J.; Gambino, R. J. *J. Vac. Sci. Technol.* **1977**, *14*, 152.

65. Weiss, B. L.; Hartnagel, H. L. *Int. J. Electronics* **1976**, *41*, 185.

66. Su, C. Y.; Lindau, I.; Chye, P. W.;Skeath, P.; Spicer, W. E. *Phys. Rev. B* **1982**, *25*, 4045.

67. Hughes, G.; Ludeke, R. *J. Vac. Sci. Technol. B* **1986**, *4*, 1109.

68. Bertness, K. A.; Friedman, D. J.; Mahowald, P. H.; Yeh, J. J.; Wahi, A. K.; Lindau, I.; Spicer, W. E. *J. Vac. Sci. Technol.* **1986**, *4*, 1102.

69. Landgren, G.; Ludeke, R.; Jugnet, Y.; Morar, J. F.; Himpsel, F. J. *J. Vac. Sci. Technol. B* **1984**, *2*, 351.

70. Spicer, W. E.; Chye, P. W.; Garner, C. M.; Lindau, I.; Pianetta, P. *Surf. Sci.* **1979**, *86*, 763.

71. Spicer, W. E.; Lindau, I.; Pianetta, P.; Chye, P. W.; Garner, C. *Thin Solid Films* **1979**, *56*, 1.

72. Ranke, W.; Jacobi, K. *Surf. Sci.* **1979**, *81*, 504.

73. Mönch, W. *Surf. Sci.* **1983**, *132*, 92.

74. Mönch, W. *Surf. Sci.* **1986**, *168*, 57.

75. Pianetta, P.; Lindau, I.; Garner, C. M.; Spicer, W. E. *Phys. Rev. B* **1978**, *18*, 2792.

76. Wilmsen, C. W.; Kee,; Geib, *J. Vac. Sci. Technol.* **1979**, *16*, 1434.

77. Bartels, F.; Mönch, W. *Surf. Sci.* **1984**, *143*, 31.

78. Petro, W. G.; Hino, I.; Eglash, S.; Lindau, I.; Su, C. Y.; Spicer, W. E. *J. Vac. Sci. Technol.* **1982**, *21*, 405.

79. Webb, C.; Lichtensteiger, M. *J. Vac. Sci. Technol.* **1982**, *21*, 659.

80. Lieht, M.; Lüth, H. *J. Vac. Sci. Technol.* **1979**, *16*, 1200.

81. Cohen, C.; Siejka, J.; Berti, M.; Drigo, A. V.; Bentine, G. G.; Pribat, D.; Jannetti, E. *J. Appl. Phys.* **1984**, *55*, 40.

82. Corallo, C. F.; Asbury, D. A.; Pipkin, M. A.; Anderson, T. J.; Hoflund, G. B. *Thin Solid Films* **1986**, *139*, 299.

83. Goddard, W. A.; Barton, J. J.; Redondo, A.; Mcgill, T. C. *J. Vac. Sci. Technol.* **1978**, *15*, 1274.

84. Ranke, W.; Xing, Y. R.; Shen, G. D. *Surf. Sci.* **1982**, *122*, 256.

85. Lucovsky, G. *J. Vac. Sci. Technol.* **1982**, *20*, 761.

86. Ludeke, R.; Koma, A. *J. Vac. Sci. Technol.* **1976**, *13*, 241.

87. Alonso, M.; Soria, F. *Surf. Sci.* **1987**, *182*, 530.

88. Dorn, R.; Lüth, H.; Russell, *Phys. Rev. B* **1974**, *10*, 5049.

89. Pianetta, P.; Lindau, I.; Garner, C.; Spicer, W. E. *Phys. Rev. Lett.* **1976**, *37*, 1166.

90. Ludeke, R. *Solid State Commun.* **1977**, *21*, 815.

91. Mele, E. J.; Joannopoulos, J. D. *Phys. Rev. Lett.* **1978**, *40*, 341.

92. Pianetta, P.; Lindau, I.; Garner, C.; Spicer, W. E. *Phys. Rev. Lett.* **1975**, *35*, 1356.

93. Pianetta, P.; Lindau, I.; Garner, C.; Spicer, W. E. *Phys. Rev. B.* **1977**, *16*, 5600.

94. Gregory, P. E.; Spicer, W. E. *Surf. Sci.* **1976**, *54*, 229.

95. Ranke, W.; Xing, Y. R.; Shen, G. D. *J. Vac. Sci. Technol.* **1982**, *21*, 426.

96. Landgren, G.; Ludeke, R.; Morar, J. F.; Jugnet, Y.; Himpsel, F. J. *Phys. Rev. B* **1984**, *30*, 4839.

97. Mele, E. J.; Joannaopoulos, J. D. *Phys. Rev. B* **1978**, *18*, 6999.

98. Chye, P. W.; Piannetta, P.; Lindau, I.; Spicer, W. E. *J. Vac. Sci. Technol.* **1977**, *14*, 917.

99. Iwasaki, H.; Mizokawa, Y.; Nishitani, R.; Nakamura, S. *Surf. Sci.* **1979**, *86*, 811.

100. Ludeke R.; Koma, A. *CRC Crit. Rev. Solid St. Mater. Sci.* **1975**, *5*, 259.

101. Iwasaki, H.; Mizokawa, Y.; Nishitani, R.; Nakamura, S. *Jpn. J. Appl. Phys.* **1978**, *17*, 315.

102. Bartels, F.; Surkamp, L.; Clemens, H. J.; Mönch, W. *J. Vac. Sci. Technol. B* **1983**, *1*, 756.

103. Frankel, D. J.; Yukun, Y.; Avci, R.; Lapeyre, G. J. *J. Vac. Sci. Technol. A* **1983**, *1*, 679.

104. Iwasaki, H.; Mizokawa, Y.; Nishitani, R.; Nakamura, S. *Jpn. J. Appl. Phys.* **1979**, *18*, 1525.

105. Frankel, D. J.; Anderson, J. R.; Lapeyre, G. J. *J. Vac. Sci. Technol. B* **1983**, *1*, 763.

106. De Cellabos, I. L.; Munoz, J.; Goni, R.; Sacedon, S. *J. Vac. Sci. Technol. A* **1986**, *4*, 1621.

107. Röhkel, K.; Hartnagel, H. L. *Int. J. Electronics* **1986**, *60*, 663.

108. Demanet, C. M.; Rawsthorne, E. D.; Stander, C. M. *Surf. Int. Anal.* **1985**, *7*, 15.

109. Childs, K. D.; Luo, W. -A.; Lagally, M. G. *J. Vac. Sci. Technol. A* **1984**, *2*, 593.

110. Massies, J.; Contour, J. P. *Appl. Phys. Lett.* **1985**, *46*, 1150.

111. Mokwa, W.; Kohl, D.; Heiland, G. *Surf. Sci.* **1984**, *139*, 98.

112. Büchel, M.; Lüth, H. *Surf. Sci.* **1979**, *87*, 285.

113. Webb, C.; Lagowski, J.; Lichtensteiger, M. *Surf. Sci.* **1984**, *138*, 39.

114. Bertness, K.A.; McCants, C.E.; Chiang, T.; Spicer, W. E. *Bull. Am. Phys. Soc.* **1986**, *31*, 536.

115. Bertness, K. A.; Chiang, T.; McCants, C. E.; Mahowald, P. H.; Wahi, A. K.; Kendelewicz, T.; Lindau, I.; Spicer, W. E. *Surf. Sci.* **1987**, *185*, 544.

116. Dahlberg, S.C. *J. Vac. Sci. Technol.* **1976**, *13*, 1056.

117. Bermudez, V. M. *J. Appl. Phys.* **1983**, *54*, 6795.

118. Bermudez, V. M.; Williams, R. T.; Long, J. P.; Rife, J. C.; Wilson, R. M.; Tuttle, A. E.; William, Jr., G. P. *J. Vac. Sci. Technol. A* **1987**, *5*, 541.

119. So, S. K.; Ho, W. *Appl. Phys. A* **1988**, *47*, 213.

120. Rosenberg, A. J. *J. Phys. Chem. Solids* **1960**, *14*, 175.

121. Rosenberg, A. J.; Butler, J. N.; Meena, A. A. *Surf. Sci.* **1966**, *5*, 1108.

122. Arthur, J. R. *J. Appl. Phys.* **1967**, *38*, 4023.

123. Van Velzen, W. J. M.; Morgan, A. E. *Surf. Sci.* **1973**, *39*, 255.

124. Morgan, A. E. *Surf. Sci.* **1973**, *40*, 360.

125. Froitzheim, H.; Ibach, H. *Surf. Sci.* **1975**, *47*, 713.

126. Gregory, P. E.; Spicer, W. E.; Ciraci, S.; Harrison, W. A. *Appl. Phys. Lett.* **1974**, *25*, 511.

127. Mark, P.; Chang, C.; Creighton, W. F.; Lee, B. W. *CRC Crit. Rev. Sol. Stat. Mater. Sci.* **1975**, *5*, 189.

128. Shirley, D. A. *J. Vac. Sci. Technol.* **1975**, *12*, 280.

129. Thurmond, C. D.; Schwartz, G. P.; Kammlott, G. P.; Schwartz, B. *J. Electrochem. Soc.* **1980**, *127*, 1366.

130. Schwartz, G. P.; Gualtiere, G. J.; Kammlott, G. W.; Schwartz, B. *J. Electrochem. Soc.* **1979**, *126*, 1737.

131. Grunthaner, F. J.; Grunthaner, P. J.; Vasquez, R. P.; Lewis, B. F.; Maserjian, J. *J. Vac. Sci. Technol.* **1979**, *16*, 1443.

132. Skeath, P.; Su, C. Y.; Chye, P. W.; Piannetta, P.; Lindau, I.; Spicer, W. E. *J. Vac. Sci. Technol.* **1979**, *16*, 1439.

133. Grunthaner, P. J.; Vasquez, R. P.; Grunthaner, F. J. *J. Vac. Sci. Technol.* **1980**, *17*, 1045.

134. Yamasaki, K.; Sugano, T. *J. Vac. Sci. Technol.* **1980**, *17*, 959.

135. Lucovsky, G. *J. Vac. Sci. Technol.* **1981**, *19*, 456.

136. Harrison, B.; Wyatt, M.; Gough, K. G. *Catalysis* **1985**; *5*, 127.

137. Ibbotson, D. E.; Wittrig, T. S.; Weinberg, W. H. *Surf. Sci.* **1981**, *110*, 294.

138. Bringans, R. D.; Bachrach, R. Z. *J. Vac. Sci. Technol. A* **1983**, *1*, 676.

139. Pao, Y.; Liu, D.; Lee, W. S.; Harris, J. S. *Appl. Phys. Lett.* **1986**, *48*, 1291.

140. Larsen, P. K.; Pollmann, J. *Solid State Commun.* **1985**, *53*, 277.

141. Lagowski, J.; Kaminska, M.; Parsey, J. M.; Gatos, H. C.; Lichtensteiger, M. *Appl. Phys. Lett.* **1982**, *41*, 1078.

142. Pearton, S. J. *J. Appl. Phys.* **1982**, *53*, 4509.

143. Pretzer, D. D.; Hagstrum, H. D. *Surf. Sci.* **1966**, *4*, 265.

144. Mokwa, W.; Kohl, D.; Heiland, G. *Phys. Rev. B* **1984**, *29*, 6709.

145. Astaldi, C.; Sorba, L.; Rinaldi, C.; Mercuri, R.; Nannarone, S.; Calandra, C. *Surf. Sci.* **1985**, *162*, 39.

146. Antonangeli, F.; Calandra, C.; Colavita, E.; Nannarone, S.; Rinaldi, C.; Sorba, L. *Phys. Rev. B* **1984**, *29*, 8.

147. Bringans, R. D.; Bachrach, R. Z. *Solid State Commun.* **1983**, *45*, 83.

148. Hou, X.; Yang, S.; Dong, G.; Ding, X.; Wang, X. *Phys. Rev. B* **1987**, *35*, 8015.

149. Förster, A.; Spitzer, A.; Lüth, H. *Surf. Sci.* **1986**, *172*, 174.

150. Mattern-Klosson, M.; Ding, X.; Lüth, H.; Spitzer, *Surf. Sci.* **1983**, *129*, 1.

151. Matz, R.; Lüth, H. *Surf. Sci.* **1982**, *117*, 362.

152. Winters, H. F. *J. Appl. Phys.* **1978**, *49*, 5165.

153. Coburn, J. W.; Winters, H. F. *J. Vac. Sci. Technol.* **1979**, *16*, 391.

154. Hughes, E. E. *J. Chem. Phys.* **1961**, *35*, 1531.

155. Shaw, D. W. *J. Electrochem. Soc.* **1981**, *128*, 874.

156. Oelhafen, P.; Freeouf, J. L.; Pettit, G. D.; Woodall, J. M. *J. Vac. Sci. Technol. B* **1983**, *1*, 787.

157. Mizokawa, Y.; Iwasaki, H.; Nishitani, R.; Nakamura, S. *J. Electron Spectrosc. Rel. Phenom.* **1978**, *4*, 129.

158. Sheka, I. A.; Chaus, I. S.; Mityureva, T. T. *The Chemistry of Gallium*; Elsevier Publishing: New York, 1966; pp 41-48.

159. Sato, T.; Nakamura, T. *J. Chem. Tech. Biotechnol.* **1982**, *32*, 469.

160. Perkin Elmer 5000 Series ESCA Systems Manual, Version 2.0, Section IV: Theory of Operation.

161. Perkin Elmer 5000 Series ESCA Systems Manual, Version 2.0, Section III.

162. Briggs, D. In *Practical Surface Analysis by Auger and X-ray Photoelectron Spectroscopy*; Briggs, D., Seah, M. P., Eds.; John Wiley and Sons: New York, 1983; p 362.

163. Sen, S. *Electrical Studies on Ion-Etched n-GaAs(100) Surfaces*, Master's thesis, Virginia Polytechnic Institute and State University, 1987.

164. Cole, E. D.; Johnson, P. J. unplublished results at Virginia Polytechnic Institute and State University, 1986.

165. Cole, E. D. *Electrical Analysis of Low Energy Argon Ion Bombarded GaAs*, Ph.D. Dissertation, Virginia Polytechnic Institute and State University, 1988.

166. Holtz, M. *Raman-Scattering Studies of the Structure of Ion-Implanted GaAs*, Ph.D. Dissertation, Virginia Polytechnic Institute and State University, 1987.

167. Feng, G. *Optical Studies of Ion Bombarded GaAs*, Ph.D. Dissertation, Virginia Polytechnic Institute and State University, 1989.

168. Bertrand, P. A. *J. Vac. Sci. Technol.* **1981**, *18*, 28.

169. Shirley, D. A. *J. Vac. Sci. Technol.* **1975**, *12*, 280.

170. Holloway, P. H.; Bhattacharya, R. S. *J. Vac. Sci. Technol.* **1982**, *20*, 444.

171. Norton, P. R. *J. Catal.* **1975**, *36*, 211.

172. Wilmsen, C. W. *Thin Solid Films* **1976**, *39*, 105.

173. Vasquez, R. P.; Lewis, B. F.; Grunthaner, F. J. *Appl. Phys. Lett.* **1983**, *42*, 293.

174. Roberts, M. W. In *Advances in Catalysis*; Eley, D. D., Pines, H., Weisz, P. B., Eds.; Academic Press: New York, 1980; Volume 29, pp 76,81-82.

175. McIntyre, N. S. In *Practical Surface Analysis by Auger and X-ray Photoelectron Spectroscopy*; Briggs, D., Seah, M. P., Eds.; John Wiley and Sons: New York, 1983; p 410.

176. Wagman, D. D.; Evans, W. H.; Parker, V. B.; Halow, I.; Bailey, S. M.; Schumm, R. H.; *National Bureau of Standards Technical Note*; **1968**, 270-3.

177. Szymonski, M.; Battacharya, R. S. *Appl. Phys.* **1979**, *20*, 207.

178. *Handbook of Chemistry and Physics*, 61st ed.; Weast, R. C., Astle, M. J., Eds.; The Chemical Rubber Co.: Florida, 1981; pg D-221.

179. *Handbook of Chemistry and Physics*, 66th ed.; Weast, R. C., Astle, M. J., Beyer, W. H., Eds.; The Chemical Rubber Co.: Florida, 1986; pp E62-63.

180. Bussing, T. D.; Holloway, P. H.; Wang, Y. X.; Moulder, J. F.; Hammond, J. S. *J. Vac. Sci. Technol. B* **1988**, *6*, 1514.

181. Feng, G. F.; Holtz, M.; Zallen, R.; Epp, J. M.; Dillard, J. G.; Cole, E.; Johnson, P.; Sen, S.; Burton, L. C. *Mat. Res. Soc. Sym. Proc.* **1987**, *93*, 381.

182. Masterton, W. L.; Slowinski, E. J.; Stanitski, C. L. *Chemical Principles*, 5th ed.; Saunder Coll. Pub.: Philadelphia, 1981; p A6.

183. Aspnes, D. E.; Kelso, S. M.; Olson, C. G.; Lynch, D. W. *Phys. Rev. Lett.* **1982**, *48*, 1863.

184. Williams, R. E. *Gallium Arsenide Processing Techniques*; Artech House: Massachusetts, 1984; pp 59,260.

185. Feng, G. F.; Zallen, R.; Epp, J. M.; Dillard, J. G. *Phys. Rev. B* in press.

186. Feng, G. F.; Zallen, R. *Bull. Am. Phys. Soc.* **1987**, *32*, 517.

187. Kittel, C. *Introduction to Solid State Physics*, 6th ed.; John Wiley and Sons: New York, 1986.

188. Private communication with Alf Siochi.

189. Carter, G.; Navinšek, B.; Whitton, J. L. In *Sputtering by Particle Bombardment II: Sputtering of Alloys and Compounds, Electron and Neutron Sputtering, Surface Topography*; Behrisch, R., Ed.; Springer-Verlag: Berlin, 1983; pp 231-270.

190. Shevchik, N. J.; Tejada, J.; Cardona, M. *Phys. Rev. B* **1974**, *9*, 2627.

191. Scherzer, B. M. U. In *Sputtering by Particle Bombardment II: Sputtering of Alloys and Compounds, Electron and Neutron Sputtering, Surface Topography*; Berisch, R., Ed.; Springer-Verlag: New York, 1983.

192. Wagner, C. D. In *Practical Surface Analysis by Auger and X-ray Photoelectron Spectroscopy*; Briggs, D., Seah, M. P., Eds.; John Wiley and Sons: New York, 1983; Appendix 4.

193. Wagner, C. D.; Riggs, W. M.; Davis, L. E.; Moulder, J. F. *Handbook of X-Ray Photoelectron Spectroscopy*; Muilenberg, G. E., Ed.; Perkin-Elmer: 1979.

194. Roberts, M. W. In *Advances in Catalysis*, Volume 29; Eley, D. D., Pines, H.; Weisz, P. B., Eds.; Academic Press: New York, 1980; p 70.

195. Bertness, K. A.; Mahowald, P. H.; McCants, C. E.; Wahi, A. K.; Kendelewicz, T.; Lindau, I.; Spicer, W. E. *Appl. Phys. A* **1988**, *47*, 219.

196. Ying, Z.; Ho, W. *Phys. Rev. Lett.* **1988**, *60*, 57.

197. Lucovsky, G.; Bauer, R. S. *Solid State Commun.* **1979**, *31*, 931.

198. Gasser, R. P. H. *An Introduction to Chemisorption and Catalysis by Metals*; Oxford University Press: New York, 1985; p 40.

199. Ranke, W.; Jacobi, K. *Prog. Surf. Sci.* **1981**, *10*, 1.

The vita has been removed from
the scanned document